

**Steady-State and Transient Thermal Modeling of
Solid Electrolysis (SOXE) within the Mars Oxygen
In-Situ Resource Utilization Experiment**

by

Justine Nikole Schultz

B.S. Aerospace Engineering
B.S. Mechanical Engineering
West Virginia University (2015)

Submitted to the Department of Aeronautical and Astronautical
Engineering
in partial fulfillment of the requirements for the degree of
Masters of Science in Aeronautical and Astronautical Engineering
at the

MASSACHUSETTS INSTITUTE OF TECHNOLOGY

May 2022

© Massachusetts Institute of Technology 2022. All rights reserved.

Author
Department of Aeronautical and Astronautical Engineering
May 17, 2022

Certified by.....
Jeffrey A. Hoffman
Professor of the Practice of Aerospace Engineering, Department of
Aeronautics and Astronautics
Thesis Supervisor

Accepted by
Jonathan P. How
R. C. Maclaurin Professor of Aeronautics and Astronautics Chair,
Graduate Program Committee

Steady-State and Transient Thermal Modeling of Solid Electrolysis (SOXE) within the Mars Oxygen In-Situ Resource Utilization Experiment

by
Justine Nikole Schultz

Submitted to the Department of Aeronautical and Astronautical Engineering
on May 17, 2022, in partial fulfillment of the
requirements for the degree of
Masters of Science in Aeronautical and Astronautical Engineering

Abstract

Humankind has always felt the need to understand our place in the universe. The most direct next step for humankind to accomplish the colossal task of understanding and exploring our place in the solar system is to send people to Mars. This ambitious task requires improved understanding and performance of in-situ resource utilization on Mars' surface as humans prepare to visit Mars. The Mars Perseverance Rover, which landed on the Martian surface on 18 February, 2021, contained the Mars Oxygen In-Situ Resource Utilization Experiment (MOXIE) as an experimental payload to demonstrate the capabilities of in-situ resource utilization by producing oxygen (O_2) out of the abundant carbon dioxide (CO_2) that makes up a majority of the Martian atmosphere.

Accurate and high fidelity modelling of internal temperatures of the Solid Oxide Electrolysis (SOXE) stack are crucial to understanding operational performance of MOXIE. Weight, energy, space, and complexity constraints limited the ability to add internal temperature sensors to the flight instrument MOXIE. Tests are being conducted on the Martian surface with limited sensor data available to understand the degradation and performance of the SOXE stack in various operational conditions. A high fidelity model has been created utilizing COMSOL to understand the thermal impact of ambient conditions and empirical data on any given location of the SOXE stack, both internal to the flow path and external. This transient model was validated against data from JPL's MOXIE testbed laboratory and continued model validation as new data is down-linked from the MOXIE flight model aboard NASA's Perseverance Rover.

This thesis gives an overview of the thermal system and corresponding thermal and multi-physics modelling of MOXIE. Since MOXIE is an experimental instrument that is confined to the Martian surface with limited sensors, the accurate modelling of detailed thermal data can provide an insight to the instrument's performance. Similarly, analytical experiments can be conducted utilizing the multi-physics model to predict the results of a warm-up routine and an oxygen-producing run prior to experimenting in the harsh and unforgivable Martian atmosphere. The model will contribute to understanding the performance and thermal response of creating oxygen

on the Martian surface to aid in human exploration.

Thesis Supervisor: Jeffrey A. Hoffman

Title: Professor of the Practice of Aerospace Engineering, Department of Aeronautics and Astronautics

Acknowledgments

I am so humbled to be a part of a team with such passion and expertise in spaceflight. I never would have dreamed that I would work among the scientists and engineers that produced oxygen on a different planet for the first time. I am so thankful for my experience in every aspect.

Thank you to my advisor, Professor Jeffrey Hoffman, for recruiting me to join the MOXIE family and trusting me with this work. I will never forget both the excitement and nerves during our team call waiting for confirmation of the first oxygen production on Mars. I joined this team not knowing the unknown. I am grateful of both the research skills and technical skills I gained during this experience, all during a global pandemic.

Thank you to Michael Hecht, our MOXIE leader. Your excitement and engagement is contagious and I hope our paths cross again as humans continue making strides to living on Mars.

Thank you to Asad Aboobaker and Jen Hua for the mentorship and the material provided to allow me to complete my research.

Thank you to Joe Hartvigsen, my COMSOL and thermal engineering mentor. I have learned so much during this process thanks to your guidance.

Thank you to my funding sponsor, GE Aviation, for championing for me and allowing to pursue my higher education.

To my family: Thank you to my parents, Kristina and Ed Schultz. You provided a home and upbringing that was loving and encouraging for me to follow my dreams. Thank you to my sisters, Alexa and Viktoria, for letting me ramble on for countless hours about my fascination with space and encouraging me to continue my education.

Finally, I would like to thank my fiance, Chris Bolster. You have constantly motivated me by leading by example through your work ethic. I truly believe that with your support, I can accomplish anything.

Contents

1	Introduction	10
1.1	Mars Perseverance Rover	10
1.1.1	MOXIE	11
1.1.2	Carbon Dioxide Acquisition and Compression (CAC)	13
1.1.3	Solid Oxide Electrolysis (SOXE) Subsystem	13
1.1.4	Monitor and Control Subsystem	18
2	Thermal Modelling System	20
2.1	Thermal Modelling	20
2.2	MOXIE Thermal Model	22
2.2.1	SOXE	22
3	Material Properties	24
3.1	Inconel 600	26
3.2	Refrasil UC 100-48	28
3.3	Compressed MinK	30
3.4	Copper Alloy UNS C15715	32
3.5	Scandium-Stabilized Zirconia	32
3.6	CFY Cr Alloy	35
3.7	Aerogel	38
3.8	Carbon Dioxide	39
4	Modelled Thermodynamics	41
4.1	Conduction	41
4.2	Radiation	41
4.3	Convection	43
5	Model Set-up	45
5.1	Previous and Existing Models	45
5.2	Model Geometry Simplification	46
5.3	Meshing	47
5.4	Boundary Conditions	49
5.4.1	Aerogel	50
5.4.2	Ambient Temperature	51
5.5	Steady-State	54

5.6	Transients	55
5.6.1	Warm-Up	55
5.6.2	Heater Controller	56
6	Results	58
6.1	Steady-State	58
6.1.1	Labelling and Notation	59
6.1.2	Baseline Thermal Model Values	61
6.1.3	Steady-State Model Validation and Comparison to Experimental Results	63
6.1.4	Thermal Model Study: Impact of Heater Variation	66
6.1.5	Ambient (RAMP) Conditions Impact	70
6.2	Transient	71
6.2.1	Transient Model Validation and Comparison to Experimental Results	73
6.2.2	Transient Results	74
7	Model Improvement Plan	76
7.1	Next Steps	76
A	Steady-State Results	78

List of Figures

1-1	MOXIE System CAD Model [10]	12
1-2	MOXIE Subsystem Diagram[18]	12
1-3	Chemical Reaction through SOEC [16]	14
1-4	MOXIE Subsystem Components [17]	15
1-5	SOXE Subsystem Components	16
1-6	SOXE System Labeled Diagram	17
1-7	SOXE Thermocouple Sensor Locations [17]	18
2-1	MOXIE System Component Breakdown [17]	21
2-2	MOXIE System Component Breakdown[15]	22
2-3	Interaction Diagram, Top Three Layers of SOXE Assembly Stack [9]	23
3-1	Material Map of SOXE Components [15]	25
3-2	Material Location of Inconel 600	26
3-3	COMSOL Input Inconel 600 Heat Capacity as Function of Temperature [3]	27
3-4	COMSOL Input Inconel 600 Conductivity as Function of Temperature[3]	28
3-5	Material Location of Refrasil Cloth	29
3-6	COMSOL Input Refrasil Cloth Conductivity as Function of Temperature	29
3-7	Material Location of Compressed Mink-K	30
3-8	COMSOL Input Min-K Heat Capacity as Function of Temperature [3]	31
3-9	COMSOL Input Min-K Conductivity as Function of Temperature [3]	31
3-10	Material Location of Scandium Zirconia	33
3-11	COMSOL Input Scandium Zirconia Heat Capacity as Function of Temperature [3]	34
3-12	COMSOL Input Scandium-Stablized Zirconia Conductivity as Function of Temperature [3]	35
3-13	Material Location of CFY Interconnects	36
3-14	COMSOL Input CFY Heat Capacity as Function of Temperature [3]	36
3-15	COMSOL Input CFY Conductivity as Function of Temperature [3]	37
3-16	COMSOL Input CFY Thermal Diffusivity as Function of Temperature [3]	37
3-17	COMSOL Input Aerogel Conductivity Coefficient as Function of Temperature	38
3-18	Location of Carbon Dioxide Internal to SOXE	39

4-1	Incoming Irradiation (left), Outgoing Radiosity (right) [6]	42
4-2	Boundaries Selected for Radiation-to-Ambient Condition (selected in blue)	43
5-1	Previous MOXIE Thermal Model[11]	45
5-2	Full Model 3-D Tetrahedron Meshing	48
5-3	Zoomed in View of 3-D Tetrahedron Meshing on Electrolyte-Interconnect Layering	49
5-4	Full SOXE assembly with Aerogel Insulation	50
5-5	Constant RAMP Temperature Boundary Condition Locations	51
5-6	Radiation to Ambient Boundary Condition to Represent Aerogel	53
6-1	TC5	60
6-2	Labelling Convention, X-Y Plane View of SOXE Stack Interconnect	61
6-3	Thermal Model Steady-State, Z-Y Plane View	63
6-4	Cross-Section Temperature Validation with Test JSA006 OC10	65
6-5	Heater Temperature Sweep Results, Volumetric Average Temperatures within Thermal Model Steady-State	67
6-6	SOXE Stack 3D Volumetric Thermal Analysis at Baseline Heater Temperatures	68
6-7	SOXE Stack 3D Volumetric Thermal Analysis at Heater Temperature Baseline -5 degC	69
6-8	SOXE Stack 3D Volumetric Thermal Analysis at Heater Temperature Baseline +5 degC	70
6-9	SOXE Stack Temperatures vs. Variation of Ambient (RAMP) Temperatures	71
6-10	COMSOL Transient Model for TC5 (blue) vs. Empirically Recorded Results for TC5 (red)	73
6-11	Analytical Heater Temperature (Orange) and SOXE Internal Temperature vs. Time	74

List of Tables

3.1	Component Material List	24
3.2	COMSOL Input UNS C15715 Material Properties [4]	32
5.1	COMSOL Meshing Properties for Free-Tetrahedral	47
5.2	COMSOL Algebraic Multi-Grid Solver	54
5.3	COMSOL Newton Nonlinear Solver	55
5.4	COMSOL Time-Dependent Solver	55
5.5	COMSOL Proportional Integration Controller for Heaters	56
6.1	Model Output Average Volume Temperatures for Each Layer of SOXE Cell at Baseline	62
6.2	Detailed Model Output Temps for Each Layer of SOXE Cell at Baseline Heater (degC)	62
6.3	Absolute Error Used for Validation of Steady-State COMSOL Model at Thermocouple Locations	64
6.4	Temperature Range of Steady-State COMSOL Model vs. Test JSA006 OC07 and Test JAS006 OC08	64
6.5	Temperature Sweep of Top and Bottom Heater Conditions	66

Chapter 1

Introduction

Humankind has looked to the sky with fascination long before Mars was first observed through Galileo's telescope. This red planet, named after the ancient Roman god of war, claimed its spot in the solar system as Earth's neighbor and humankind's goal for cosmic exploration. A short cosmic trip to Mars will be the furthest any human will have ever travelled throughout all of Earth's written history. An intrepid exploration of this distance requires engineering and consideration for aspect of life on the Mars surface due to the distance and corresponding challenges. All exploration of the red planet in the past has not contained human life, and while still an engineering feat, there is more uncharted innovation required to prepare for a human exploration.

One major aspect of preparing for humans on the martian surface is the ability to obtain oxygen, which is required for both breathing for sustaining human life and as an oxidizer for rocket combustion, required for the return to Earth. Mars has an atmosphere of 95.5 % carbon dioxide (CO_2) and the remaining is comprised of mostly argon and nitrogen, compared the the Earth's atmosphere of 21% oxygen (O_2). [12], The Mars Perseverance rover was sent to Mars in July 2020 with an experiment on board to demonstrate in situ oxygen production with the use of the abundant CO_2 that comprises the martian atmosphere.

1.1 Mars Perseverance Rover

Among other experiments to search for ancient life on the surface of the red planet, one experiment aboard the rover has the unique main objective of demonstrating the first ever in-situ resource utilization (ISRU) on another planet. In situ resources is an increasingly important study as humans push further into the cosmos, increasing the quantity of resources required to sustain life. The aforementioned experiment, Mars Oxygen In-Situ Resource Utilization Experiment (MOXIE), incurs oxygen by converting carbon dioxide from the atmosphere to carbon monoxide and oxygen via electrolysis. This process of producing oxygen is pertinent for human visits to Mars and to ensure the launch vehicle is capable of returning to Earth.

1.1.1 MOXIE

A majority of the oxygen required for a Mars mission is required as the oxidant supplied to the Mars ascent vehicle that will shuttle humans from the surface of the red planet back to Earth. NASA's Mars mission architecture study estimated that the quantity of oxygen required for a CH₄/O₂ propulsion system is 400 metric tons for a direct return flight to Earth. Producing oxygen in-situ on the Martian surface would provide a 32% mass savings overall, which is a major constraint to the mission design. [7]

MOXIE is a demonstrator and proof of concept with two primary objectives. The first primary goal is to show feasibility of producing oxygen in-situ on the Martian surface utilizing the Mars atmosphere. The second is using the system design as a baseline for increased production size for the first human mission and the design will be matured to run continuously for 14 months as the results of the operating performance is studied. The production goal for MOXIE is to produce greater than 99.6% pure oxygen during segmented operation when sufficient rover power becomes available. [18] The experiment sits within the body of the Mars Perseverance Rover, confined to a gold plated containment and consists of three main subsystems[16]:

1. Carbon Dioxide Acquisition and Compression (CAC)
2. Solid Oxide Electrolysis (SOXE)
3. Monitor and Control System (MCS)

The figure below is a model representation of the MOXIE system, self-contained in a 23.9 x 23.9 x 30.9 cm case that is mounted within the Perseverance Rover.

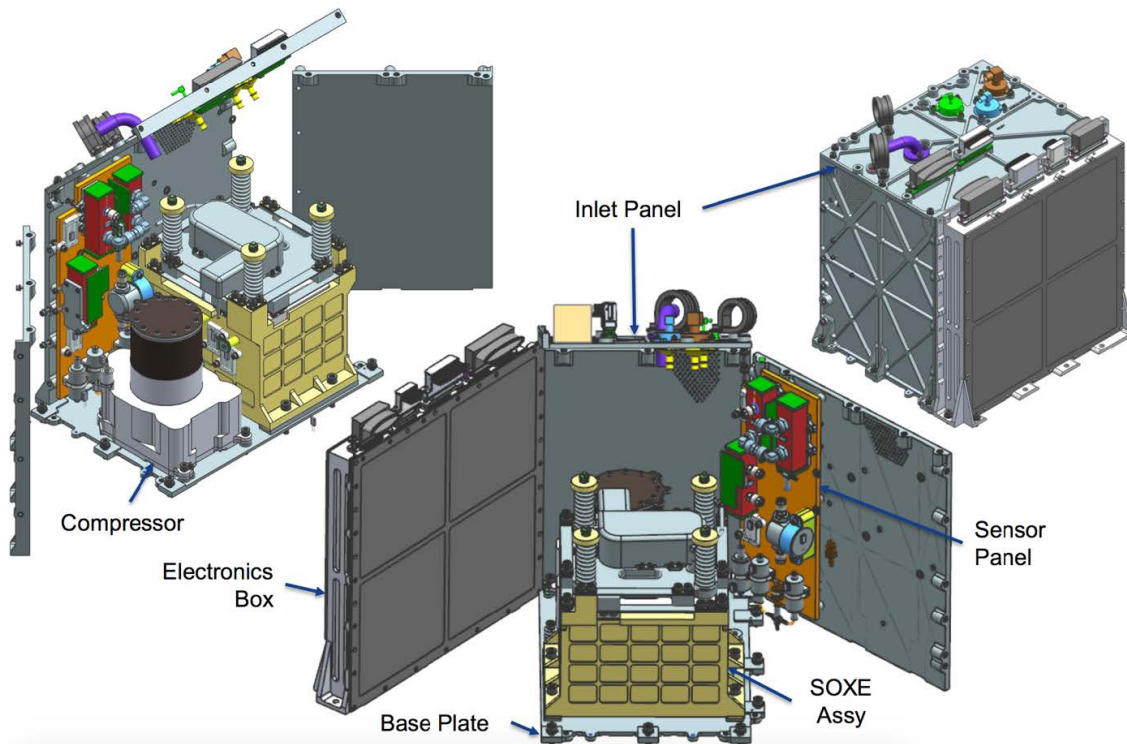


Figure 1-1: MOXIE System CAD Model [10]

The compressor in this figure is part of the CAC assembly with access to the atmosphere through the inlet panel. The SOXE Assembly is secured by a spring-loaded containment and will be elaborated on further as this is the subsystem model in this thesis. The electronics box and the sensor panel make up the MCS and are partial used for the thermal SOXE model.

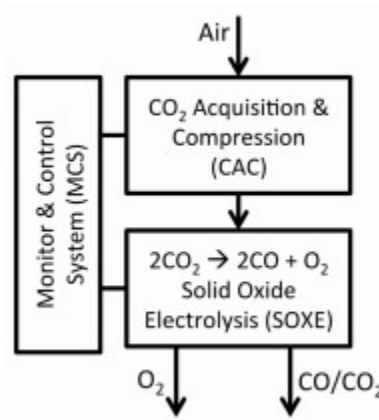


Figure 1-2: MOXIE Subsystem Diagram[18]

The block diagram for these subsystems is shown in Figure 1-2. MOXIE operates by drawing rover power to operate the electric heaters in the Solid Oxide Electrolysis (SOXE) subsystem and powers the scroll compressor that inhales atmospheric gases through the CO₂ Acquisition and Compression (CAC) subsystem. The compressed CO₂ becomes an input to SOXE. Within the SOXE system, the gas is flowed through the solid oxide electrolysis stack, converting the carbon dioxide to carbon monoxide and oxygen via electrolysis. Atmospheric gases other than CO₂ pass through the system and are released into the Mars atmosphere through the cathode exhaust. Oxygen then passes through the electrolyte to the anode where the oxygen purity is measured and returned to the atmosphere.

Each step of the system is detailed below in the corresponding subsections.

1.1.2 Carbon Dioxide Acquisition and Compression (CAC)

The carbon dioxide acquisition and compression system (CAC)'s main objective is to draw in Mars atmosphere and compress the gas to a usable pressure, increasing the flow velocity to be directed to the inlet of the SOXE.

This operation is achieved through a scroll compressor. The compressor draws in the Martian atmosphere while running at approximately 3500 RPM, which is then flowed into the SOXE subsystem at a flow rate of approximately 60 g/hr. As Hinterman et. al suggests, previous concern that pressure oscillations of the compressor could impact that the operation of oxygen production was mitigated by the plenum chamber. The design modulates the oscillations, verified by testing at JPL. The findings of the study concluded that the press oscillations from the compressor are minimal and so the continuous flow through the inlet of SOXE can be assumed. [11]

1.1.3 Solid Oxide Electrolysis (SOXE) Subsystem

The objective of the SOXE subsystem is the electro-chemical process of creating oxygen from the carbon dioxide rich atmosphere. This produces a bi-product of carbon monoxide to fulfill the following net chemical reaction:



The solid oxide electrolysis cell (SOEC), composed of repeating layers of porous cathode and anodes at high temperatures. Each layer of the cathode and anode are separated by a scandium-doped zirconia ceramic electrolyte as illustrated in the figure below.

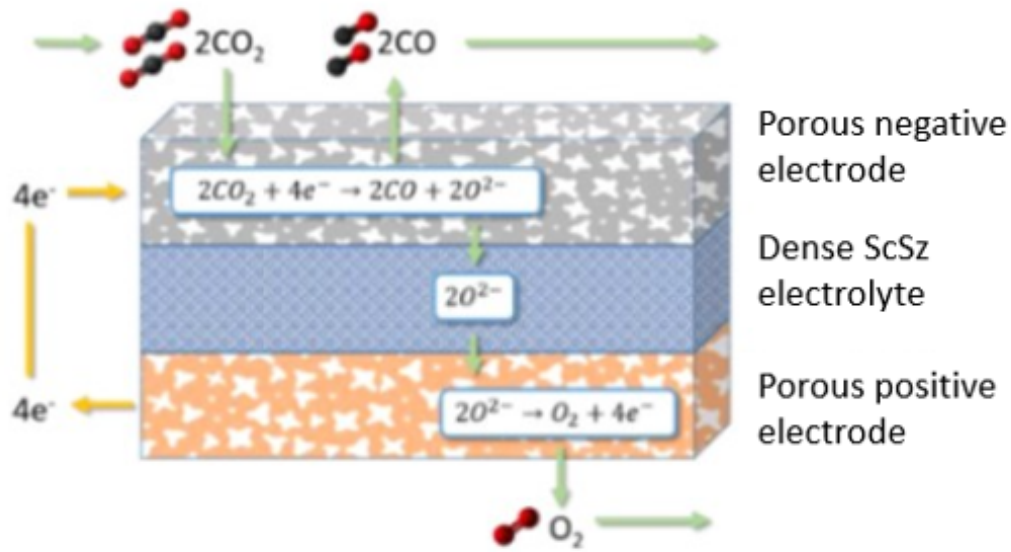
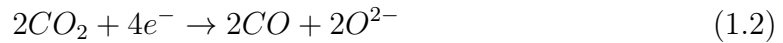


Figure 1-3: Chemical Reaction through SOEC [16]

The compressed and preheated CO_2 flows through the cathode to the catalytic site as an electric potential is applied. This precipitates the following reaction[19]:



The negatively charged O^{2-} is directed through the scandium-stabilized zirconia (ScSZ) electrolyte to the positively porous electrode where the O^{2-} ions are oxidized. This produces an oxygen molecule and is represented as:



Component Breakdown

Figure 1-4 is the layers of the MOXIE system and subsystem. The blue arrows indicate layering. The arrows point toward layers that are underneath their predecessor.

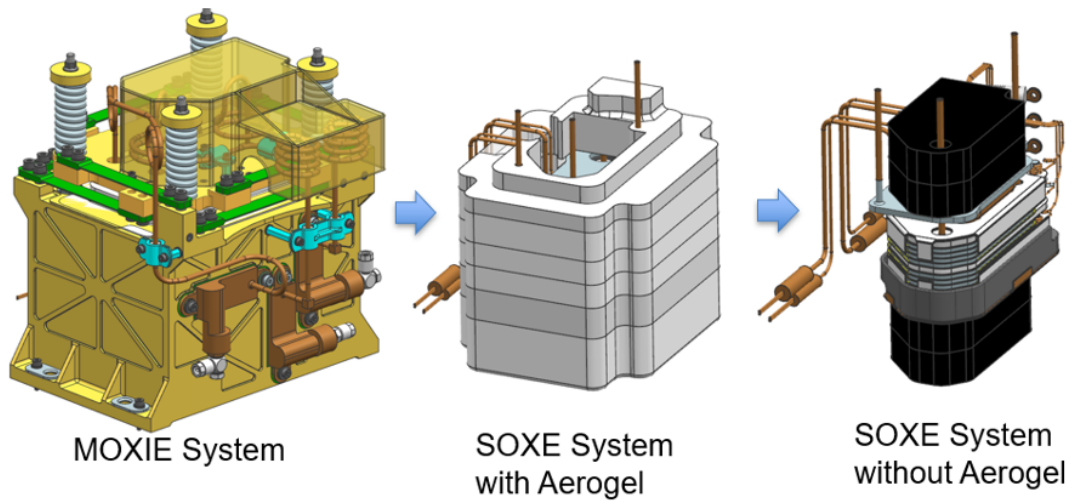


Figure 1-4: MOXIE Subsystem Components [17]

The first image of the gold cube is the full MOXIE system with the external configurations. The second image is the SOXE system with the insulating aerogel visible (white). Following the blue arrow to the third image shows the SOXE subsystem that present underneath the aerogel layer.

Figure 1-5 is the CAD model of the subsystem that is thermally modeled in this research with appropriate labelling.

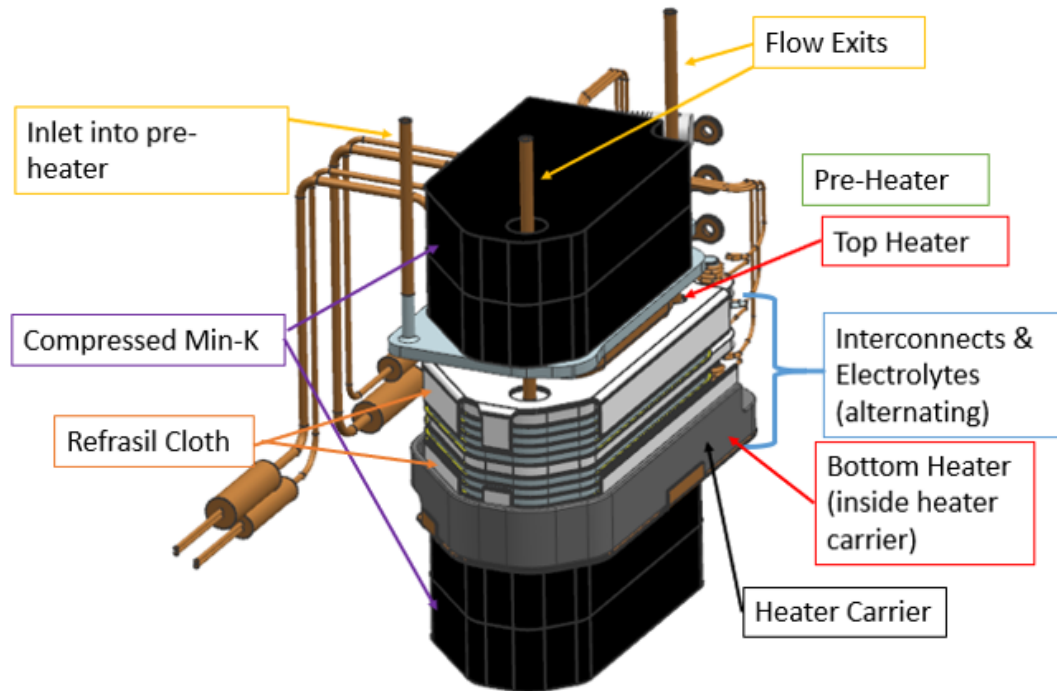


Figure 1-5: SOXE Subsystem Components

The SOXE subsystem is made up the the following components:

1. Compressed Min-K
2. Gas Flow Path Preheater
3. Refrasil Cloth Electrolytes and Interconnects (alternating layers of SOXE Stack)
4. High Temperature Heaters
5. Heater Carriers
6. Aerogel Insulation

Naming Conventions

The following naming conventions are used throughout this paper to denote order and orientation of the components.

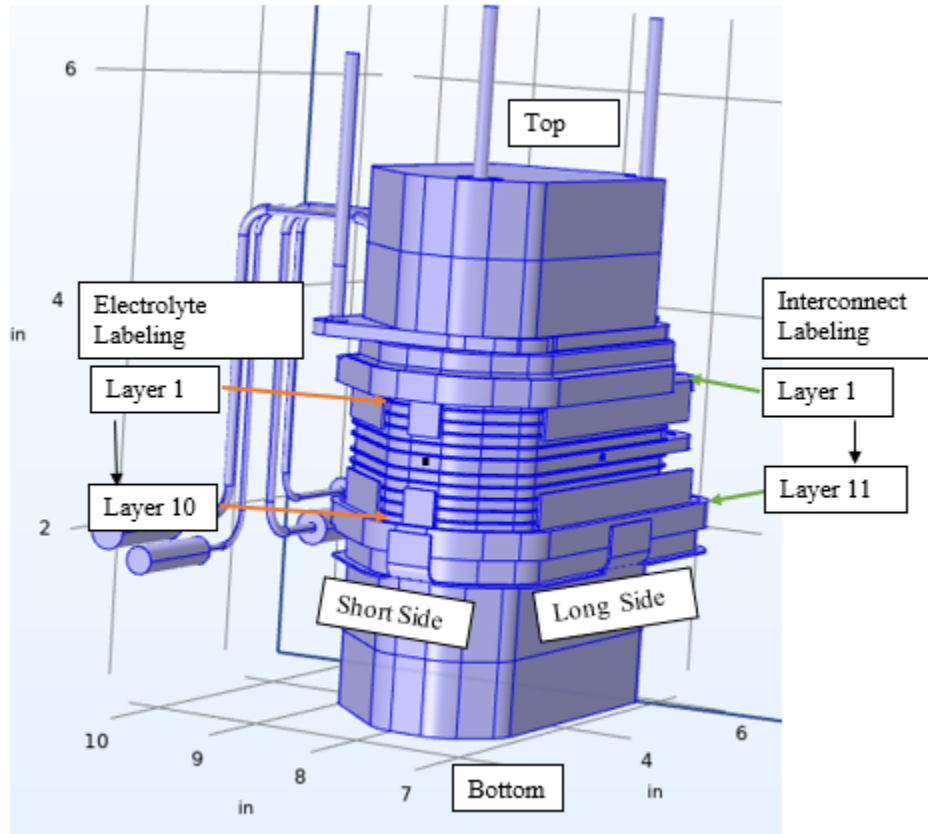


Figure 1-6: SOXE System Labeled Diagram

As noted in Figure 1-6, the top of the subsystem denotes the beginning of the numbering sequence. Each layer of interconnect in the stack is labeled 1 through 11, where interconnect layer 11 is the layer closest to the bottom. The interconnects are the thicker layers of the stack. The heater carriers and refrasil cloths obstruct the view to the top-most and bottom-most layers in Figure 1-6.

Figure 1-7 is an expanded view to expose the full SOXE stack and layers. The same numbering pattern is true for the labeling of the electrolytes, which are alternating layers between the interconnects. There are 10 electrolyte layers and therefore the top electrolyte is labelled as 1, and the layer closest to the bottom is layer 10. The short side and long side are used to differentiate between the edges of the stack. This notation is used for both the electrolyte and interconnect layers. Since perfect symmetry cannot be assumed, it is useful to characterize the sides individually.

Another important naming convention is the location of the thermocouples. The thermocouples were used in the laboratory testing and the results from this testing are used to calibrate the thermal model and determine errors.

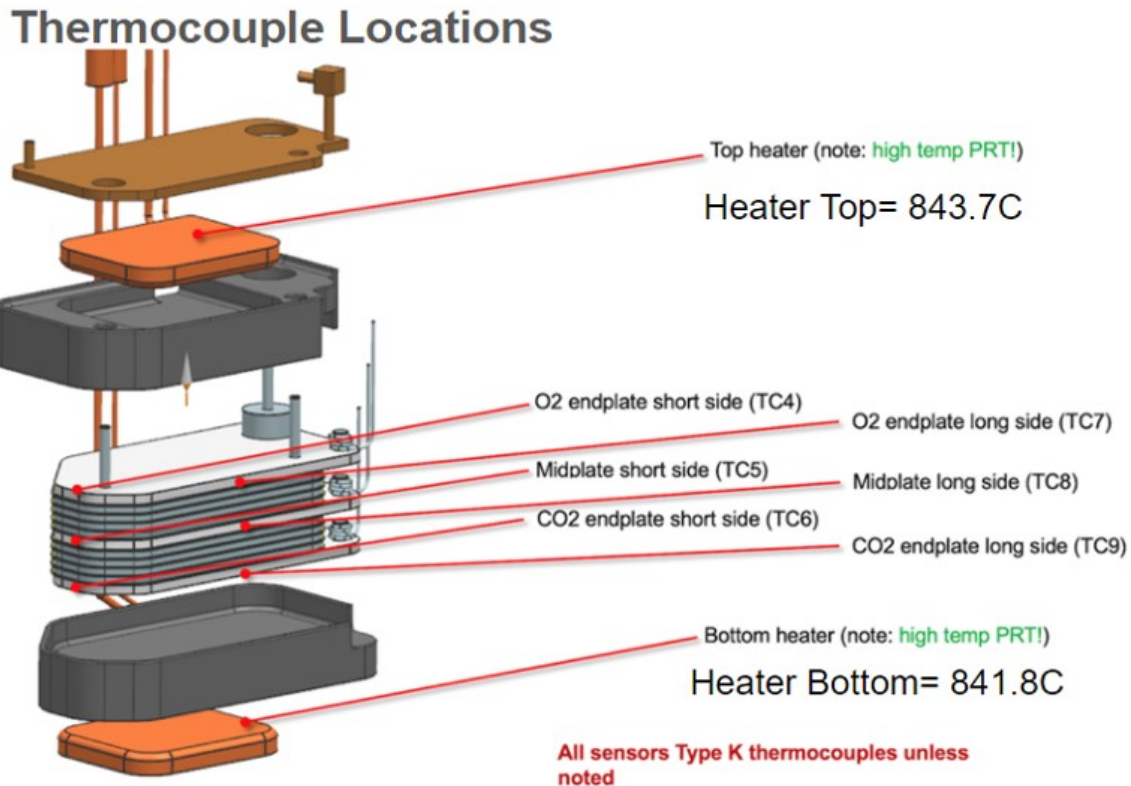


Figure 1-7: SOXE Thermocouple Sensor Locations [17]

As seen in Figure 1-7 the 6 thermocouples (TC) are labelled from top to bottom, beginning on the short side and numerically continuing on the long side.

1.1.4 Monitor and Control Subsystem

The monitoring and control system (MCS) characterizes the states of the inlet gas, pump health, state of the electrochemical process, and the outlet gas composition. Figure ?? indicates the system sensors and locations. Pressure and temperature measurements are taken at the exit of the inlet filter to characterize the gas stream entering the scroll pump [16]. The SOXE inlet gas flow rate is characterized by an orifice plate calibrated for a pressure drop, flow rate, relationship. The controlled processes include

1. The scroll pump speed
2. SOXE inlet gas heater temperature

3. SOXE temperature
4. SOXE voltage
5. Outlet gas analysis system temperature

This thesis focuses on the the thermal system and includes modelling of the SOXE temperature control. The thermal control objective is to achieve an internal SOXE stack operational temperature of 800 degC while electrolysis is occurring. There are not direct measurements available due to physical constraints since adding temperature sensors internally would obstruct the flow path. The inability to take direct measurements introduces the crux of this thesis.

The thermal control is regulated using the top and bottom heaters as the primary thermal controllers without direct internal thermal measurements. The overall system can provide oxygen production performance and efficiency, but there are unknowns with the performance for each individual layer. The thermal model created in this thesis can address this knowledge gap. The true internal temperatures of each layer within the SOXE stack can influence oxygen production efficiency and performance on per-layer breakdown. This level of detail is available from the high fidelity temperature analytical model that has been developed and is explained in this thesis.

Chapter 2

Thermal Modelling System

This section contains the thermal system and corresponding modelling that is included in the high fidelity COMSOL model. The full thermal cycle of MOXIE can be broken down into the following steps:

1. Heater Warm-Up Transient
2. Heater Steady-State
3. Compressor "ON" Transient, Flow Initiated
4. Compressor "ON" Steady-State (Electrolysis)
5. Compressor "OFF" Heater Cool-down Transient

This research includes the details to build a model and validate stages 1 and 2 of the thermal cycle. Since this model will be used as the foundation for further thermal modelling of stages 3-5, COMSOL was used as the modelling software due to its ability to build a multiphysics model. The model was built using a bifurcated process to ensure that mode is high fidelity, validated by using ground-tested empirical data. The first part was creating and validating a steady-state thermal model for the heater warm-up followed by the creation of the transient warm-up routine to match the empirical data.

2.1 Thermal Modelling

The thermal configuration is pictured in Figure 2-1 contains the overall thermal connections and boundaries. The two SOXE heaters (top heater and bottom heater) are the heat sources that use the control system to regulate the internal SOXE stack temperature of an optimal temperature of 800 degC +/- 10 degC. The stack is insulated by the surrounding aerogel on the sides and the compressed min-K above the top heater and below the bottom heater.

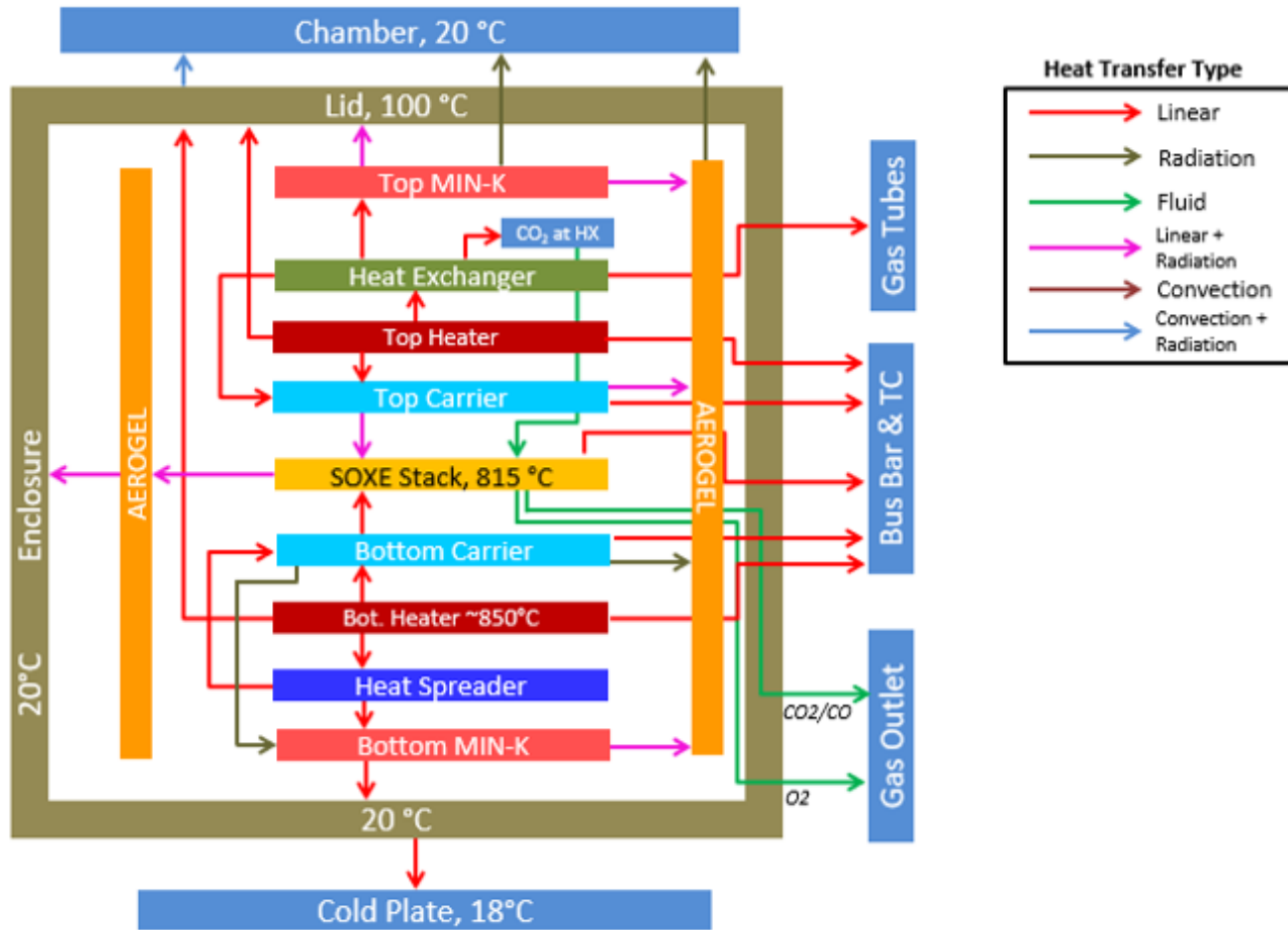


Figure 2-1: MOXIE System Component Breakdown [17]

Figure 2-1 shows the flow of the Martian atmosphere, which is 96% Carbon Dioxide, as it travels through the compressor and into the SOXE assembly. As the SOXE stack produces oxygen, carbon dioxide byproduct and oxygen are measured as they flow out of the SOXE stack. The two primary heat sources are the top heater and the bottom heater in the diagram. In order for the system to create oxygen, the electrolysis process must be initiated by carbon dioxide rich atmosphere flowing through the stack while the SOXE stack is at the appropriate activation temperature of 800 degC. The aforementioned step is thermal cycle step 4: Compressor "ON" Steady-State (Electrolysis). Prior to electrolysis, the system must heat up (Heater Warm-Up Transient) and remain at a constant temperature (Heater Steady-State).

The SOXE stack temperature in Figure 2-1 is 815 degC since that is the target steady-state temperature that the SOXE stack should be prior to the initiation of flow, and therefore electrolysis. The initial target temperature prior to electrolysis being approximately 15 degC warmer than the target SOXE stack temperature during operation (800 degC). The reason for this difference between the target start-up

and target operational temperature is because electrolysis is an endothermic reaction. Therefore, in order to produce the appropriate operational temperature, the internal temperature must be slightly higher prior to the flow of gas and electrolysis to account for the initial temperature reduction.

2.2 MOXIE Thermal Model

The main purpose of the research captured in this thesis is the build of a model with high fidelity to better understand the thermal system of the SOXE subsystem.

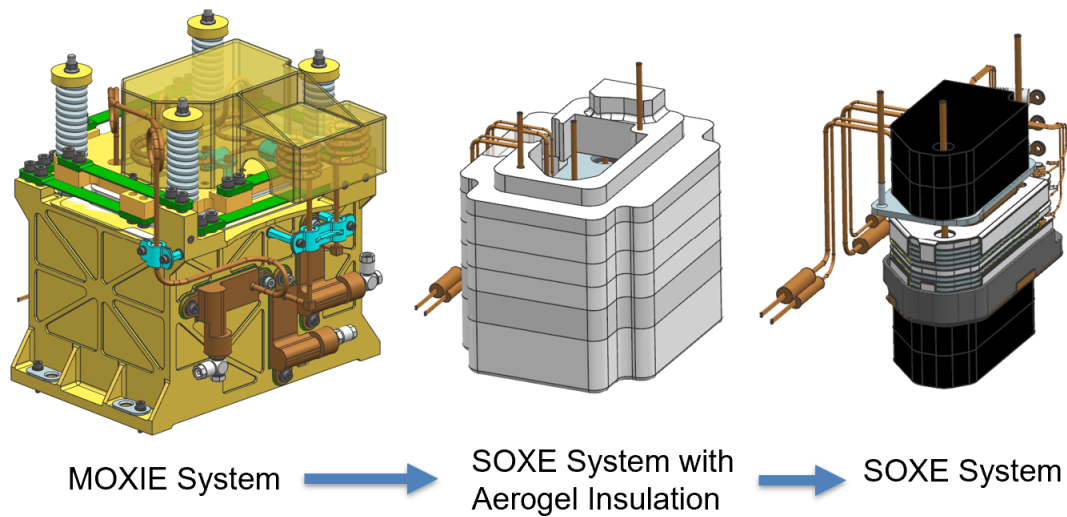


Figure 2-2: MOXIE System Component Breakdown[15]

The full 3D MOXIE system is depicted in Figure 2-2, where "MOXIE System" is the full flight hardware, "SOXE Systems with Aerogel Insulation" is the SOXE system, and "SOXE System" is the SOXE system without the insulation (Aerogel).

As seen in Figure 2-2, the total MOXIE system contains external configurations and containment. The external configurations that are visible in the "MOXIE System" is open to the Rover Avionics Mounting Panel (RAMP) temperature of the Perseverance Rover. For the purposes of this study, all additional configurations outside of the "SOXE System with Aerogel" are not modelled. Substantiation of this decision is detailed in the Model Set-up Chapter.

2.2.1 SOXE

This thesis primarily contains the details of the thermal system of the Solid Oxide Electrolysis Subsystem with the use of the control system for the thermal warm-up routine of the SOXE system prior to the airflow through the system via use of the CAC. The focal thermal system of interest is the Solid Oxide Electrolysis Stack

(SOXE Stack). This is because of the sensitive thermal equilibrium of the SOXE stack required to efficiently and effectively produce oxygen through the electrolysis process.

In order to accurately model the thermal response during the warm-up transient thermal cycle, the PI controller simulation was added to the thermal model for the top and bottom heater using the same control gain as the flight model. Additional details on how the PI controller was modelled are found in Chapter 5.

The flow of oxygen and carbon dioxide are in Figure 2-3 which also shows the top half of the SOXE assembly stack.

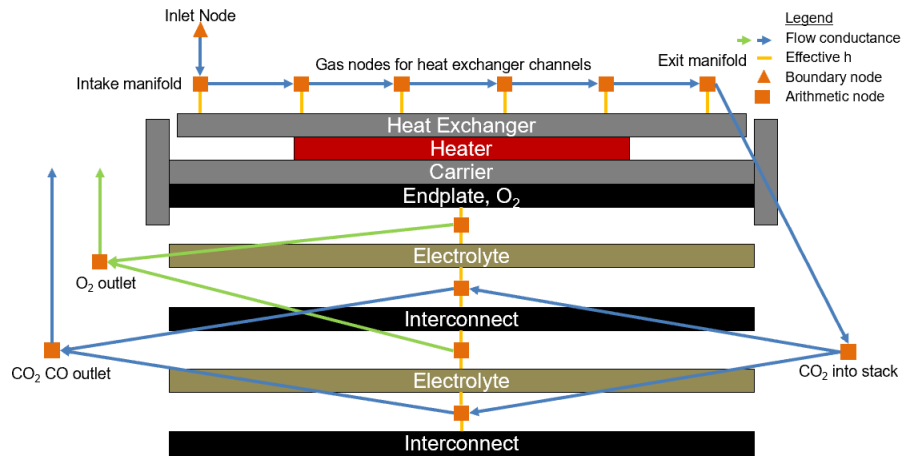


Figure 2-3: Interaction Diagram, Top Three Layers of SOXE Assembly Stack [9]

Figure 2-3 is a cross-section of the top three layers of the SOXE assembly stack. The gold and black alternating interconnects and electrolytes make up the SOXE Stack where in oxygen production, the carbon dioxide flows through each layer of the stack at excitation temperature, causing electrolysis to occur.

At the top of the diagram is the interaction between the heater, preheater (labeled heater exchanger), and heater carrier (labeled top carrier). Conduction is the main thermal interaction between each of these layers, however there is convective gaseous flow internal to the preheater. This is where the carbon dioxide-rich Martian atmosphere enters through the inlet manifold and enters into the preheater prior to flowing through the SOXE stack layers that consist of repeating interconnects and electrolytes. Note that there are connection nodes between each layer of interconnect-electrolyte and the gaseous flow between each layer. Therefore conduction and convection are modelled between each layer. Additionally, while at high temperatures, radiation is not negligible and is added as an interaction between each parallel layer.

Chapter 3

Material Properties

Accurate material characteristics has one of the largest impacts on ensuring the thermal model is high fidelity and matches the empirical values recorded during ground testing of the flight model. This section goes into details of the input material properties used in the COMSOL model. Figure 3-1 provides the overview of the material breakdown of SOXE stack with alternating interconnect and electrolyte layers and Table 3.1 provides a wholistic view of the materials used in the full SOXE subsystem that are modelled.

Table 3.1: Component Material List

COMPONENT	MATERIAL
SOXE heaters (x2)	Inconel 600
SOXE Inlet gas preheater	Inconel 600
SOXE Exhaust Heat Exchangers (x3)	Inconel 600
Sensors Inlet Heat Exchangers (x2)	Aluminum 6061-T651
SOXE Heater Carriers (x2)	Copper Alloy (UNS C15715)
SOXE Interconnects and End Plates (x11)	CFY
SOXE Electrolyte (x10)	Scandium-Stabilized Zirconia (ScSZ)

The list of materials that are modelled in COMSOL are listed below:

1. Inconel 600
2. Refrasil UC 100-48
3. Compressed MinK
4. Copper Alloy UNS C15715
5. Scandium-Stabilized Zirconia (ScSZ)
6. Chromium-Iron-Yttrium (CFY) Alloy

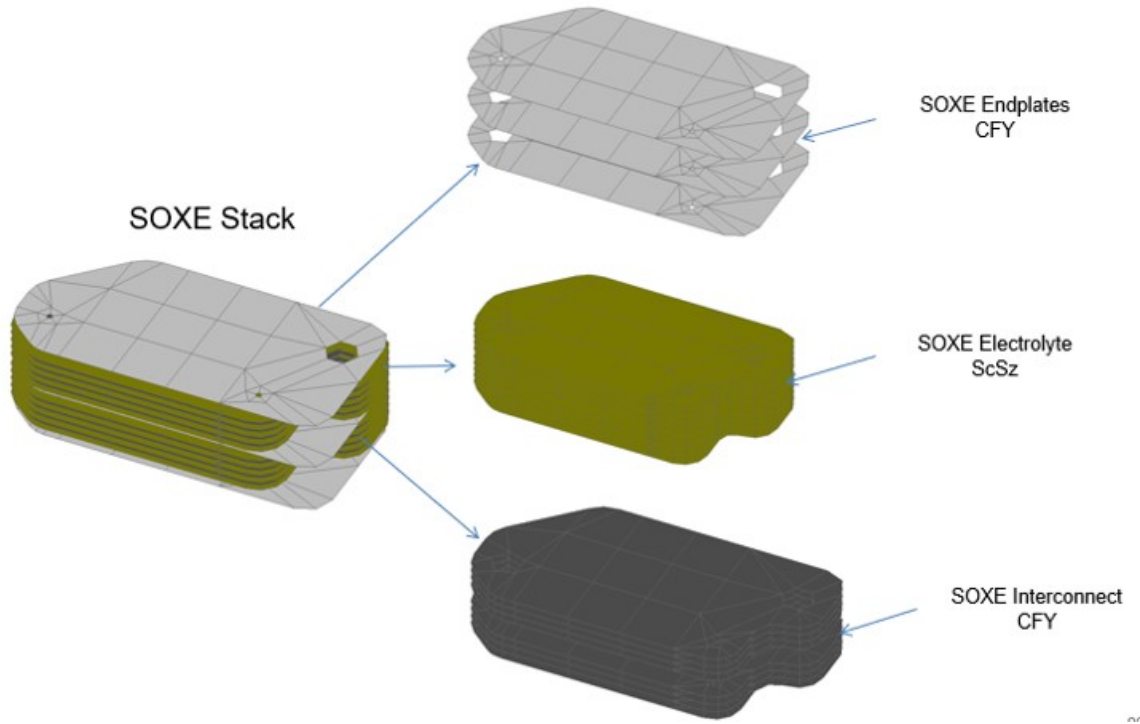


Figure 3-1: Material Map of SOXE Components [15]

7. Aerogel

8. Carbon Dioxide

The high fidelity is maintained for the transient warm-up period by introducing the thermal properties of thermal conductivity (k), heat capacity (c_p), and thermal diffusivity (D) as functions of temperature. The heat capacity is a measure to describe the amount of heat energy at a constant pressure to precipitate a temperature change for a unit mass. The thermal diffusivity is a measure of thermal inertia. Thermal diffusivity is defined as:

$$D = k/(\rho C_p) \quad (3.1)$$

Thermal diffusivity is used where either the heat capacity constant or thermal conductivity constant is undefined or poorly defined. For sensitive thermal transient modelling, it is important to include thermal diffusivity if the density of the material with temperature is unknown or has non-negligible variation.

The temperature dependent functions are input as discrete functions where the points are linearly interpolated, unless otherwise stated. Details of each material are listed in the following sections. It should be noted that all materials are modelled as solids with the exception of carbon dioxide, which is modelled as a gaseous fluid and is added to be representative of the Martian atmosphere.

3.1 Inconel 600

The material Inconel 600 is nickel-based composite metal that is tolerant of high temperatures. This material is used on the components highlighted in blue in Figure 3-2 which include the preheater and Tayco high temperature heaters.

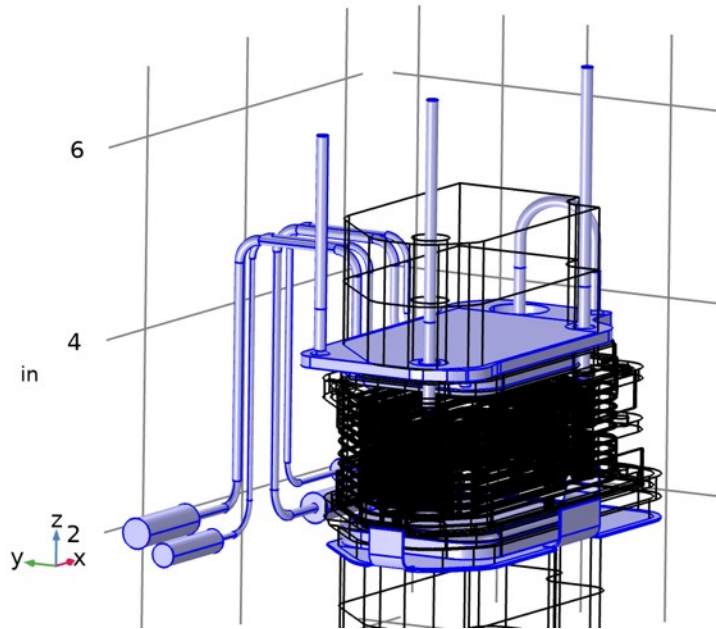


Figure 3-2: Material Location of Inconel 600

This material is used on the Tayco heaters to warm-up the internal stack to an overshoot temperature and maintain temperatures of 800 degC during oxygen production. [15] This is achieved by setting the heater temperatures to 843.7 degC and 841.8 degC for the top and bottom heaters, respectively. More details regarding the thermal controls are found in Model Set-Up. Figure 3-3 demonstrates the heat capacity as a function of temperature and Figure 3.1 shows thermal conductivity as a function of temperature.

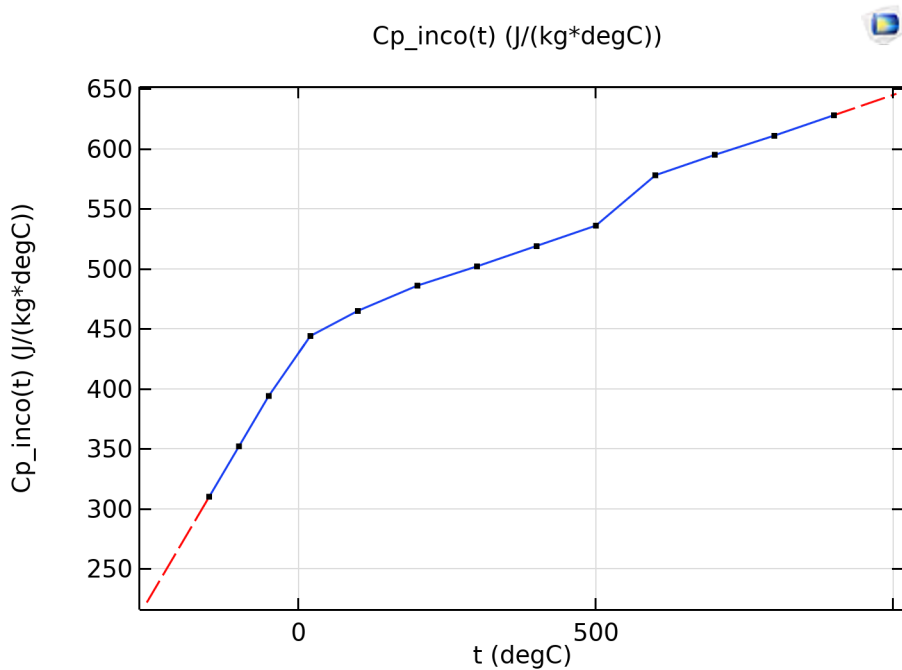


Figure 3-3: COMSOL Input Inconel 600 Heat Capacity as Function of Temperature [3]

The input heat capacity coefficient of Inconel 600 is in 3-3 which is a function of temperature to maintain high fidelity. The curve is an empirically based on material curves, where temperatures outside of the provided empirical data is extrapolated using a best fit line curve. There is a level of uncertainty introduced by extrapolating the data because the empirically derived heat capacity coefficient provided is known only between -50 degC and 800 degC. However, this uncertainty is deemed to be nominal since the time the system spends at temperatures over the 800 degC is limited and the system does not see a temperature below 20 degC.

Similarly, the conductivity coefficient as a function of temperature is also extrapolated for temperature values outside of -50 degC and 800 degC range. As noted by the the dashed red lines on 3-3, linear extrapolation of the curve is used. For values above 800 degC, it is assumed to have a constant conductivity coefficient because the change in coefficient tapers off with higher temperatures.

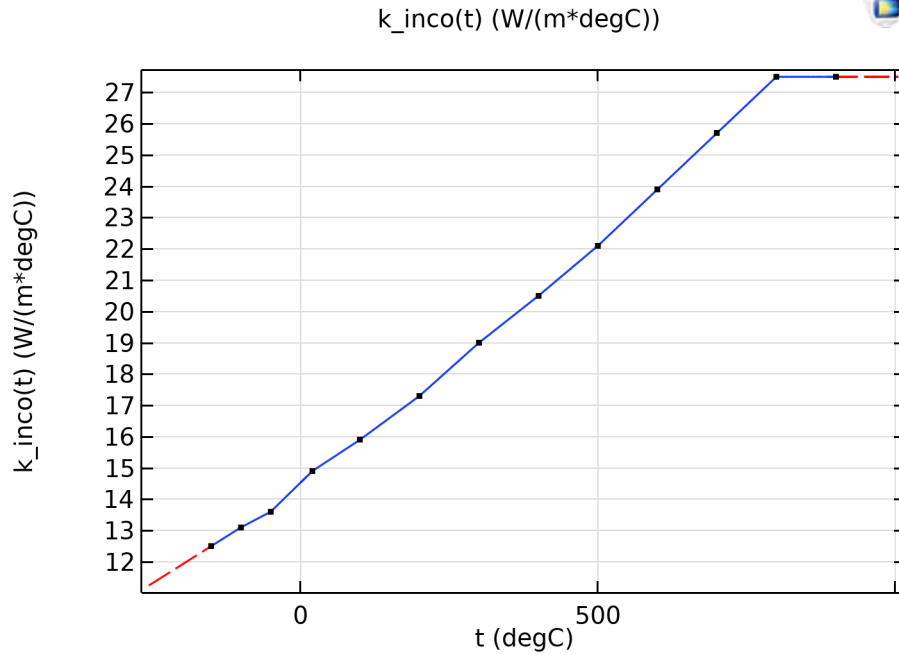


Figure 3-4: COMSOL Input Inconel 600 Conductivity as Function of Temperature[3]

It should be noted that the top heater is also used for inlet gas preheating as the flow of carbon dioxide travels throughout the preheater labyrinth. The inlet gas preheater component, also made of Inconel 600, is used to preheat the pressurized carbon-dioxide-dominant Martian atmosphere before delivery to the SOXE stack. The optimal temperature for the electrolysis reaction is 800 degC +/- 10 degC. The preheater is vital to decrease the temperature gradient across the SOXE stack in order to create a more consistent oxygen production. However, the preheater also serve the functional purpose of holding the stack secure and transporting the carbon dioxide and oxygen into and out of the stack.

3.2 Refrasil UC 100-48

Refrasil UC 100-48 is a cloth-like material that is located in between the heater carriers and the SOXE stack. Initially the Refrasil cloth was added to disperse the stresses that were introduced due to the spring loaded enclosure. However, it was found that the Refrasil cloth also had the added benefit of providing additional insulation to the SOXE stack. The location of the Refrasil cloth is highlighted in blue in 3-5

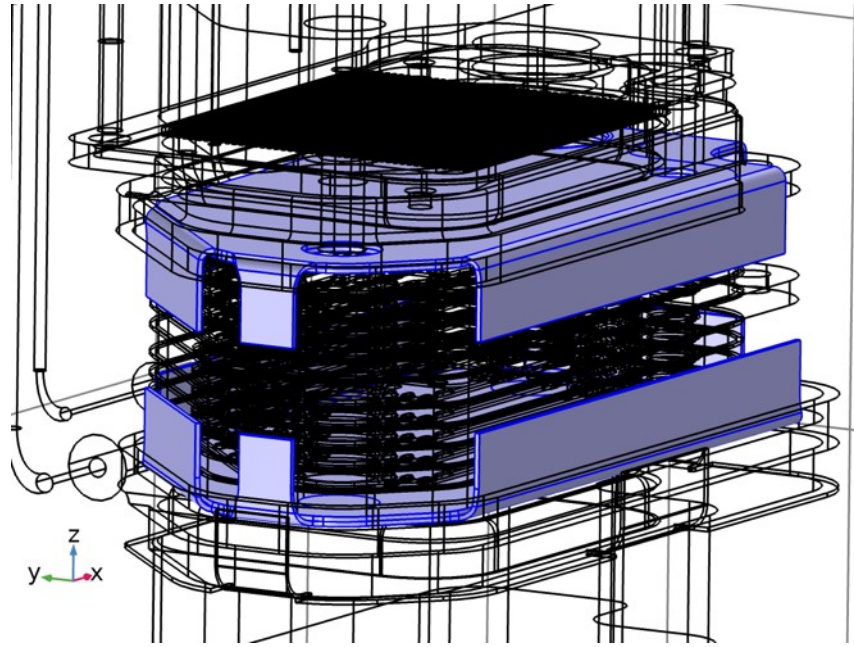


Figure 3-5: Material Location of Refrasil Cloth

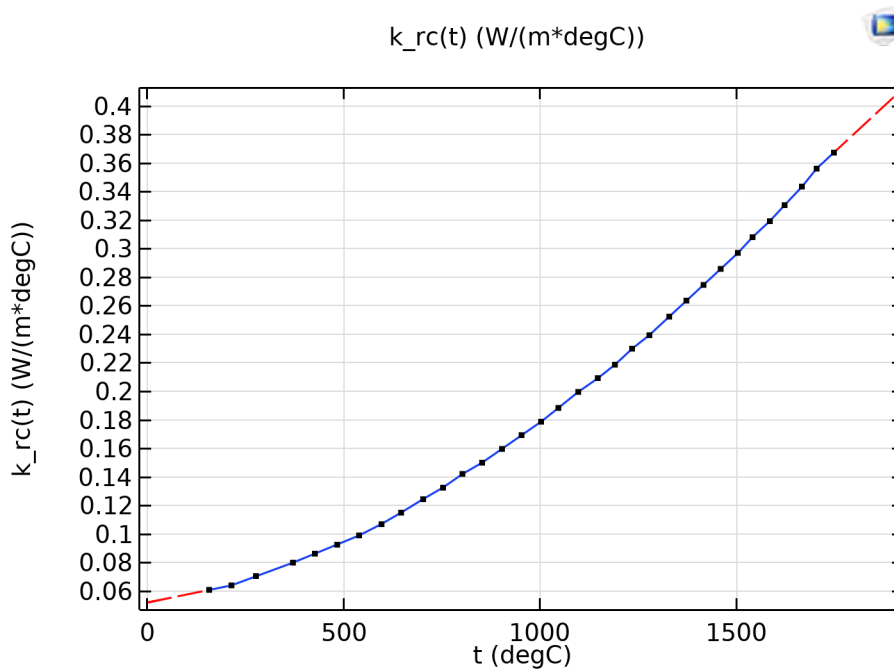


Figure 3-6: COMSOL Input Refrasil Cloth Conductivity as Function of Temperature

The material is only model to have conductive interaction between components for this model. This assumption is made due to the low thickness of the material and because there is no airflow that would come into contact with the material for convection to be a significant factor.

3.3 Compressed MinK

Compressed Min-K is added primarily to help dampen the compressing spring load while maintaining high thermal insulation properties.

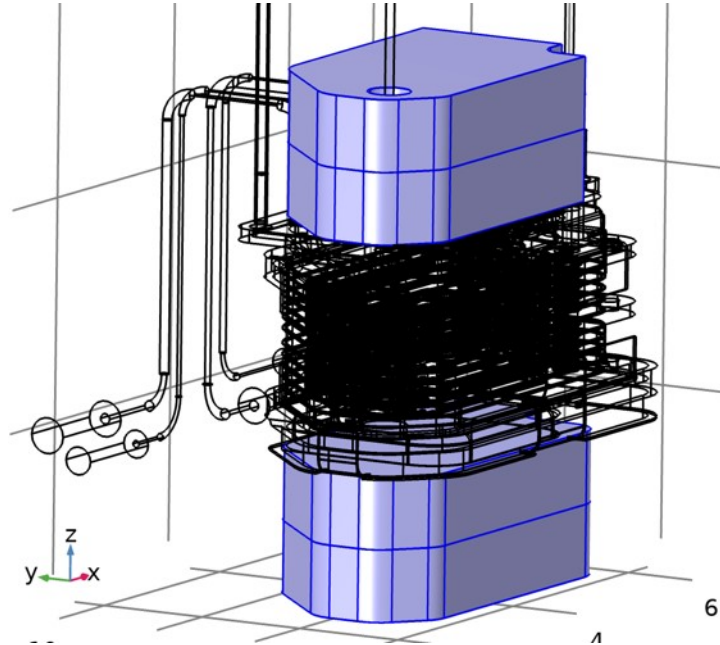


Figure 3-7: Material Location of Compressed Mink-K

Highlighted in blue, reference 3-7, the compressed Min-K is approximately the same thickness as the insulator Aerogel that surrounds the rest of the SOXE stack. However, the main geometric difference between Aerogel and Compressed Min-K is that Min-K does not have consistent thickness, unlike the Aerogel. This is due to the complex geometry of the preheater and inlet tub geometry. Therefore, the 3D volume of the Compressed Min-K remains a part of the high fidelity thermal model, unlike the Aerogel, which is reduced to a 2D boundary condition due to its consistent thickness.

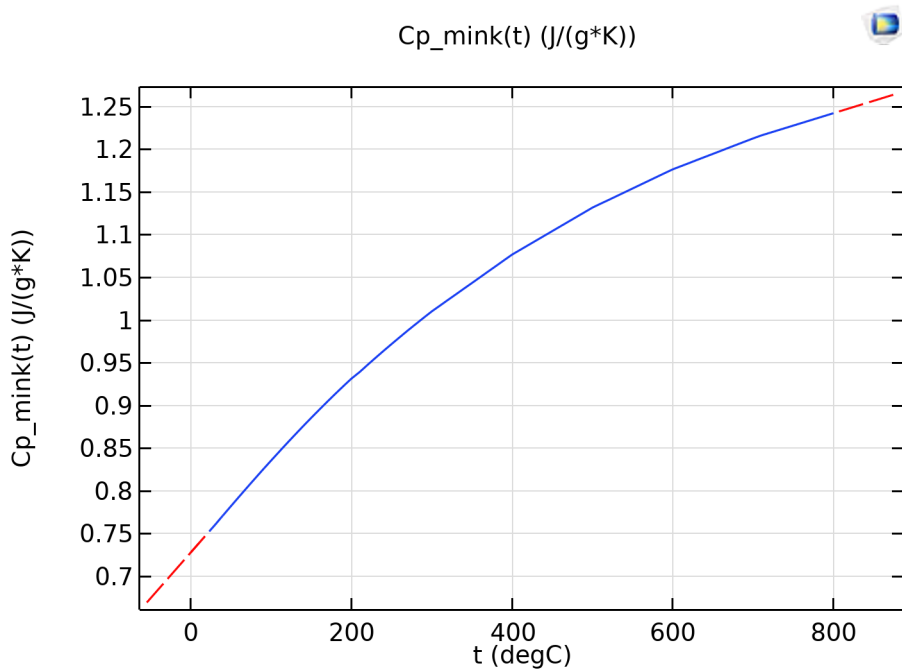


Figure 3-8: COMSOL Input Min-K Heat Capacity as Function of Temperature [3]

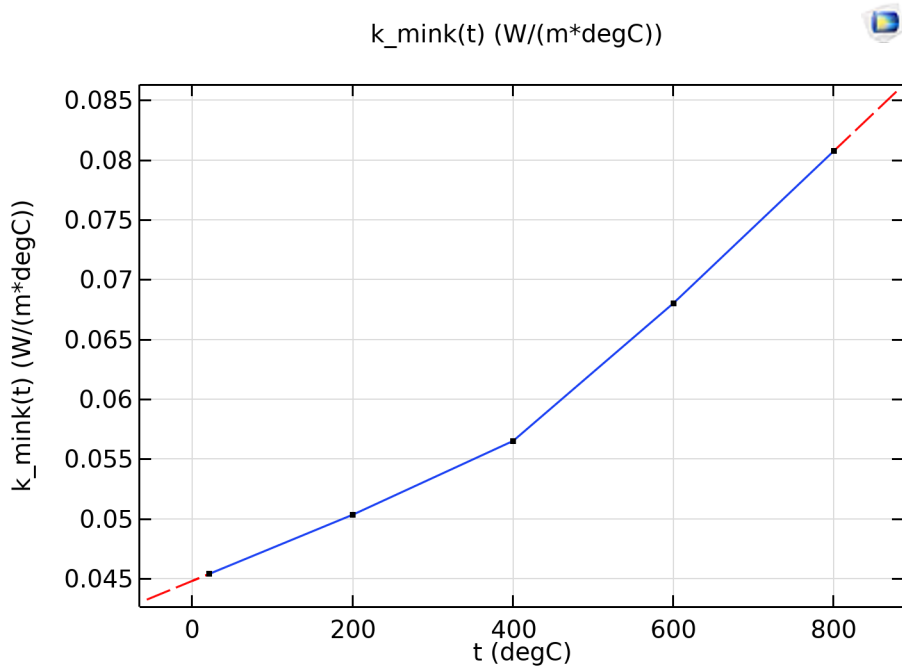


Figure 3-9: COMSOL Input Min-K Conductivity as Function of Temperature [3]

The heat capacity and conductivity coefficients are temperature dependent, again based on empirical data with values only available through the temperature range

from 20 degC to 800 degC. Both coefficients are extrapolated for values outside of this range with linear extrapolation using a slope of the nearest empirical best fit curve.

3.4 Copper Alloy UNS C15715

The heater carriers are made of the copper alloy UNS C15715. The purpose of the heater carrier is to retain heaters and allow the transfer of heat from the heaters into the SOXE stack.

PROPERTY	VALUE	UNIT
Thermal Conductivity (k)	320	W/(m·K)
Density (ρ)	8900	kg/m ³
Heat Capacity (C_p)	425	J/(kg·K)

Table 3.2: COMSOL Input UNS C15715 Material Properties [4]

There is a high temperature distribution within the heater carrier, making this component a high thermo-elastic stress region, specifically where there are notches in the geometry.

3.5 Scandium-Stabilized Zirconia

Scandium-stabilized zirconia is the electrolyte selected inside of the SOXE stack. The electrolyte stack layers alternate with the CFY Chromium alloy interconnects to modularize the electrolysis reaction. The layers of the scandium zirconia is highlighted in blue in Figure 3-10.

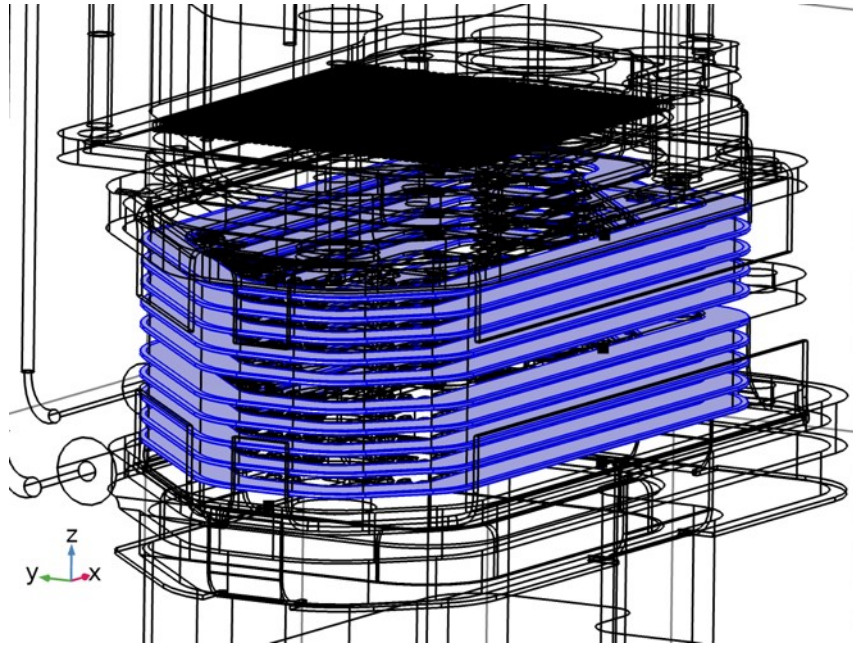


Figure 3-10: Material Location of Scandium Zirconia

The heat capacity and conductivity coefficients of the electrolyte material are both temperature based to maintain the model high fidelity. As seen, there is only material data available between 20 degC and 800 degC for the heat capacity coefficient, where the value is linearly extrapolated based on the closest near curve to the extrapolation point.

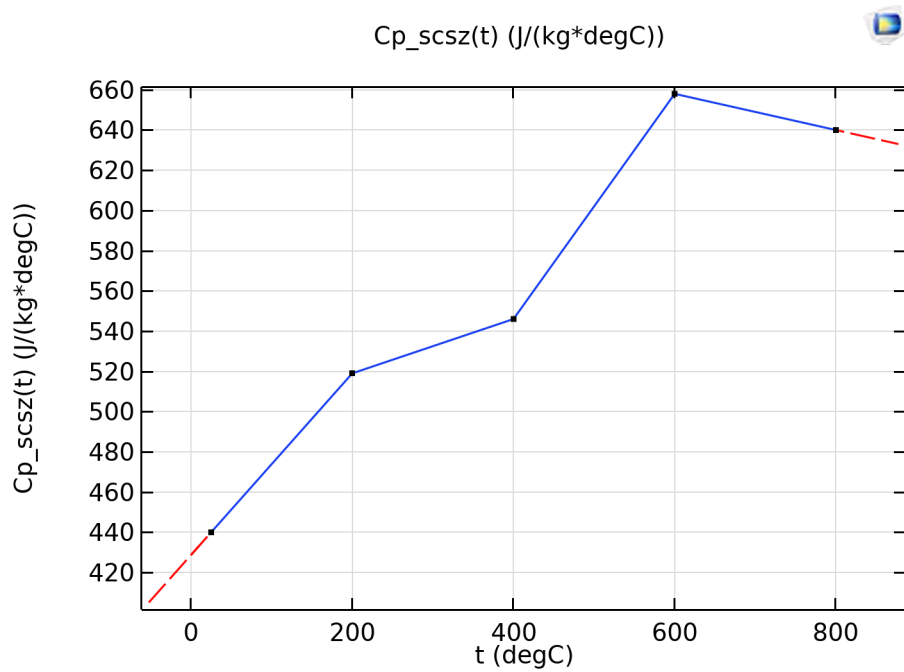


Figure 3-11: COMSOL Input Scandium Zirconia Heat Capacity as Function of Temperature [3]

The extrapolation is represented by the red dashed line. This introduces some uncertainty since there is limited heat capacity coefficient data with this material. The coefficient curve is made up of discrete heat capacity coefficient values and the model linearly interpolates the coefficient values for temperatures in between the discrete points.

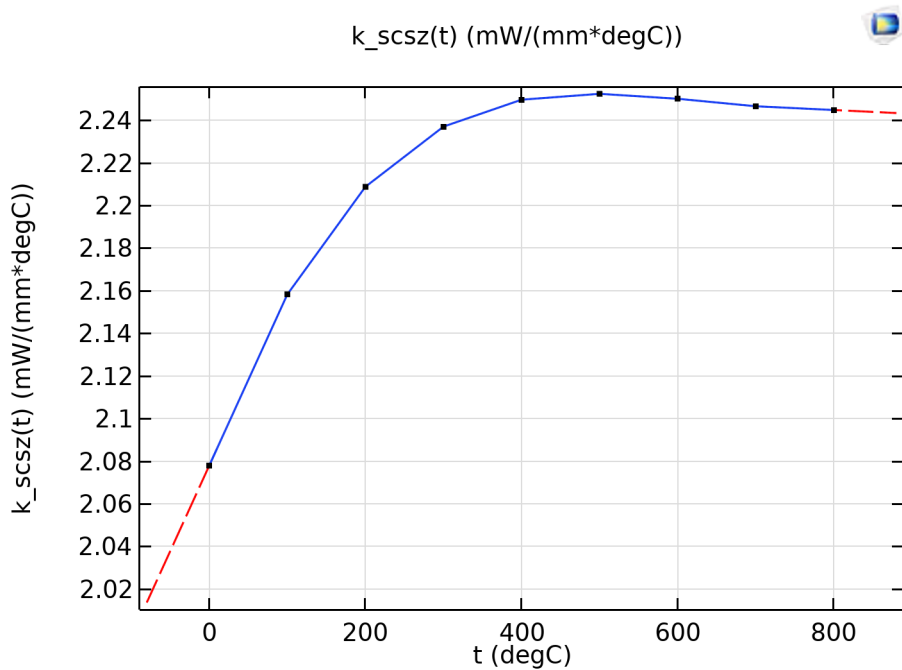


Figure 3-12: COMSOL Input Scandium-Stablized Zirconia Conductivity as Function of Temperature [3]

Figure 3-12 is the conductivity coefficient as a function of temperature. From visual inspection, the curve is more continuous than the heat capacity coefficient. This suggests that there is less uncertainty introduced by the linear interpolation and extrapolation used for values outside of the temperature range.

3.6 CFY Cr Alloy

Chromium-iron-yttrium (CFY) alloy is the material used for the SOXE stack end plates (3) and interconnects (8). Both the interconnects and end plates serve as the same function, creating the boundary in between the electrolyte layers for electrolysis to occur. However, the difference between the end plates and the interconnects are the geometry and secondary functions.

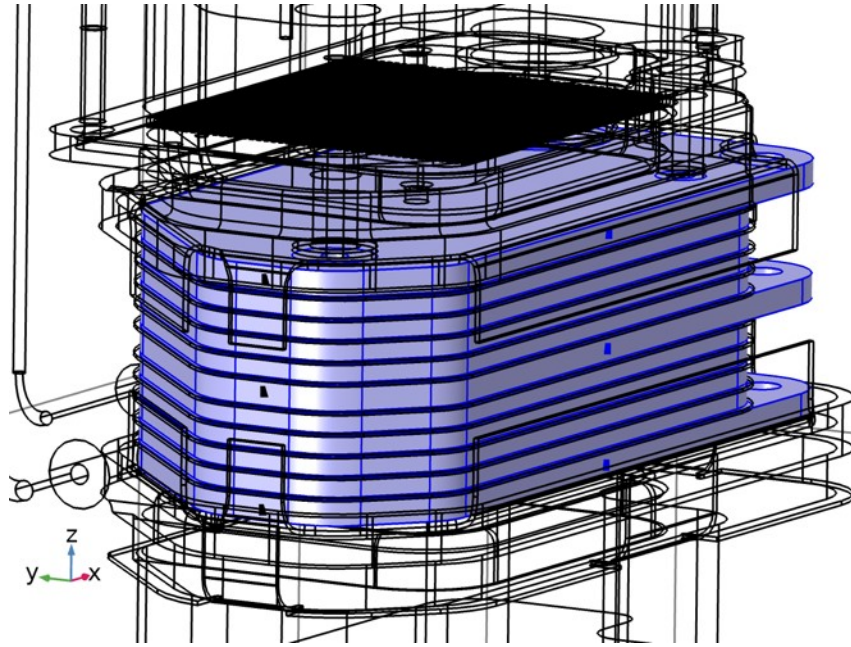


Figure 3-13: Material Location of CFY Interconnects

The end plates and the interconnects are highlighted in blue in Figure 3-13. The end plates, consisting of top, middle, and bottom end plates are thicker in geometry and have additional protruding material tabs to provide surface area for the electric wiring to coil about, securing the electric current through the stack.

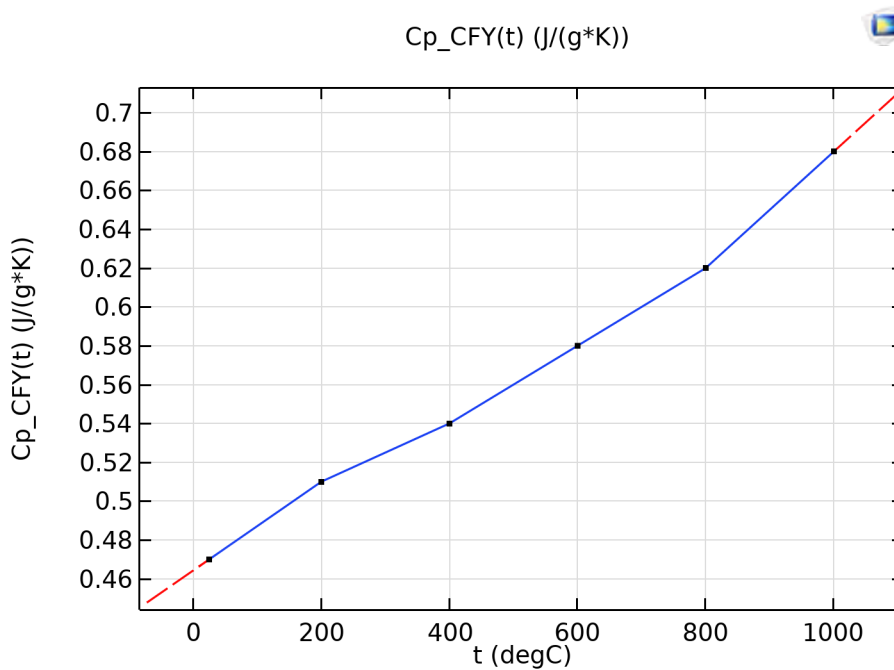


Figure 3-14: COMSOL Input CFY Heat Capacity as Function of Temperature [3]

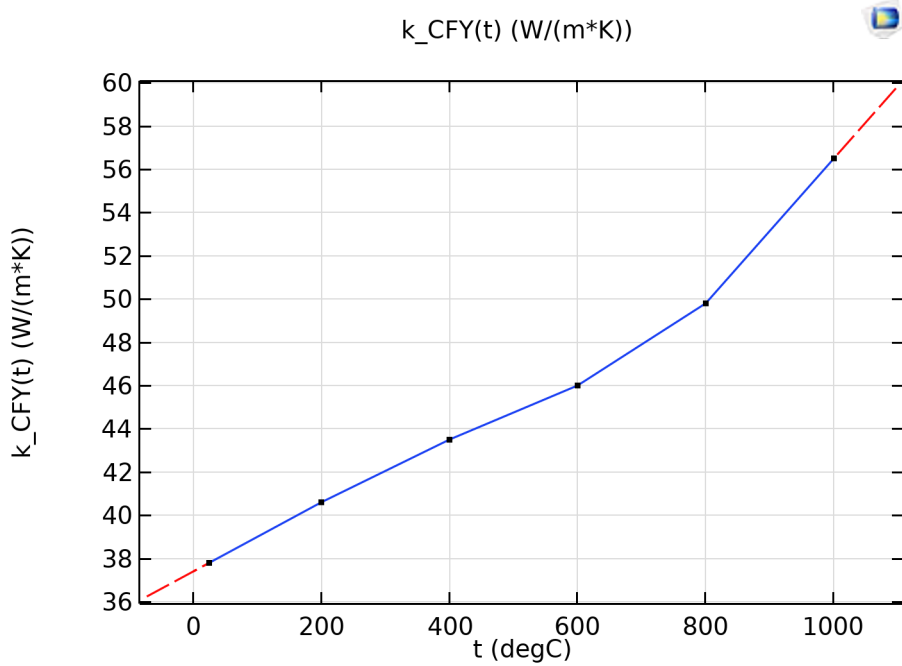


Figure 3-15: COMSOL Input CFY Conductivity as Function of Temperature [3]

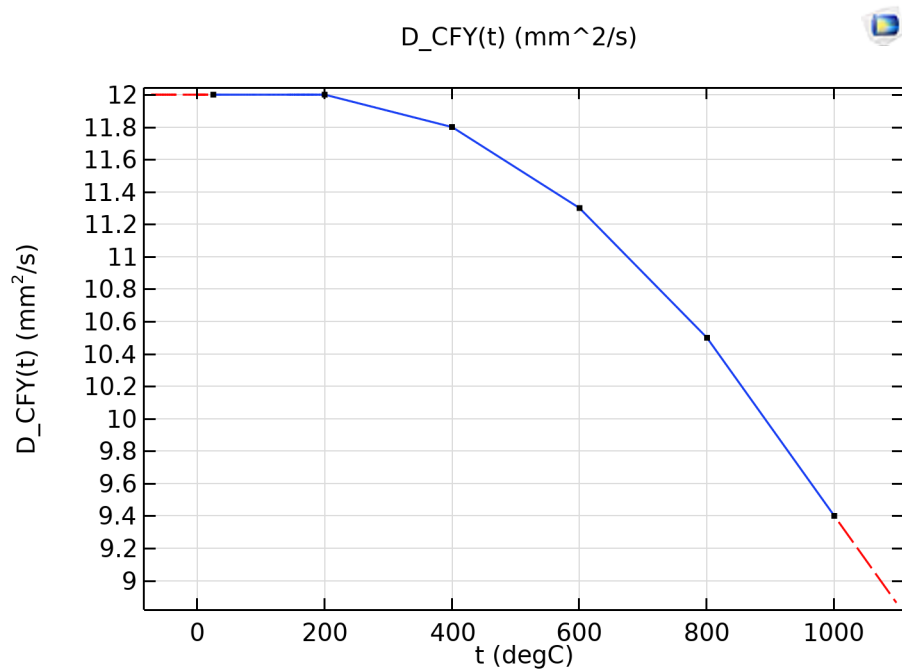


Figure 3-16: COMSOL Input CFY Thermal Diffusivity as Function of Temperature [3]

Thermal diffusivity is used for the transient thermal model for the interconnects. This is because density for all solid materials in this model were input as constants and were assumed to not vary density with temperature. The SOXE stack is the focal of the thermal model, of which a majority the volume consists of the interconnects. In order to provide a high fidelity transient model, thermal diffusivity is explicitly added as a function of temperature for the interconnect materials to account for any thermal-dependent density variation. The material property curves use linear extrapolation for temperatures outside the available coefficient temperature range and linear interpolation for temperature values between discrete points.

3.7 Aerogel

Aerogel is the insulation used to maintain high temperatures within the system required for MOXIE operation and to protect the remainder of rover from damage that could instill from the MOXIE operational temperatures . The 3d substance of aerogel was not modelled in COMSOL for computation time improvements, however the properties are included to create boundary conditions. Figure 3-17 shows the temperature-dependent conductivity coefficient of aerogel.

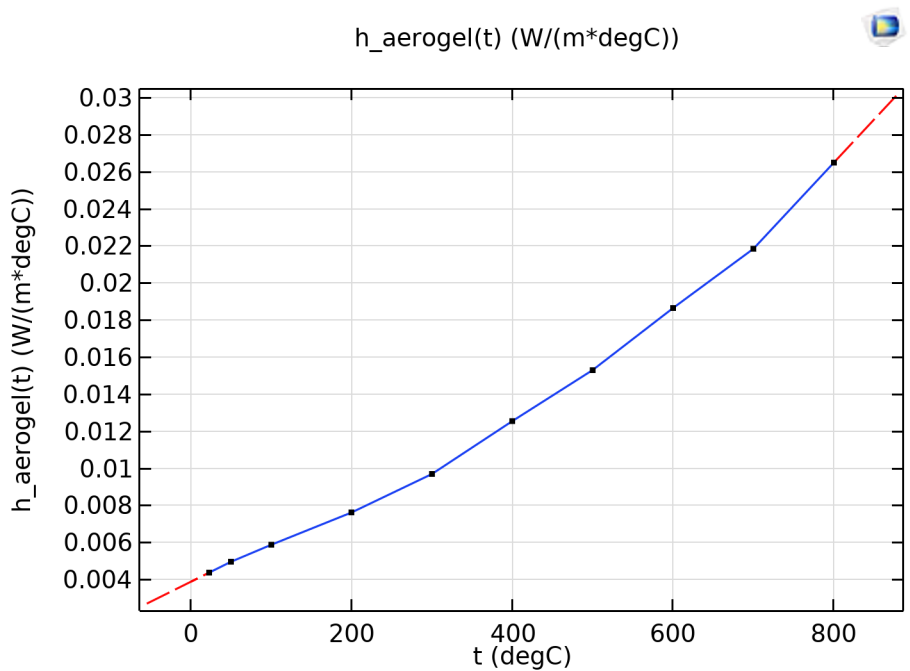


Figure 3-17: COMSOL Input Aerogel Conductivity Coefficient as Function of Temperature

The value is calculated using linear interpolation based on the temperature of the aerogel. Linear extrapolation is used for temperature values outside of the available

material data. This assumption has negligible impact on the model since the temperature of aerogel throughout the operation of MOXIE never exceeds the upper bound of 800 degC nor is less than the 10 degC lower bound.

3.8 Carbon Dioxide

The final material included in the model is the gaseous flow of carbon dioxide, which represents the Martian atmosphere. As previously mentioned, it is assumed that all flow through the gaseous chambers is represented by carbon dioxide. There is low density of the Martian atmosphere, therefore there are low convection effects and subsequent thermal impacts prior to the MOXIE cycle step where the compressor is activated. After the compressor is turned on, the carbon dioxide rich atmosphere is pressurized after it flows through the compressor.

Figure 3-18 shows the volume of carbon dioxide internal to the SOXE assembly. The three tube-shaped volumes are the inlet and exit flow manifolds of the carbon dioxide into and out of the system. The top flat layer shows the labyrinth that the flow is required to navigate in the preheater. From the preheater, the carbon dioxide volume fills the flow paths in between each layer of interconnect and electrolyte.

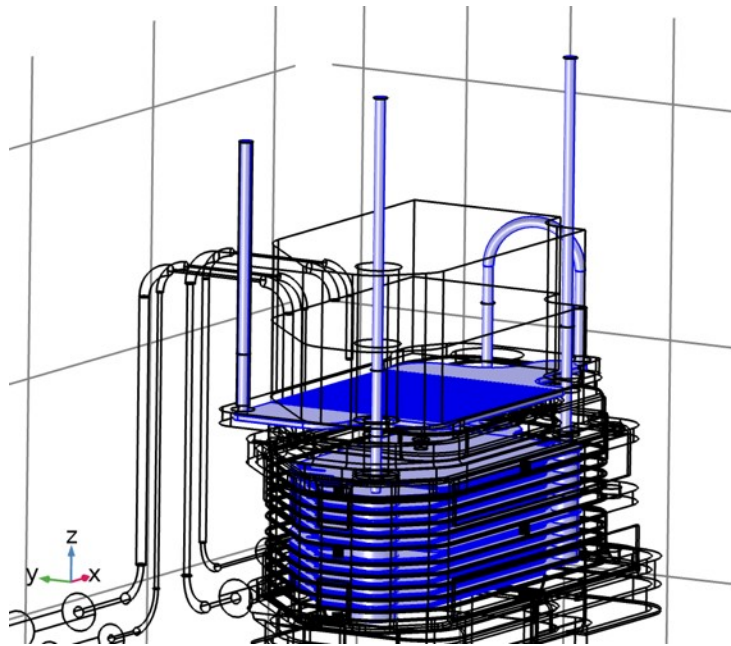


Figure 3-18: Location of Carbon Dioxide Internal to SOXE

For this thesis, it is acceptable to assume 100% carbon dioxide to represent the Martian atmosphere. Carbon Dioxide is represented by the following continuous functions for temperature values from 220 to 600 Kelvin.

$$C_p = 459.913258 + 1.86487996T^1 - 0.00212921519T^2 + 1.22488004E - 6T^3$$

$$k = -0.00132472616 + 4.13956923E - 5T^1 + 6.70889081E - 8T^2 - 2.11083153E - 11T^3$$

where the unit of Cp is [J/(Kg K)], unit of k is [W/(m*K)], and temperature is in Kelvin. The equations are standard equations from COMSOL to represent gaseous carbon dioxide. Properties at temperature values above 600 Kelvin are not extrapolated and assumed to be constant based on the COMSOL standard material properties for carbon dioxide. These standards infer the thermal conductivity for carbon dioxide temperatures over 600K is to be a constant of 0.0431[W/(m*K)] and heat capacity for the same condition to be a constant of 1076.9 [J/(kg*K)].

Chapter 4

Modelled Thermodynamics

This section provides a breakdown of the thermodynamic assumptions and governing physics that impact the high fidelity thermal model. The three thermodynamic responses are convection, conduction, and radiation. The primary thermal impact is from conduction, followed by radiation, and trace thermal impacts from convection.

4.1 Conduction

The governing equation for solving the heat transfer applies to both solids and fluids through interface connection is described as

$$\rho C_p (\delta T / \delta t) + \rho C_p \mathbf{u} \cdot \nabla T + \nabla \cdot \mathbf{q} = Q \quad (4.1)$$

where ρ is the density, Q is representative of additional heat sources, \mathbf{q} is the heat flux through conduction, \mathbf{u} is the unit velocity vector, and T is absolute temperature of the element that is being calculated [6]. The variable C_p is the heat capacity which is based on the material property at constant pressure and is a function of temperature. Also a function of temperature is k , thermal conductivity, which used with the temperature gradient to evaluate the conductive heat flux, \mathbf{q} .

$$\mathbf{q} = -k \nabla T \quad (4.2)$$

4.2 Radiation

At the high internal temperatures of system, there are two types of radiation that have an impact on the thermodynamic response:

1. Surface-to-Surface Radiation
2. Surface-to-Ambient Radiation

The surface-to-surface radiation occurs between each layer of the SOXE stack since the surfaces of the stack are parallel. There may be additional radiation occurring between each layer since the surfaces are not completely parallel due to the nodules on the interconnect surface. However, for simplification it is assumed that the surfaces are parallel and the direction of radiation is perpendicular to the surface. Figure 4-1 shows the general case with outgoing diffusive reflectivity ρ_d , refraction index n , and specular reflectivity ρ_s .

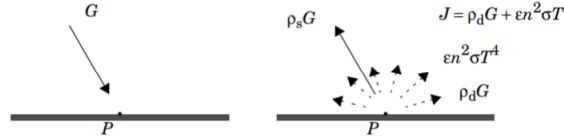


Figure 4-1: Incoming Irradiation (left), Outgoing Radiosity (right) [6]

The surface-to-surface radiation uses the Jacobian matrix of the discrete model partly filled instead of the more common sparse matrix. [6] The additional nonzero elements in the matrix correspond to the radiosity degrees of freedom and is computationally expensive but necessary for the high fidelity model. The general equation for the surface-to-surface radiation is:

$$\epsilon = 1 - (\rho_d + \rho_s) \quad (4.3)$$

$$q = \epsilon(G - n^2 \sigma T^4) \quad (4.4)$$

The inward radiative heat flux is represented by q , ϵ is emissivity, J is total radiosity. Total radiosity is the sum of diffusively reflected and emitted radiation. Absorptivity is not included in this form of the equation since the objects are assumed to be opaque. By assuming that the surfaces are parallel, the refraction index is set to 1.

The surface-to-ambient radiation equation is used to represent the heat loss from the system through radiation. This includes radiation from the external surfaces of the SOXE stack and heaters into the aerogel boundary.

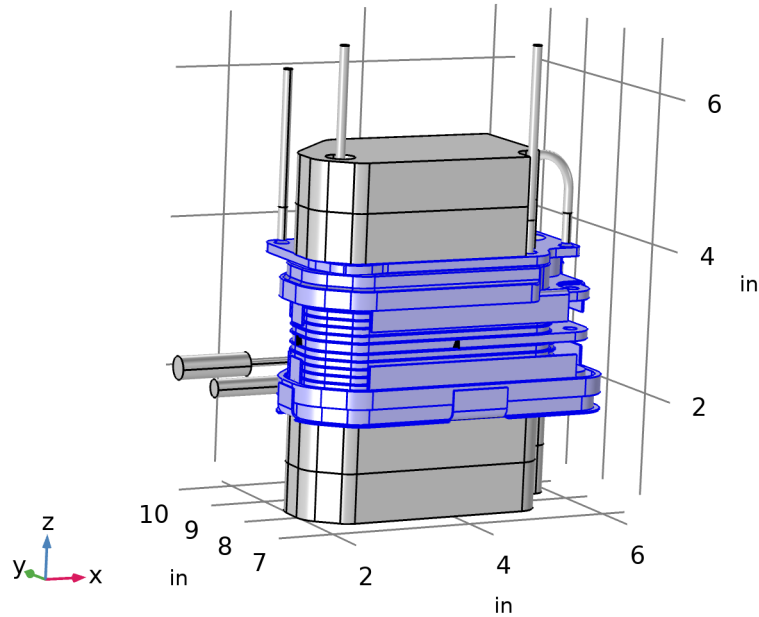


Figure 4-2: Boundaries Selected for Radiation-to-Ambient Condition (selected in blue)

Figure 4-2 shows the boundaries that are impacted by the surface-to-ambient radiation heat flux. These boundaries face the insulation aerogel which is not modeled in 3D for computation time improvement. More details on this boundary condition are found in Chapter 5.

4.3 Convection

Trace amounts of convection are modelled but not utilized in this thesis. This is because this thesis only contains the thermal steps prior to the compressor being turned on, which activates the pressurization and subsequent fluid flow of carbon dioxide through the system. Convection physics have been added and are model with the following equation

$$-n \cdot q = \rho \Delta H u \cdot n \quad (4.5)$$

$$\Delta H = \int_{T_{upstream}}^{T2} C_p dT + \int_{P_{upstream}}^{PA} 1/\rho(1 - \alpha_p T^2) dp \quad (4.6)$$

Equation 4.6 is the convection coefficient calculation using the temperature dependent heat capacity coefficient of the carbon dioxide (C_p) integrated over the temper-

ature of the nodal location to the upstream temperature ($T_{upstream}$). The upstream pressure ($P_{upstream}$) is set to 0.095 psi for the conditions modelled in this thesis. The inlet temperature is set to the ambient (RAMP) temperature.

The convection is based on the properties of the inlet tube into SOXE. This inlet is where the martian atmosphere flow (assumed carbon dioxide) from the compressor would continue to feed into SOXE. There is no flow through the system for the conditions modelled therefore the velocity in all coordinates are zero and convection is negated. This value can be added for the study of additional thermal studies and is expanded on in Chapter: Model Improvement Plan. Even though there is no flow through the SOXE stack, there is still heat transfer through the low pressure carbon dioxide via the modelled fluid conduction.

Chapter 5

Model Set-up

5.1 Previous and Existing Models

A preliminary SOXE system thermal model was created prior to this thesis. At the time the preliminary model was built, there were still unknowns on many features including the warm-up cycle model specifics, select material properties, and detailed geometries. The previous model made assumptions to significantly simplify the materials and geometry, which precipitated a computationally-efficient model that could provide overall approximate temperatures for initial design and preliminary studies. This user-friendly model was presented by Eric Hinterman, a previous graduate student at MIT, and is summarized in the figure below.

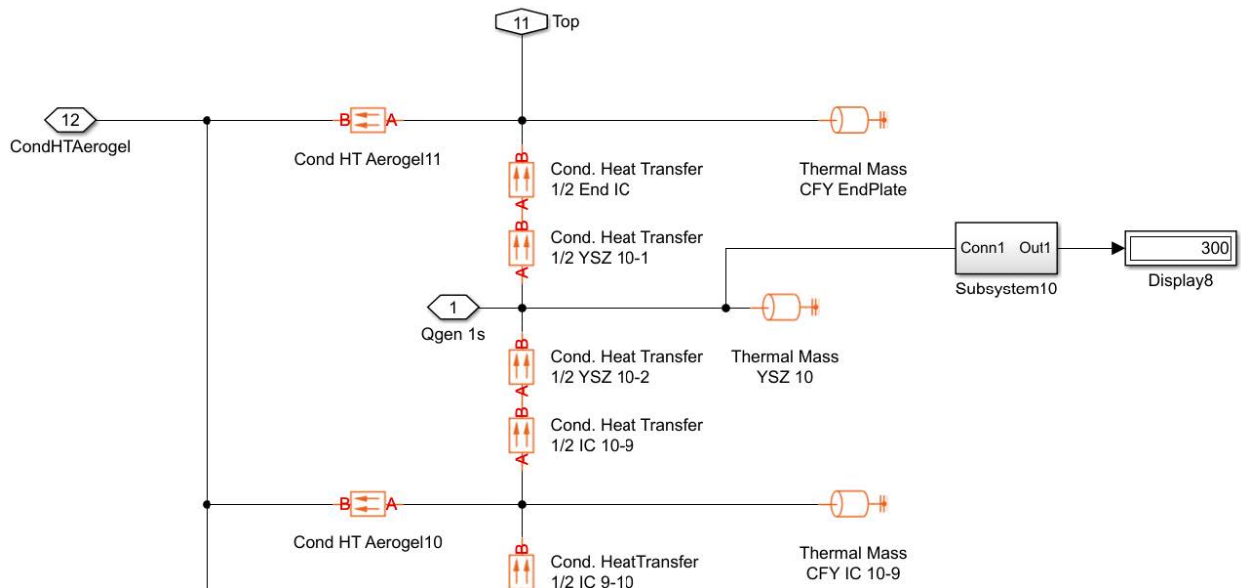


Figure 5-1: Previous MOXIE Thermal Model[11]

This model, though user-friendly and efficient, is a simplified thermal model of the system. It can be noted in the diagram that the 3D geometry and asymmetry of the

true SOXE stack are not considered and the stack layering is simplified. In addition, the material properties that are temperature dependent were simplified and one value at 400 deg C was used to represent the material as a method of simplification. [11] Due to these assumptions, Hinterman acknowledges the addition of "grey factors" to account for the variation caused in order to validate the model.

The previous model output overall temperature of the SOXE stack and does not include the ability to determine temperature planes on each layer of the SOXE stack. This level of high fidelity temperature analysis became a point of interest for the team due to the performance sensitivity of the temperature on each layer of the SOXE stack.

The research objectives that drove the current model were:

1. Build a geometrically accurate 3D model that is capable of thermal transients with each layer of the SOXE stack represented.
2. Apply true heat transfer properties and physics to reduce or remove the need of grey factors.
3. Determine the temperature variation between all layers of the SOXE stack to understand overall system variation.
4. Determine the temperature variation within the plane of each layer of the SOXE stack to understand performance variation within each layer.

The requirements above organically down-selected the modelling software to a 3D thermal modelling software. ANSYS was used to create an initial thermal model with a limited software licence. ANSYS was used to create a steady-state thermal model after heater warm-up and was validated with test data. However, it was determined that the model needed to include the electrolysis process, which involved incorporating gas flow and an endothermic reaction. Therefore, the modelling software was changed from ANSYS to COMSOL to incorporate COMSOL's benefits of multi-physics modelling capability in future model improvements. Further comparison and validation of the ANSYS and COMSOL model are captured in Chapter 6: Results. The details of the model set-up in this chapter focus on the COMSOL model because it was down-selected as the primary modelling software.

5.2 Model Geometry Simplification

The model in Figure 5-2 shows the components meshed in the geometry. All external components were removed as a simplifying assumption. The remaining geometry was simplified by removing details as appropriate. This included ignoring edge lines and vertices as independent components to improve meshing quality. Intermediate edge lines are seen on a single component due to the CAD creation of that object. By instructing COMSOL to ignore those edges, it prevents unnecessary high mesh density within a component. Also, external fillets and small details that are not impacted by the internal flow path were removed to improve meshing and computation time.

5.3 Meshing

Tetrahedral meshing was the primary meshing used for the model solver. The benefits of the tetrahedral meshing are that the free-tetrahedral meshing can be used on all geometries shape and the mesh size can be finely tuned for complexities in the geometry. In previous models, the geometry was simplified to remove all non-parallel curvatures so that simplified quadrilateral meshing could be used. Since this model will be used for additional analysis with airflow through the internal geometries, the details of the inner flow geometries are not removed to maintain the high fidelity of the model. The overall meshing properties are detailed in the table.

Table 5.1: COMSOL Meshing Properties for Free-Tetrahedral

DESCRIPTION	VALUE
Minimum element size	0.00012 [in]
Average element size	0.0622 [in]
Minimum element quality	0.11
Average element quality	0.61
Number of Tetrahedron Elements	20135689
Number of Triangle Elements	2288410
Number of Edge Elements	167440
Number of Vertex Element	7569

The mesh quality is a way of quantifying the overall length to width ratio elements. An optimal value for average mesh quality is close to 1, meaning that the elements have expected aspect ratios. However, for thin elements, such as the thin layers of the interconnects and electrolytes, it becomes a trade off between mesh quality and computation time. [?]

The geometry has complexities that could not be removed to improve the meshing quality. The standard guidance is to have minimum mesh quality greater than 0.1, therefore this mesh is deemed acceptable.

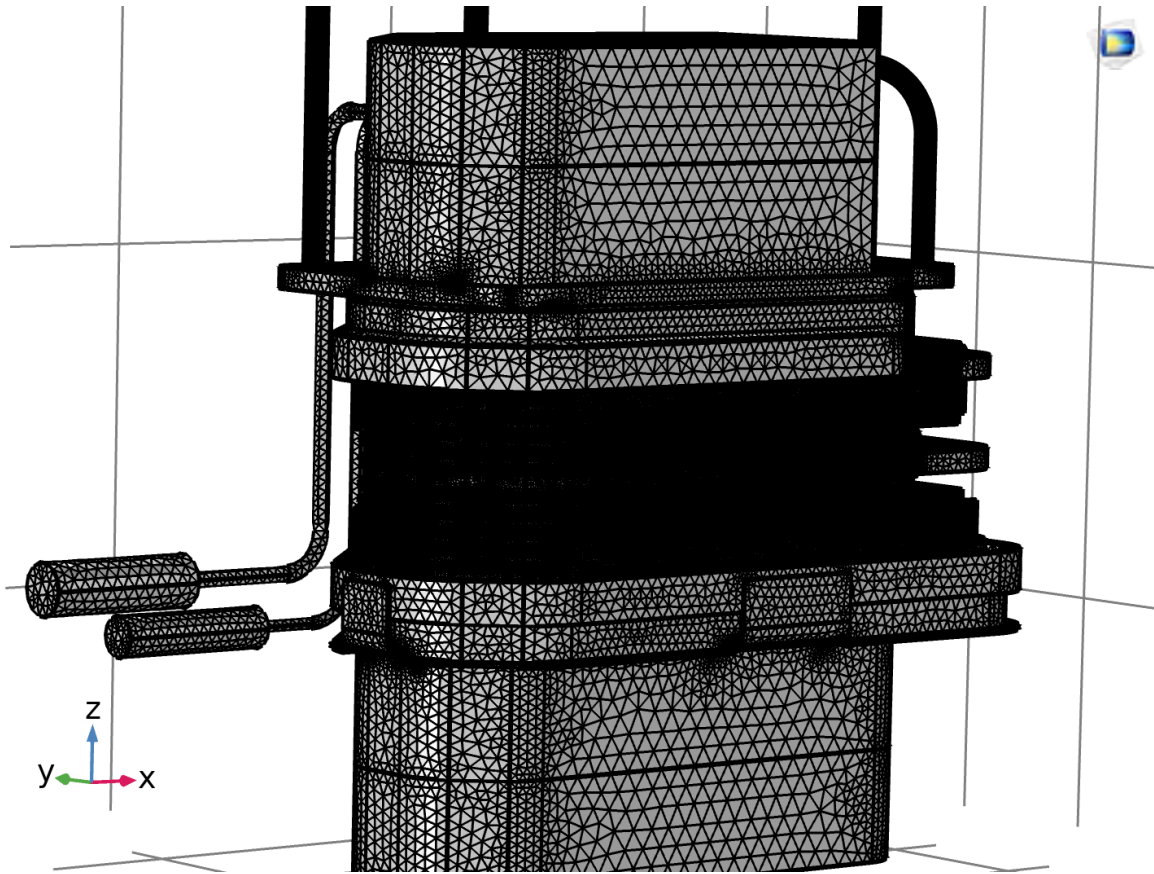


Figure 5-2: Full Model 3-D Tetrahedron Meshing

The full meshing is pictured in Figure 5-2. The size of mesh for the layers of the electrolysis stack are extremely fine for improved fidelity over the thin layers. The meshing in this location appears to be black due to the high density of the mesh. Figure 5-3 provides a zoomed in view of the interconnect and electrolyte layered meshing.

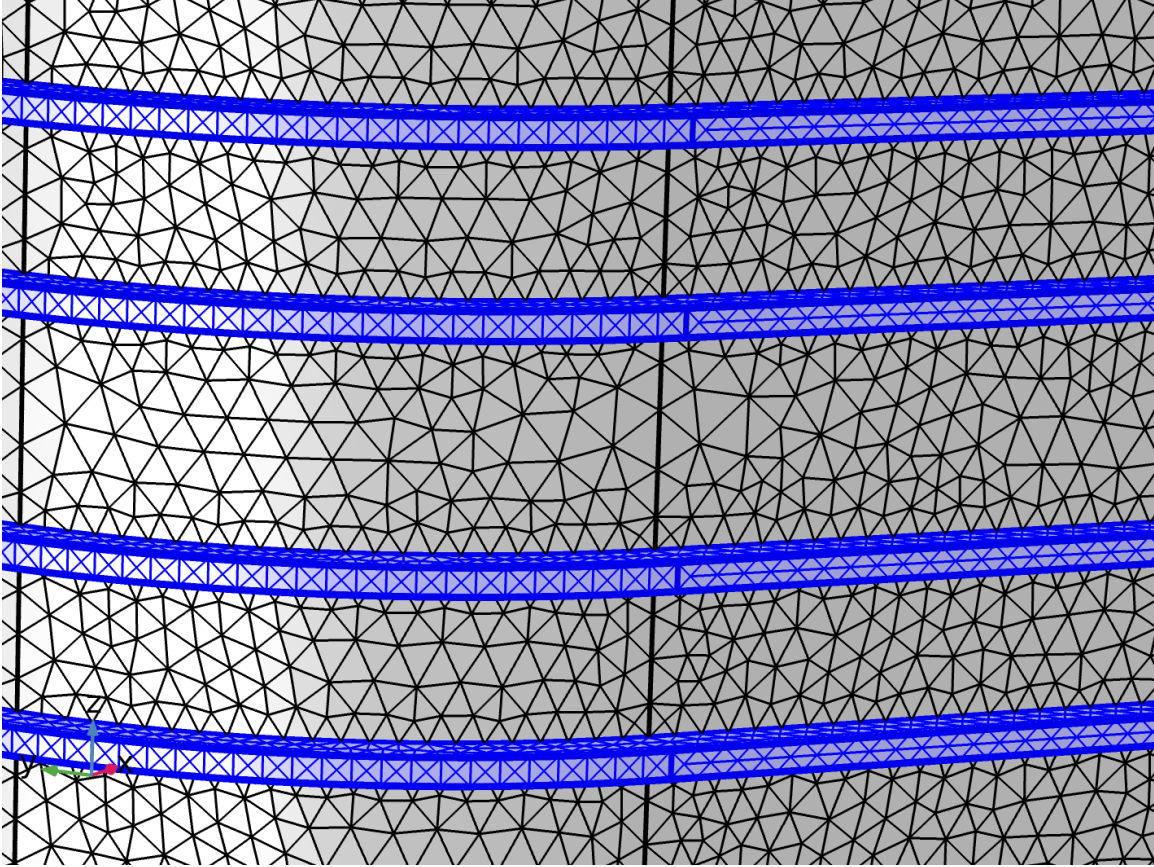


Figure 5-3: Zoomed in View of 3-D Tetrahedron Meshing on Electrolyte-Interconnect Layering

The layers of electrolyte are highlighted in blue and the interconnect layers are grey. It should be noted that the computation time is the trade-off for the high fidelity achieved by dense meshing. The following subsections in this chapter detail the model inputs and set-up conditions.

5.4 Boundary Conditions

It is important to appropriately define the boundaries of the system model in order for the model to have an optimized balance between efficacy and accuracy. Including additional components increases the number of nodes for the model to solve and therefore becomes more computationally expensive. The system thermal model extends to the exterior boundaries of the insulated aerogel layer. The aerogel engulfs the SOXE system as seen in Figure 5-4.

5.4.1 Aerogel

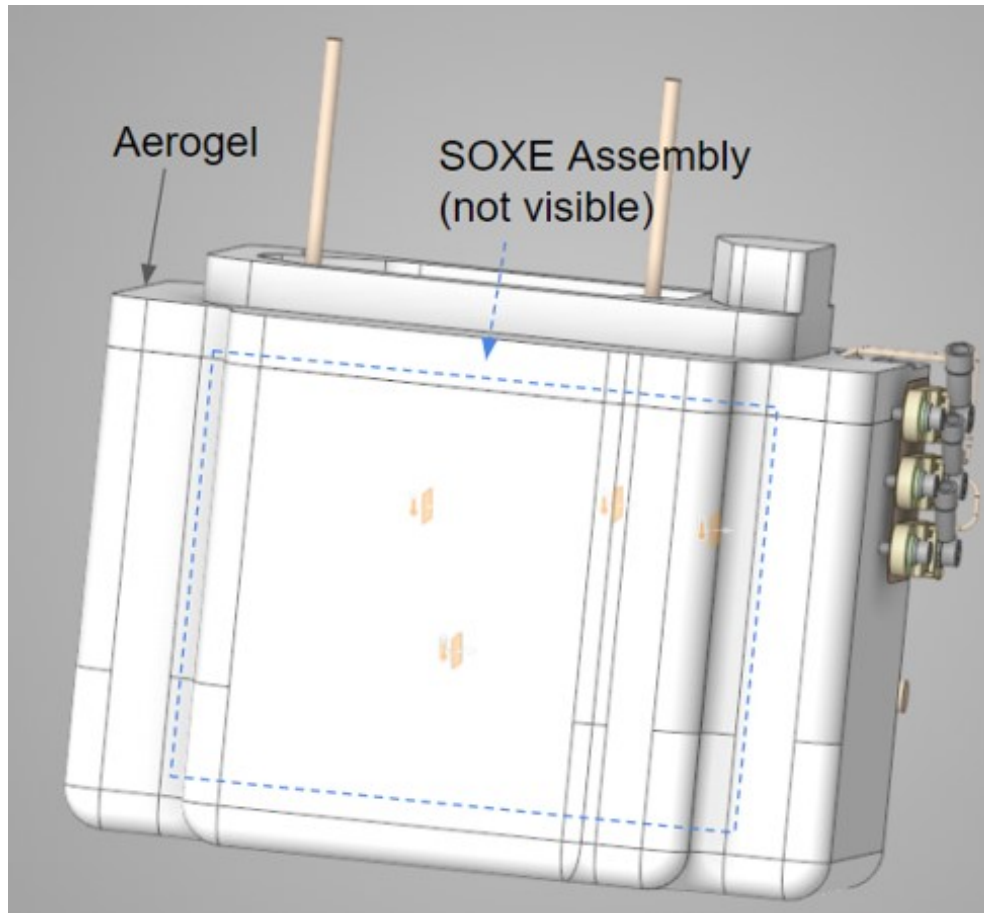


Figure 5-4: Full SOXE assembly with Aerogel Insulation

The aerogel insulation bounds the SOXE stack and is used as the beginning of the boundary condition of the model. However, the Aerogel was set as a 2D boundary condition, and the 3D geometry was not added to the model for two reasons:

1. The addition of 3D modelled aerogel increases the complexity and computation time of the model
2. The outside boundary of the aerogel is assumed to be a perfect insulator

The second reasoning for removing aerogel ensures that the heat transfer from the SOXE stack to the aerogel insulation can be simplified by applying conduction and radiation equations to the outside boundaries of the SOXE stack into the aerogel. This means that the SOXE stack can transfer heat into the aerogel, but the aerogel will maintain the thermal energy within its volume. The physics applied to represent the aerogel insulation at the model's boundary conditions are substantiated in the following section. It should be noted that convection was assumed to be negligible between the SOXE stack and the insulation due to the low pressure at reduced gravity with no forced flow.

5.4.2 Ambient Temperature

The temperature inside of MOXIE where the SOXE assembly is located is assumed to maintain the same temperature as the (RAMP) temperature prior to warm-up of the heaters. This temperature is set as the system ambient temperature and based on Earth testing is relatively consistent. The temperature is set to a value of 20 degC and is held constant through the simulation. Figure 5-5 highlights the boundary surfaces that are visible to the RAMP temperature in blue.

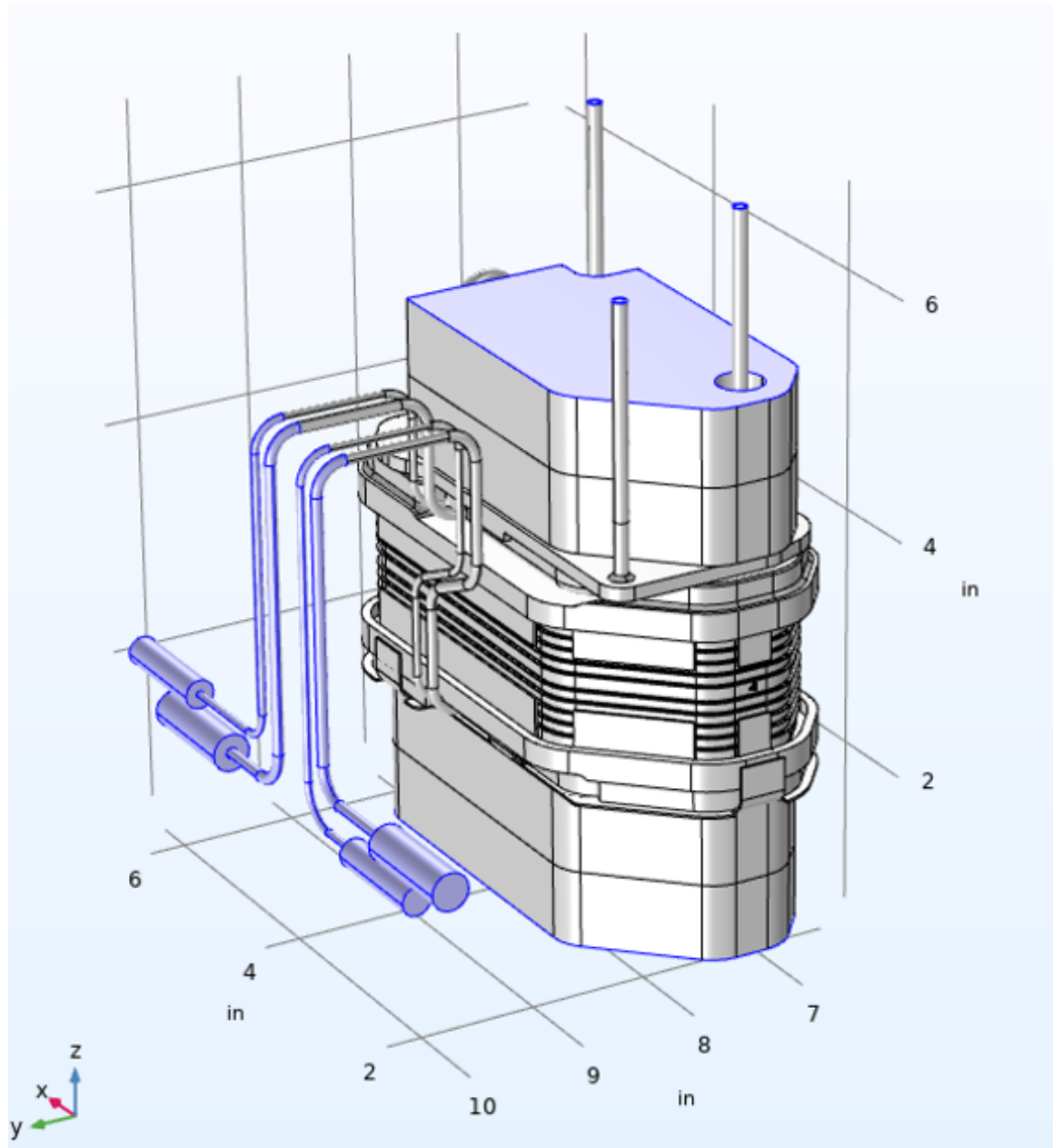


Figure 5-5: Constant RAMP Temperature Boundary Condition Locations

For ground testing on Earth, there was a cold plate place beneath the bottom

surface of the condensed min-K. There were validation runs when verifying the model that used this boundary condition to compare to the empirical data. However, it is not necessary to include this boundary condition for predictive runs of the model in the Mars environment and 20 degC was used as the boundary condition for model validation.

Radiation into Aerogel

Radiative heat transfer into and out of the aerogel is modeled between the outside surface of SOXE assembly and what would represent the inside surface of the insulating aerogel layer. The aerogel layer is reduced to a 2D surface where the outside boundary of the aerogel is equal to the RAMP temperature. There is an assumption that there is perfect insulation on the exterior boundary of the full system provided by the aerogel. The assumption for no heat loss through the exterior boundaries of the aerogel is validated and documented in the following chapter. Figure 5-6 shows the boundary surface location that represent the radiative heat transfer from the SOXE stack into the Aerogel insulating layer.

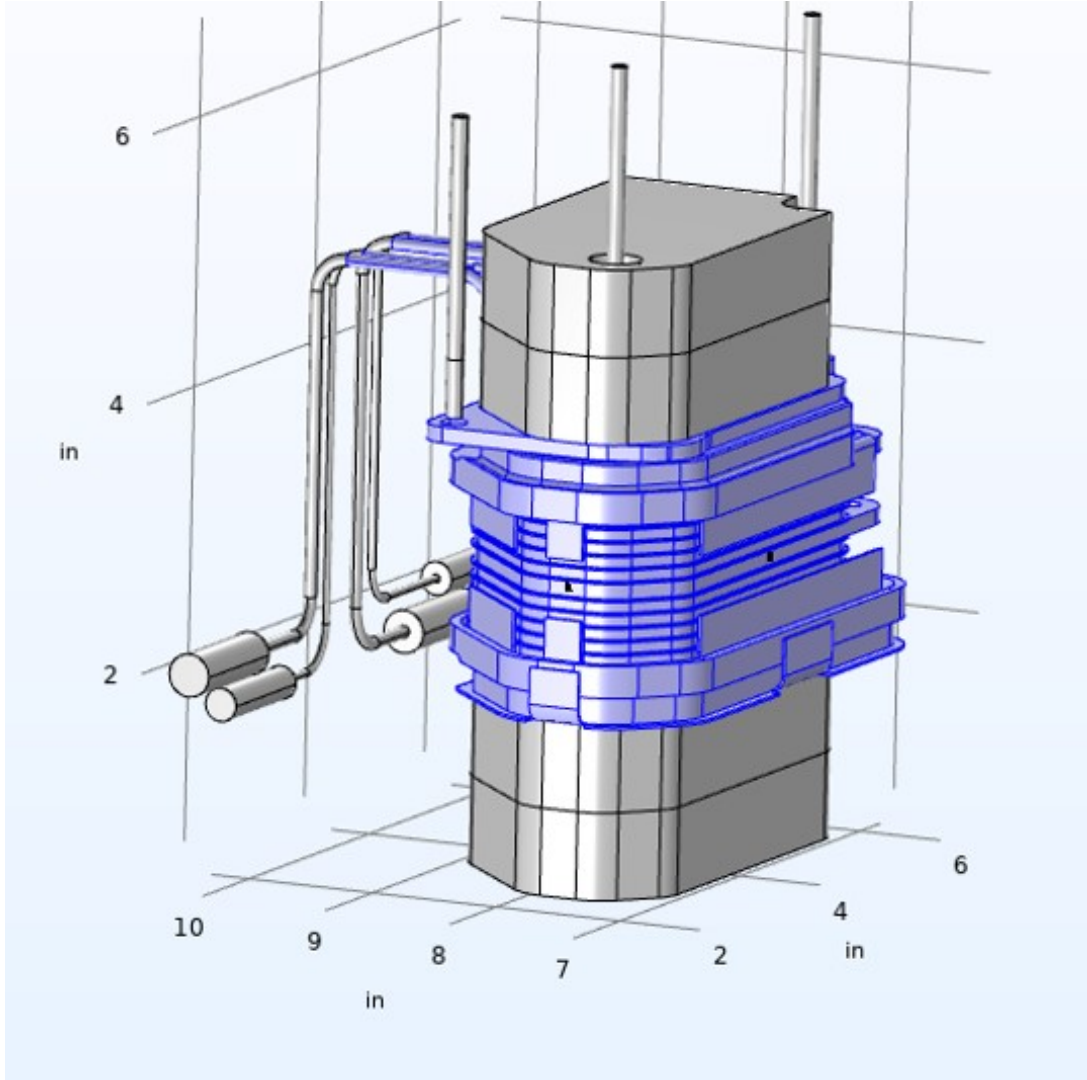


Figure 5-6: Radiation to Ambient Boundary Condition to Represent Aerogel

The surfaces highlighted in blue are the locations where radiative transfer into the aerogel is modeled. It is used via the surface-to-ambient equation, where the emissivity is a function of temperature.

Conduction into Aerogel

The second defined heat transfer on the boundary condition is conduction from the SOXE stack to the aerogel. The assumption is made that the heat flux from the sides of the SOXE stack conduct directly into the aerogel so that the flux is perpendicular with the walls of the aerogel and the SOXE stack. The long sides and short sides of the SOXE stack are modelled separately since the heat flux is calculated with thickness of the aerogel considered for the transient model. The generic equation is:

$$q_0 = -T_{SOXE} * h_{aerogel}(T_{SOXE})/t_{aerogel} \quad (5.1)$$

The variable $t_{aerogel}$ is the thickness of the aerogel and is 0.02m for the short side and 0.027m for the long side. T_{SOXE} is the temperature of the exterior boundary of the SOXE sides. This temperature is taken by using the average of the area of the sides parallel to the corresponding aerogel. The conduction coefficient $h_{aerogel}$ is calculated using linear interpolation based on the temperature dependent values. The input temperature to solve for the coefficient value is T_{SOXE} since continuity is assumed between the interior boundary of aerogel and the exterior boundary of the SOXE stack (T_{SOXE}).

Since there is low pressure and reduced gravity, convection is assumed to have a negligible impact on the heat transfer. Therefore, it is assumed the energy is conducted from the SOXE stack exterior boundaries to the aerogel insulation with no loss from convection.

5.5 Steady-State

The steady-state model was created to model the SOXE stack when the system reaches thermal equilibrium after the heaters are turned on and reach the steady-state point. The top heater is set to 843.7 degC and the bottom heater is set to 841.8 degC. The COMSOL stationary solver was used to compute the solution. For this case, the initial conditions inputs do not matter and the boundary conditions are unchanged as previous defined in this chapter. The relative tolerance in the stationary solver is set to 0.0001 using algebraic multi-grid as the linear solver. Table 5.2 contains the details of the algebraic multi-grid solver.

Table 5.2: COMSOL Algebraic Multi-Grid Solver

DESCRIPTION	VALUE
Solver Method	Generalized Minimum Residual Method
Initial Damping Factor	0.01
Preconditioning	Left
Number of Approximate Eigenvectors	25
Maximum Number of Iterations	10000

The solver method is optimal for fast convergence that uses an iterative method for general linear systems of the form $Ax = b$ [8].

Newton solver is used for nonlinear solver, a solver that is used if there is a non-convergence with the linear solver for fully coupled nodes [5]. Table 5.3 contains the details of the newton solver.

Table 5.3: COMSOL Newton Nonlinear Solver

DESCRIPTION	VALUE
Initial Damping Factor	0.01
Minimum Damping Factor	1E-6
Restriction for Step-Size Update	10
Restriction for Step-Size Increase	1
Recovery Damping Factor	0.75
Maximum Number of Iterations	50

The values in both Table 5.3 and Table 5.2 are both the COMSOL default settings for the solver methods selected. The steady-state solver is more straight forward than the transient solver so there was not need to alter the settings.

5.6 Transients

The transient solver is solved on the time unit order of minutes, ranging from 0 to 140 minutes with a standard step of 1 minute. The tolerance was reduced to 0.00001 for more computational accuracy. Table 5.4 contains the set-up details for the transient solver.

Table 5.4: COMSOL Time-Dependent Solver

DESCRIPTION	VALUE
Time Step Method	BDF
Steps Taken by Solver	Free
Maximum Order BDF	2
Minimum Order BDF	1
Consistent Initialization	Backward Euler
Initial Step for Backward Euler	0.001

Backward Euler solver can cause inaccuracies for high frequency solving, however the temperature warm-up is a slow transition so it was deemed appropriate for this thesis.

5.6.1 Warm-Up

The warm-up procedure is started by all nodes at initial temperature of 20 degC. The top and bottom heaters are then turned "on" in the simulation and controlled by the PI controller system, which is created to match the true MOXIE heater controls. The details of the heater controls as modeled in COMSOL are detailed in the following section.

5.6.2 Heater Controller

The top heater and the bottom heater are independently controlled with proportional-integration (PI) controller. The top heater is set to a target temperature of 843.7 degC and the bottom heater is targeting a temperature of 841.8 degC. This is different than previous models where the heater target temperature is 850 degC. This target values stems from two main concepts:

1. In order to achieve SOXE stack temperature of 800 degC after activation of the endothermic electrolysis reaction, the post-heater-warm-up steady-state temperature must be approximately 815 degC.
2. The temperature measurements are sensors coupled in the heater, which is the only point of temperature control. Therefore, the thermal controls needs to be in terms of setting a heater temperature to achieve an internal stack of approximately 815 degC.

The first concept captures that the initial target temperature is higher due to initial heat loss to the endothermic reaction once electrolysis reaction is activated. It is favorable for the life of the system to over heat prior to electrolysis rather than achieve a temperature less than 800 degC after activation. This prevents carbon build-up within the system and can reduce life or cause failure if significant. The second concept is a result of maintaining the steady-state temperature through heater control. In order to achieve the optimal pre-electrolysis SOXE stack temperature the heaters' temperatures must exceed the SOXE stack target since there is heat dissipation to components other than the SOXE stack. Table 5.5 contains the PI controller values that are used on the flight model and the thermal model to control the heaters.

Table 5.5: COMSOL Proportional Integration Controller for Heaters

DESCRIPTION	VALUE
Proportional Gain, Top Heater, κ_{pt}	16 (1/K)
Proportional Gain, Bottom Heater, κ_{pb}	16 (1/K)
Integral Gain, Top Heater, κ_{it}	1 (1/K)
Integral Gain, Bottom Heater, κ_{bt}	1 (1/K)
Closed-Loop Damping, ζ	1
Closed-Loop Bandwidth, ω	2 (rad/s)
Model Gain	2048 (K)

The PI controller is based on a second order system by applying a step function to the control input, defined in Equation 5.3.

$$P_0 = q_{max} * u_{ctrl} \quad (5.2)$$

where

$$Q_0 = P_0/V \quad (5.3)$$

The power limit, which is 90W for each heater is the variable q_{max} . The value for the sensor response step, u_{ctrl} , is defined by Equation 5.4.

$$u_{ctrl} = clip(u_{raw}) \quad (5.4)$$

where

$$u_{raw} = u_p + u_i \quad (5.5)$$

The clip function in Equation 5.4 limits the value to be ≥ 0 and ≤ 1 . The calculations for the time constants τ_1 and τ_2 are defined in Equation 5.6 and Equation 5.7.

$$\tau_2 = t_{63} - \tau_1 \quad (5.6)$$

$$\kappa = \omega/(2\zeta) \quad (5.7)$$

The proportional control is defined in Equation 5.8 and the integral control is defined in Equation 5.10, where e is the calculated error between the reference temperature and measured temperature at a given time.

$$u_p - \kappa_p e = 0 \quad (5.8)$$

$$du_i/dt - \kappa_i e = 0 \quad (5.9)$$

$$e = T_{ref}(t) - T_{measure}(t) \quad (5.10)$$

The equations are added into COMSOL global equations as state variables u_p and u_i . The integration of the PI controller in COMSOL provides a replica control system response to the heater control and is essential to the creation of the high fidelity thermal transient model.

Chapter 6

Results

This section contains the results and verification of the detailed thermal model and analysis. The methodology consists of creating a steady-state model first, validating the results, and then proceeding to grow the model in complexity by adding the transient warm-up portion. The steady-state results were validated by comparing the steady-state temperatures to the empirical data observed in the laboratory and the ANSYS model that was built prior to the creation of the more robust COMSOL model. The empirical data has limited temperature sensors due to the thinness of the SOXE stack materials and the size of the thermocouples. The high temperatures and extreme variation in temperatures during the heat-up and cool down process also lead to some thermocouple adhesive failure and inconsistencies in temperature readings. The next step in model validation was to create and validate the transient thermal model. This process was validated using the heater warm-up transient cycle. The control system, detailed in chapter 5, was modelled as the flight model PI controller to best replicate the ramp-up time and temperature of the empirically tested flight model. The results from the flight model are used as the validation for the transient model set-up.

6.1 Steady-State

The steady-state model was requested to create a detailed breakdown of temperature throughout the SOXE stack. A high fidelity model of each SOXE stack layer and the temperature gradients throughout is required due to the sensitivity of the ideal electrolysis temperature regime.

There are two main thermal analyses of interest in terms of understand the temperature distribution within the SOXE stack assembly:

1. The temperature gradient from top-to-bottom (along the z-axis) of the SOXE stack
2. The temperature gradient of each individual layer that make up the SOXE stack (along the x-y plane)

The first thermal analysis provides an overall understanding of how consistently the stack temperature can be controlled, and therefore overall performance of oxygen production while electrolysis is activated. The second thermal analysis provides the temperature variation within each stack layer and therefore efficiency within each SOXE stack layer. It should be noted that the second thermal analysis objective had not yet been conducted and was a point of interest to further explore the physics of the system. The small, complex, and confined geometry of each stack layer made it impossible to take temperature measurements from within the layers. Therefore validation of the model is only completed by matching the thermocouples from the exterior of the stack to the model temperature outputs in those locations. The details and results of the validation method for steady-state thermal modelling is continued in the following subsection.

6.1.1 Labelling and Notation

SOXE Assembly Labelling

The temperature sensor locations are referenced in Figure 1-7 and are labeled using the notation TC (for thermocouple), followed by a number that relates to the location of the temperature sensor.

The individual interconnect stack layers, numbered from 1 to 11 (top to bottom). The sides of the stack are referred to as the short side and the long side as labelled in Figure 1-6. The location of the 6 thermocouples are split so that 3 are on the short side and 3 are on the long side of the interconnects. To ensure model validation, the temperature probe locations added to COMSOL are located in the middle of each of the sides and are an average of surface-planar nodes.

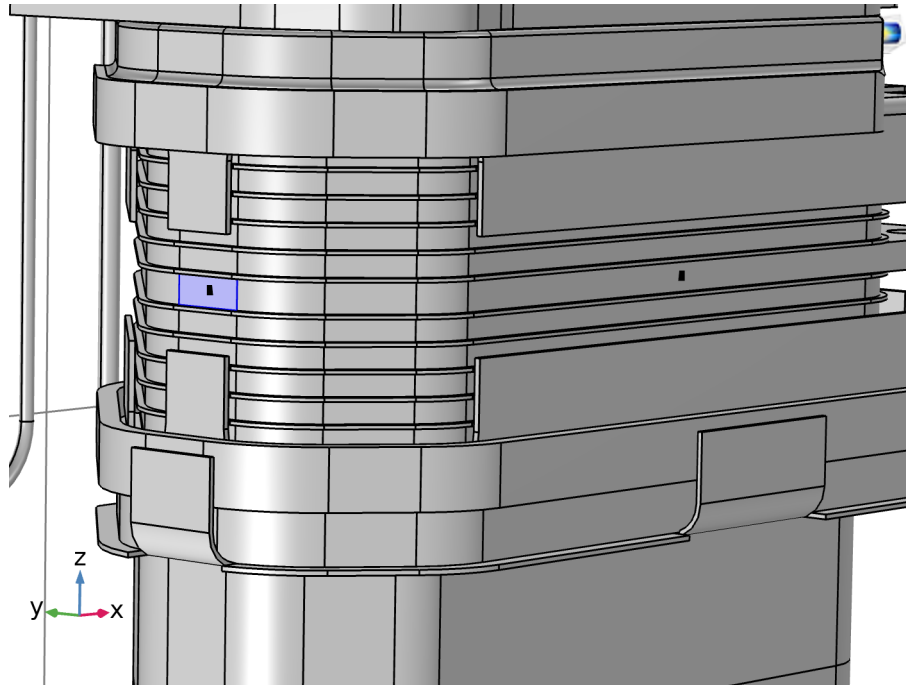


Figure 6-1: TC5

Figure 6-1 provides an example of the probe locations used within the COMSOL model. This example shows TC5 location. The highlighted blue area is the surface location where the nodal temperature is averaged to produce a temperature reading. Within the highlighted blue region is a singular point in the center of the area. This dot is the point probe for TC5. For all COMSOL thermocouple probe locations, one average and one point probe are added to verify the resultant temperature with empirical data from the thermocouples. In this thesis, the average surface temperature surrounding the node (blue area in 6-1) is reported as the COMSOL thermocouple reading used for results. The location of the nodes mimic the location of the temperature sensors recorded in laboratory testing.

Individual Stack Layer

Each layer of the SOXE stack is labelled with descriptors to be able to identify points of interest during analysis to answer the second objective of thermal model.

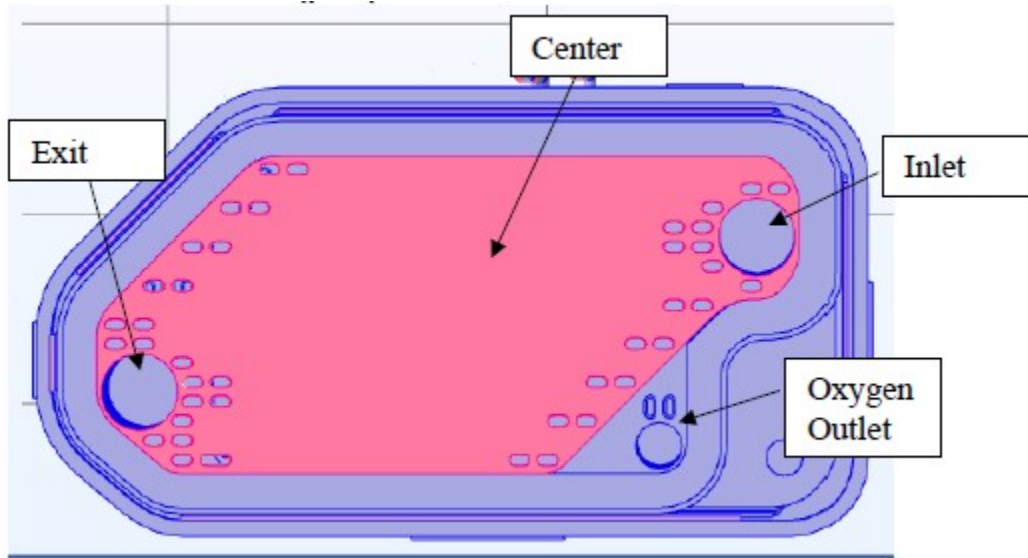


Figure 6-2: Labelling Convention, X-Y Plane View of SOXE Stack Interconnect

The inlet temperature is the average circumference edge temperature of the Martian atmosphere (carbon dioxide) passageway. The oxygen outlet temperature is the average edge temperature of circumference of the gaseous flow that has already undergone electrolysis and will continue to the exit of the system.

The exit temperature is the average planar surface temperature of the nearby surrounding location around the gas that is not converted into oxygen. This may contain trace gases from the atmosphere or carbon monoxide, which is a byproduct of the electrolysis process.

The face temperature (also called the center temperature), which is highlighted in pink in Figure 6-2 is the average planar temperature of the surface. The minimum and maximum temperatures of the face are recorded for each run to better understand the temperature range that the gaseous flow experiences. It should be noted that the minimum and maximum temperature recordings could be located in any point on face surface area and may change location for different conditions.

6.1.2 Baseline Thermal Model Values

This section contains the results of the steady-state thermal model for the baseline values. The baseline always assume steady-state heater temperature targets of 843.7 degC for the top heater and 841.8 degC for the bottom heater.

Table 6.1: Model Output Average Volume Temperatures for Each Layer of SOXE Cell at Baseline

LOCATION	AVERAGE VOLUME TEMPERATURE (degC)
Cell 1	815.07
Cell 2	812.62
Cell 3	811.44
Cell 4	810.70
Cell 5	810.30
Cell 6	809.97
Cell 7	810.67
Cell 8	811.43
Cell 9	812.52
Cell 10	814.04

The volume temperatures in Table 6.1 are calculated by taking the average temperature of all nodes with the solid component volume. The detailed breakdown of the temperatures from the model at each electrode cell layer are in Table 6.1.2.

Table 6.2: Detailed Model Output Temps for Each Layer of SOXE Cell at Baseline Heater (degC)

SOXE CELL	TEMP INLET	TEMP O ₂ OUTLET	TEMP EXIT	FACE MAX TEMP	FACE MIN TEMP	FACE AVG TEMP
Cell 1	812.48	814.48	811.21	819.35	809.63	816.96
Cell 2	810.92	812.96	810.40	813.06	809.60	814.07
Cell 3	810.10	811.88	809.85	811.72	809.34	812.59
Cell 4	809.56	811.18	809.54	810.92	809.03	811.63
Cell 5	809.28	810.81	809.48	810.50	808.75	811.10
Cell 6	809.29	810.74	810.01	810.42	808.64	810.98
Cell 7	809.80	811.08	810.89	810.85	809.54	811.33
Cell 8	810.58	811.73	812.06	811.61	810.64	812.06
Cell 9	811.63	812.70	813.59	812.74	811.82	813.20
Cell 10	813.00	814.06	815.92	814.38	813.20	814.82

These values represent the surface temperatures that carbon dioxide would be exposed to while the system is heated up, prior to electrolysis being activated. The endothermic reaction occurs due to the electrolysis process, at which point the cell temperatures would decrease.

As expected, Cell 5 contains the lowest temperatures as it is the center point between both heaters.

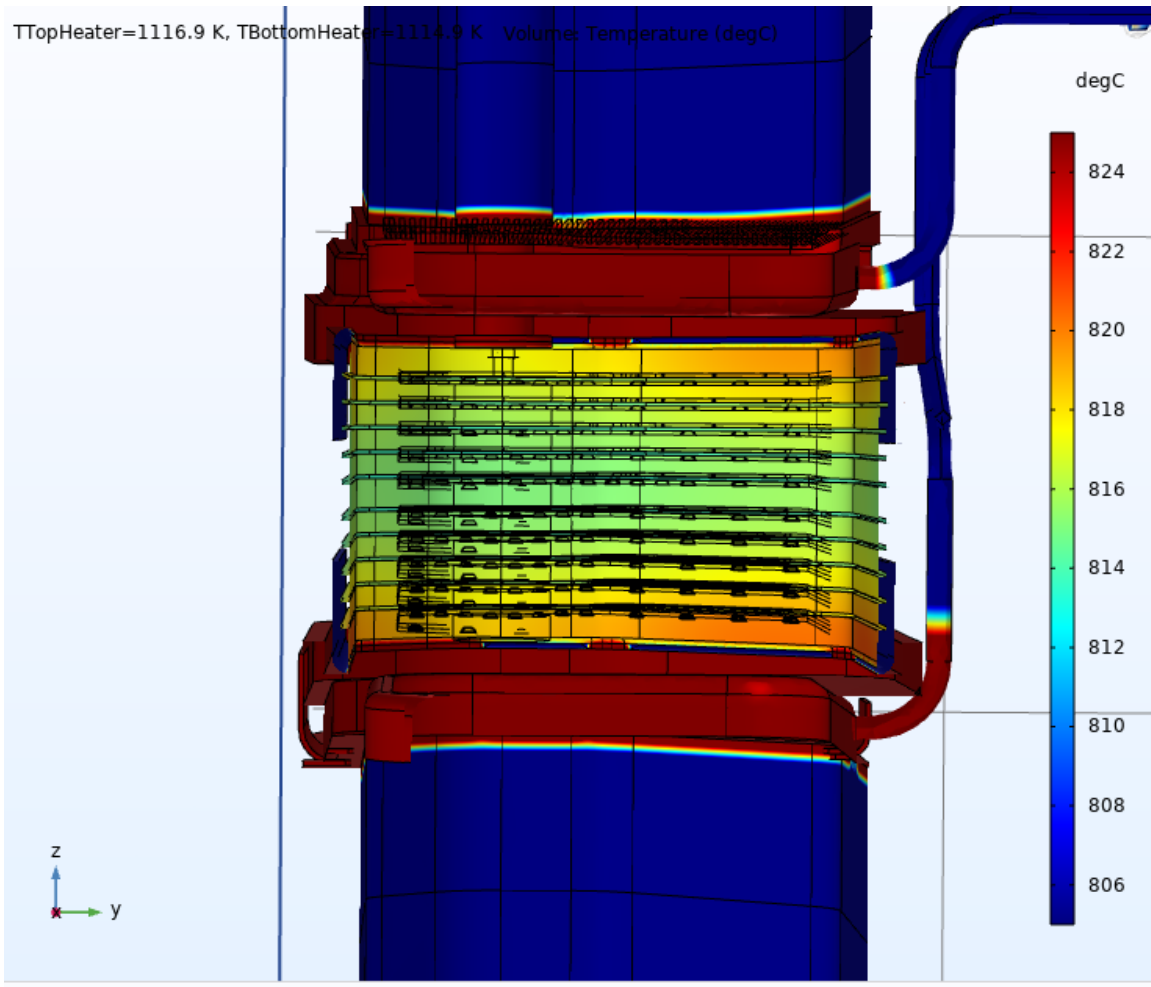


Figure 6-3: Thermal Model Steady-State, Z-Y Plane View

Figure 6-3 is a 3D visual of the temperatures in the mid-point Z-Y planar cross-sectional view. The temperature scale has been altered in the image for more comprehensive visual of the temperature variation within the stack.

6.1.3 Steady-State Model Validation and Comparison to Experimental Results

The empirical test runs OC07 and OC08 on the hardware build ID JAS006 were used for validation of the steady-state run. Table 6.3 contains the temperature sensor data recorded from the laboratory test runs and the model error compared to the model temperature.

Table 6.3: Absolute Error Used for Validation of Steady-State COMSOL Model at Thermocouple Locations

Temperatures (degC)	TC4	TC5	TC6	TC7	TC8	TC9
COMSOL Model Results	817.65	815.15	818.78	820.06	815.58	820.08
OC07 Temperature Sensor Readings	820.49	813.89	818.78	821.39	812.28	820.10
Model Error Delta vs. OC07	-2.84	1.26	0.00	-1.33	3.30	-0.02
OC08 Temp	817.19	809.79	815.18	818.28	809.00	817.19
Model Error Delta vs. OC08	0.46	5.36	3.60	1.78	6.58	2.89

The test runs for OC07 and OC08 were repeatability runs of the steady state condition. The temperatures were averaged for each thermocouple reading at the steady-state pre-electrolysis condition. As seen in Table 6.3 the model error for both runs are less than +/-7 degC, which is deemed an acceptable error. The highest difference in temperature from the model versus the test data is at TC8 from the OC08 run. The temperature ranges are expressed in Table 6.4.

Table 6.4: Temperature Range of Steady-State COMSOL Model vs. Test JSA006 OC07 and Test JAS006 OC08

Results (degC)	Min TC	Max TC	TC Range (Max-Min)
COMSOL Model	815.15	820.08	4.93
OC07	812.28	821.39	9.11
OC08	809.00	818.28	9.28

The temperature variation from empirical data is approximately 9 degC while the thermal model results have a lower range just below 5 degC.

Another validation method use was comparing the COMSOL temperature readings from a linear cross-sectional plot from experiment JSA006 OC10.

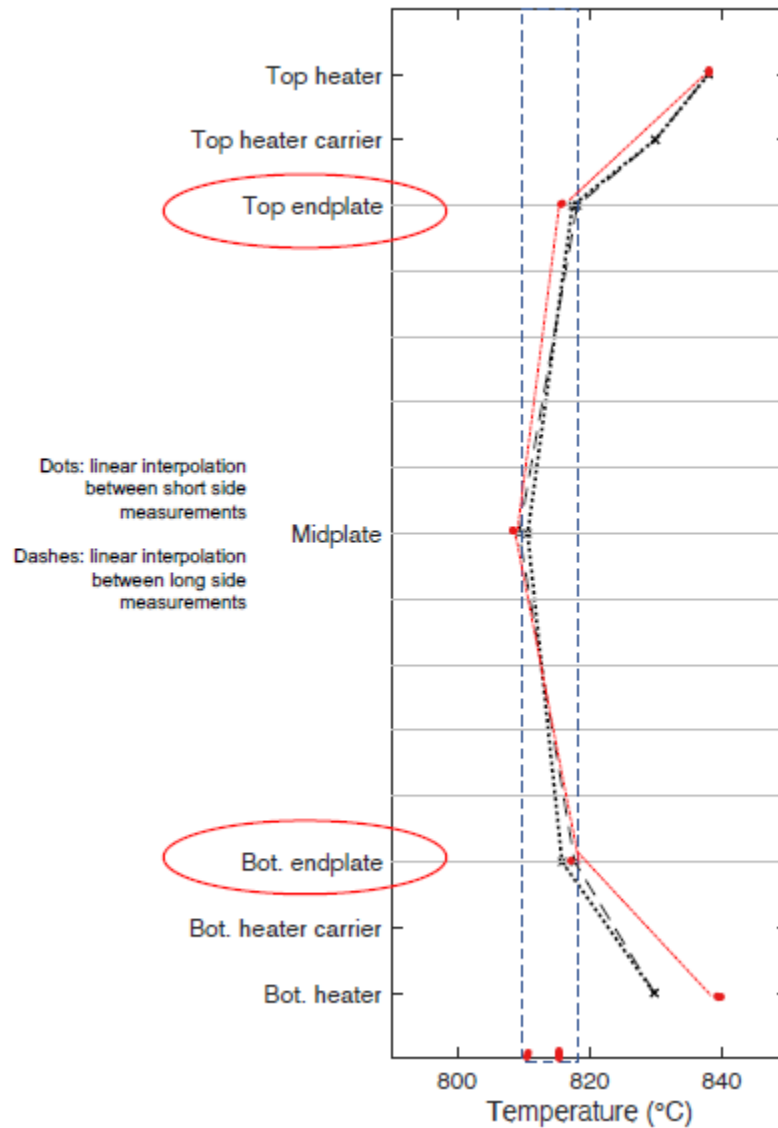


Figure 6-4: Cross-Section Temperature Validation with Test JSA006 OC10

In Figure 6-4 the points on the plot are direct measurements. The red notations represent the COMSOL thermal model results and the black notations are the experimental results. The line connecting the dots are representation of linear interpolation between the points. The blue dashed lines represents the temperature region in which all SOXE stacks are predicted to fall within based on the empirical data. The COMSOL thermal model validates and confirms this hypothesis.

6.1.4 Thermal Model Study: Impact of Heater Variation

The validated COMSOL thermal model can be used to run specific conditions and scenarios in simulation to understand the risks and performance impact of operations and future design. One example of this was the request for data from the MOXIE team to understand the SOXE stack internal temperature impact if the heaters' target temperatures were varied. A target heaters temperatures were swept by offsetting the baseline temperatures by +10, +5, -5, and -10 degC.

For this study, the ambient temperature was set to 20 degC. Martian atmospheric pressure and gravity was applied. The analysis was reviewed within the steady-state regime.

The steady-state parameter sweep was conducted using the following input heater conditions from Table 6.5.

Table 6.5: Temperature Sweep of Top and Bottom Heater Conditions

DELTA FROM BASELINE (deg C)	HEATER BOTTOM (deg C)	HEATER TOP(deg C)
-10	831.8	833.7
-5	836.8	838.7
0	841.8	843.7
5	846.8	848.7
10	851.8	853.7

The delta 0 degC temperature is the baseline heater temperature.

Heater Temperature Sweep Results

The internal interconnect values recorded in Figure 6-5 are the average volume temperatures.

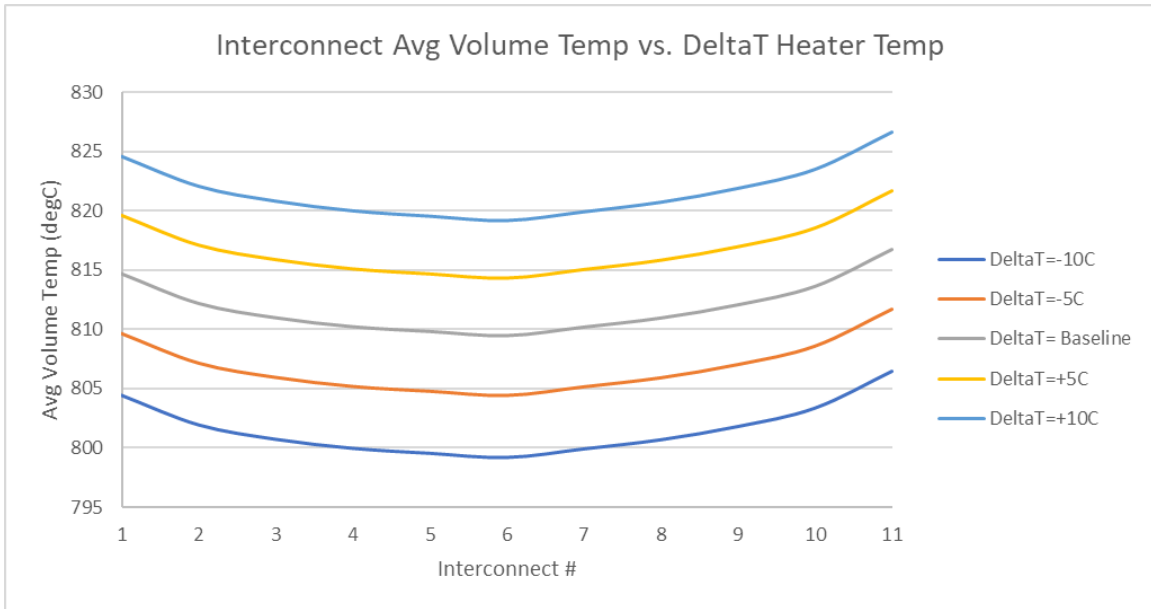


Figure 6-5: Heater Temperature Sweep Results, Volumetric Average Temperatures within Thermal Model Steady-State

As the heater temperature is offset, the internal temperature ranges and relations are offset linearly and proportionally. This result is expected as there are limited interacting physics in this condition. The 3D SOXE stack volumetric views for the baseline is represented in Figure 6-6

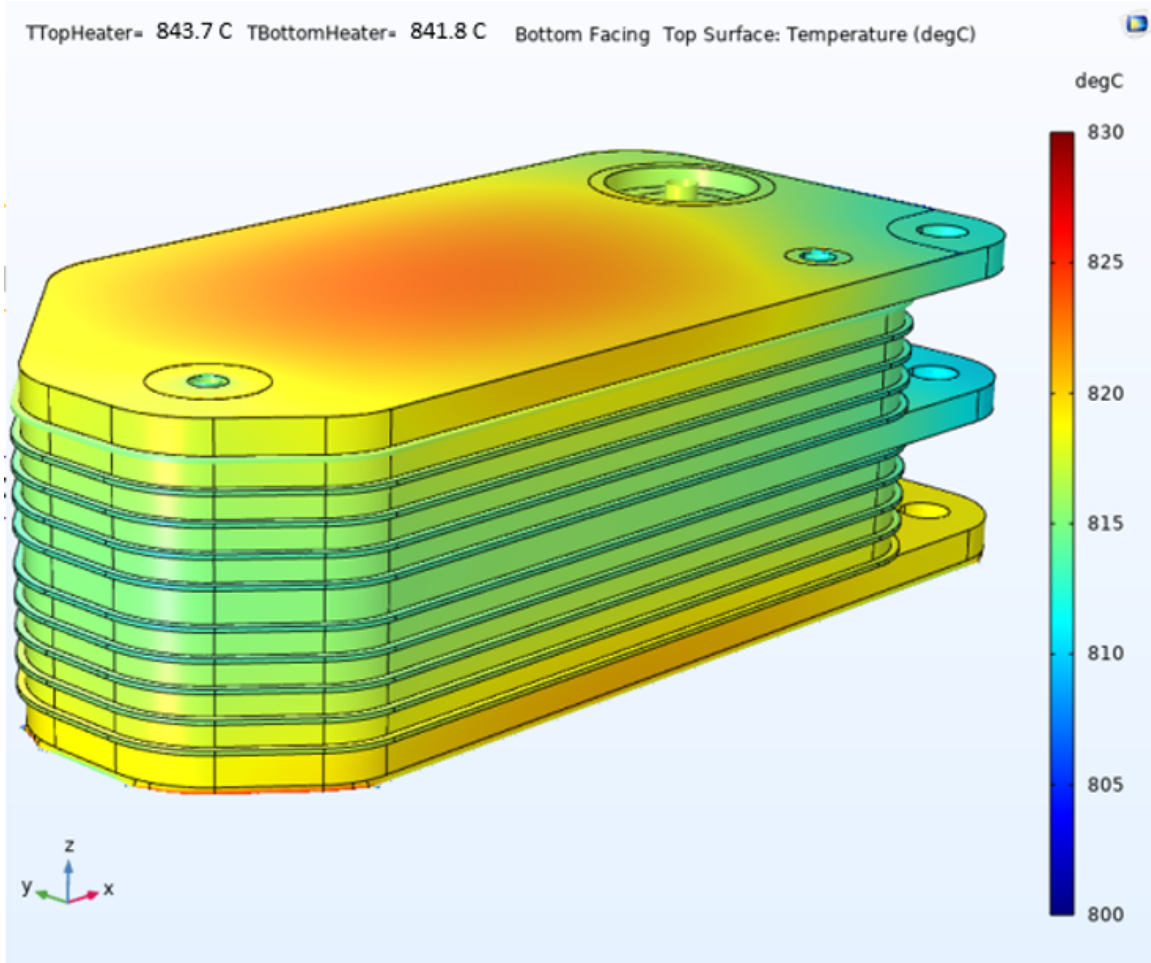


Figure 6-6: SOXE Stack 3D Volumetric Thermal Analysis at Baseline Heater Temperatures

A notable observation is that the 3 tabs that overhang the stack at the top, middle and bottom interconnects are local minimum temperatures, with the stack minimum temperature at the middle interconnect tabular overhang.

It is visible from the top interconnect that higher temperatures are centralized in the interconnect volume and have a X-Y planar temperature gradient of approximately 10 degC. This is the highest X-Y planar temperature gradient as the bottom-most interconnect near the bottom heater has a more consistent X-Y planar temperature gradient. This is likely due to the increased and consistent contact between the bottom interconnect and the bottom heater carrier. The temperature gradient lessens towards the middle of the SOXE stack.

The temperature color scale used for this baseline figure is carried through the following figures with temperature offsets for ease of comparison.

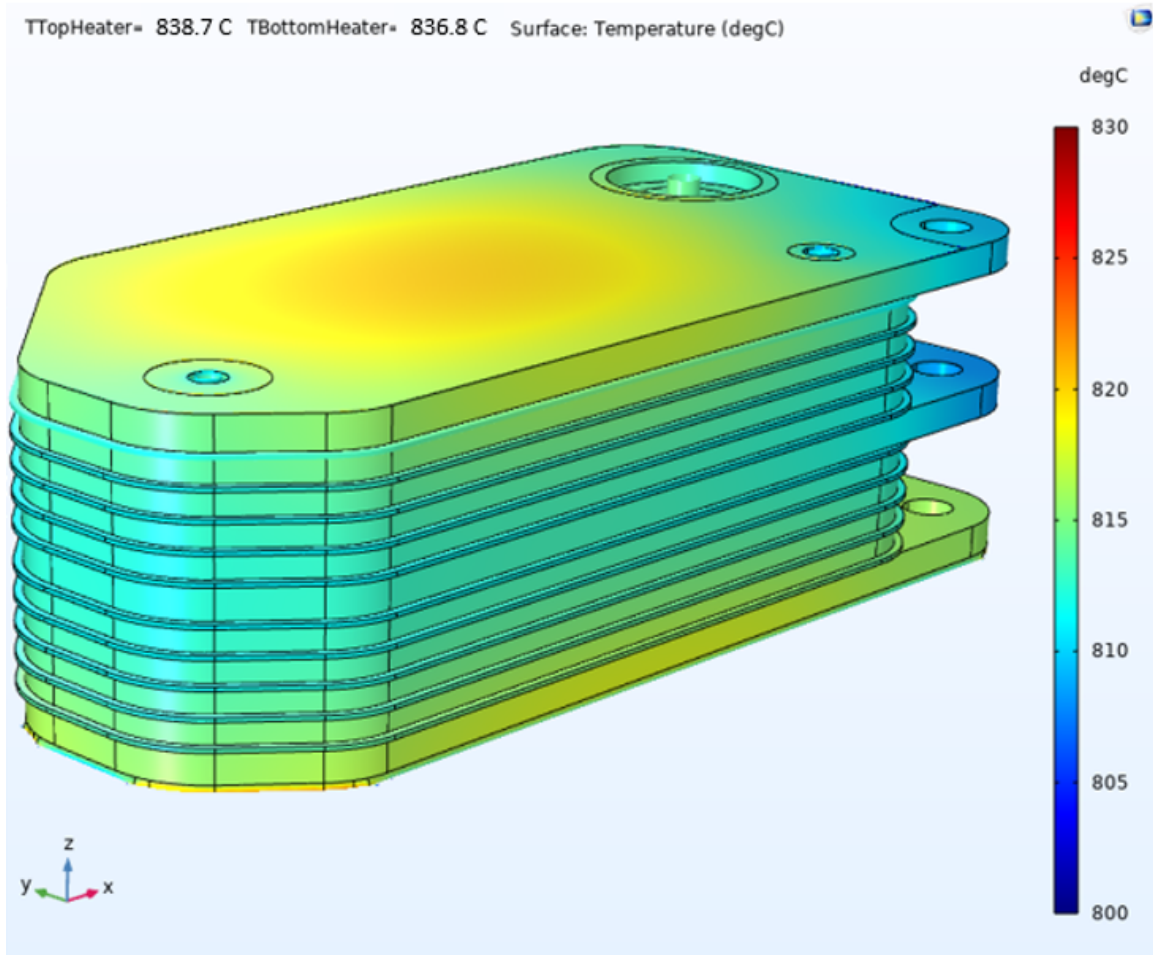


Figure 6-7: SOXE Stack 3D Volumetric Thermal Analysis at Heater Temperature Baseline -5 degC

Figure 6-7 and Figure 6-8 are images of the same view of the SOXE but with the heater temperature of variations of the baseline +5 degC and -5 degC, respectively.

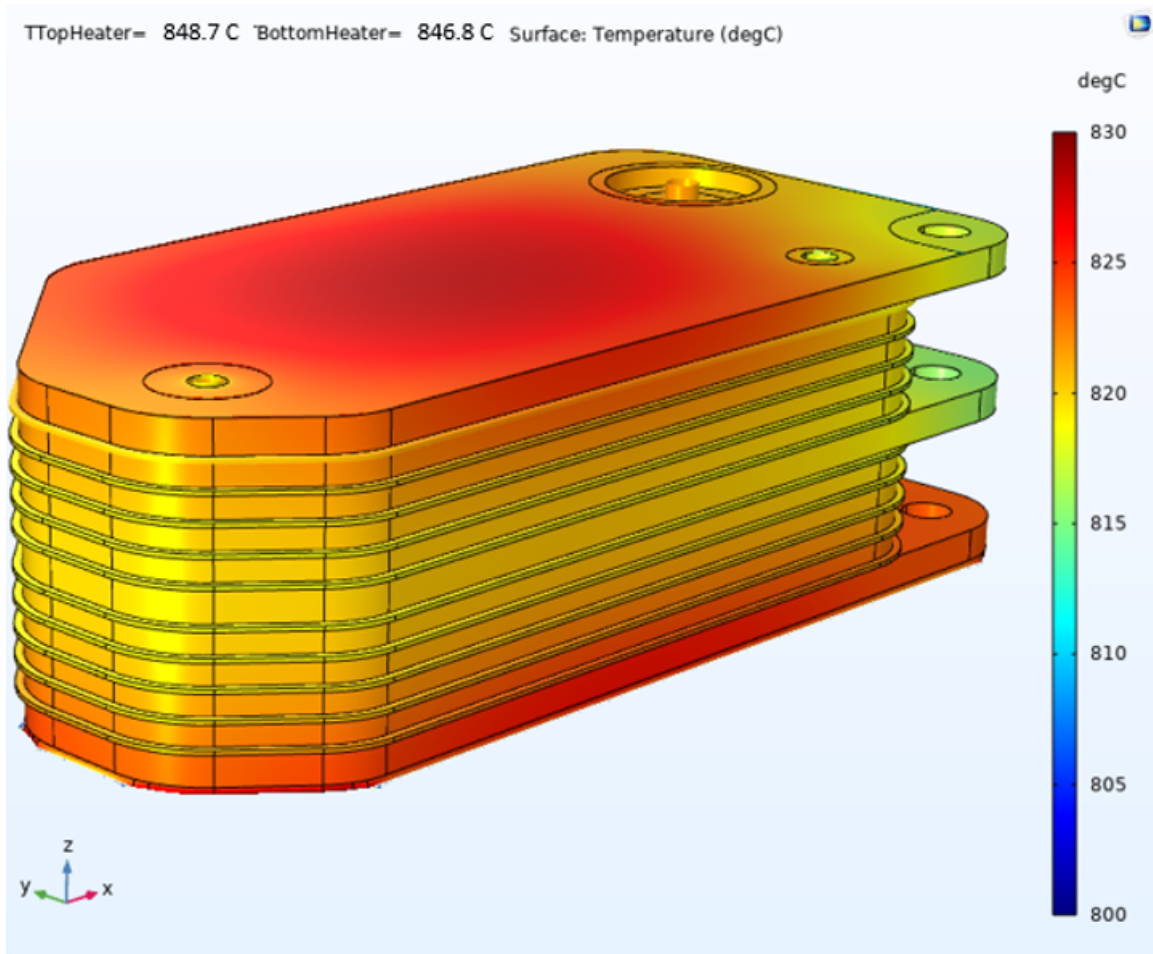


Figure 6-8: SOXE Stack 3D Volumetric Thermal Analysis at Heater Temperature Baseline +5 degC

The volumetric minimum temperature on Figure 6-7 is hotter than the average temperature of the baseline SOXE stack temperature. The minimum temperatures of Figure 6-8 dip below 805 degC towards the middle of the stack. This study demonstrates how sensitive the internal temperatures are to the heating criteria. This is especially important to note with the goal that the internal stack should be above 810 degC prior to electrolysis activation.

6.1.5 Ambient (RAMP) Conditions Impact

A study was conducted to determine the impact of the ambient temperature on the SOXE stack temperatures. The study demonstrates that ambient temperature has nominal impact on SOXE temperature.

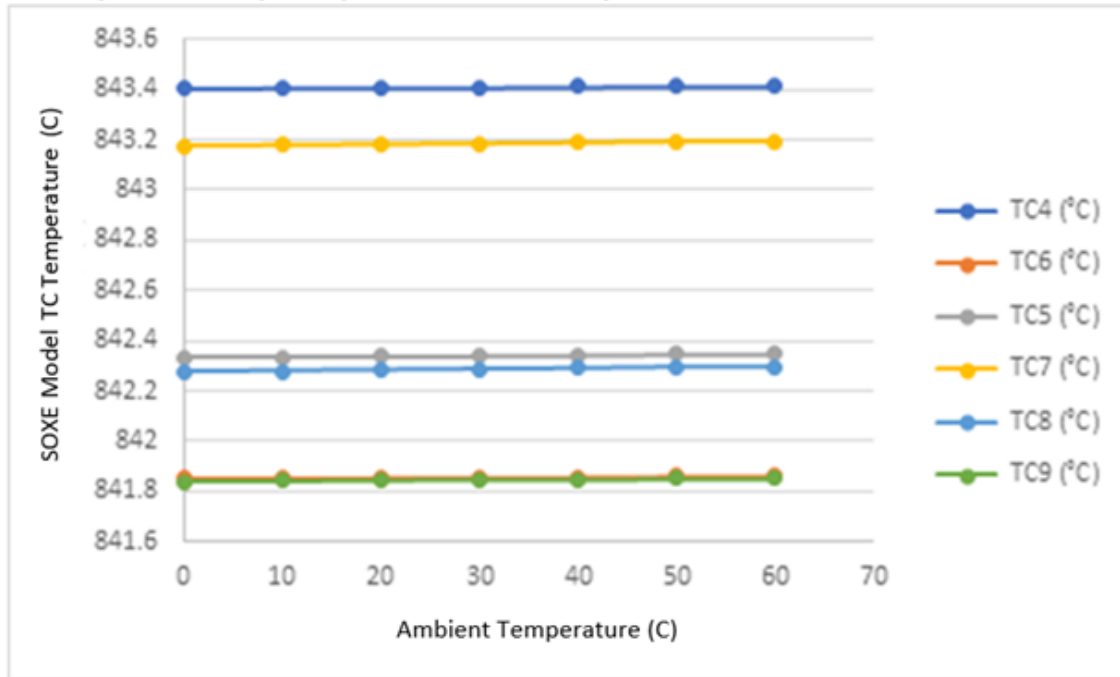


Figure 6-9: SOXE Stack Temperatures vs. Variation of Ambient (RAMP) Temperatures

Figure 6-9 shows the thermocouple readings from the model as ambient temperature is increased from 0 degC to 60 degC. This is at the steady-state condition where the heaters are set to the baseline temperatures.

6.2 Transient

The transient model was requested to create a detailed breakdown of temperature throughout the SOXE stack over time as the heaters are turned from ambient temperature. The value gained from this study provides a time offset between the heaters achieving target heater temperature and the internal SOXE cells achieving the target pre-electrolysis internal temperature of 815 degC. A high fidelity model of each SOXE stack layer and the temperature gradients throughout over each time step helps model the full system and provides a better understanding of the warm-up period.

One objective of the transient thermal model was to understand the relationship between the heater transient and the internal SOXE stack transient. The SOXE warm-up time of 180 minutes is to ensure that the interior of the SOXE stack was also at the appropriate temperature. The interior temperatures of SOXE stack cannot be measured due to space constraints as previously mentioned. Therefore the model could be used to answer the question:

Once the heater is at target temperature, how long until the internal stack reaches target temperature?

This is an important question since direct measurements cannot be taken and under-

standing the heat-up time could reduce idle time.

For simplicity of visualization, not all temperature probe locations are listed in this section, but can be found in the appendix.

There were three methods of producing a transient thermal model that were tried, two of which did not work. The methods were:

1. Set Heater Temperature
2. Set Heater Power
3. Model Heater Control System

Methods 1 and 2 did not produce a validated thermal model.

Set Heater Temperature Method

Setting the heater temperature was performed by using the empirical heater data and creating discrete data points of heater temperature at a given time. This was deemed a less ideal set-up since the input to the model set-up was from the same data set that would ultimately be used to validate the model. However, this method was attempted to determine feasibility and demonstrated a second flaw. Since the data was input as discrete data points, each time step that required a temperature increase created a step function response to the model output temperatures.

The discrete points were then converted into a continuous plot using linear interpolation in between the discrete heater temperature values. This method produced large output temperatures steps, therefore, the method of setting the heater as a power was implemented.

Set Heater Power Method

The heater system was limited to 90W, so the volumetric heater power was set on the model. This was not successful since the heated system is not at a natural thermal equilibrium without the assistance of a controller. The resulting transient would initiate a temperature runoff and the temperatures would exceed realistic temperatures.

Similar to the setting the temperature, an attempted improvement was made by inputting empirical heater power data as discrete data points over time. However, this set-up has the same limitation with model validation while simultaneously achieving model overshoot as different time points. This accrued significant error over the heater warm-up period.

Finally, it was decided to mimic the heater control system that was implemented on MOXIE. MOXIE uses a PI controller for the heater control. The feedback loop used on MOXIE to control the heaters was added to the model for a more accurate control system. Details of the PI controller set-up are found in Chapter 5. The validation method of the PI controller is detailed in the following section.

6.2.1 Transient Model Validation and Comparison to Experimental Results

PI control was added to the heaters in the thermal model by adding a feedback loop of the model's heater temperature outputs into the proportional-integral equations. The PI controller implementation of the thermal model was able to match the transient results produced on the test apparatus. This validation was more challenging than the steady-state validation since there was limited data recorded by the thermocouples during the heating period. Only TC5 from the laboratory experiment produced temperature values for the entirety of the test warm-up. Other thermocouples were either damaged or fell off during the testing.

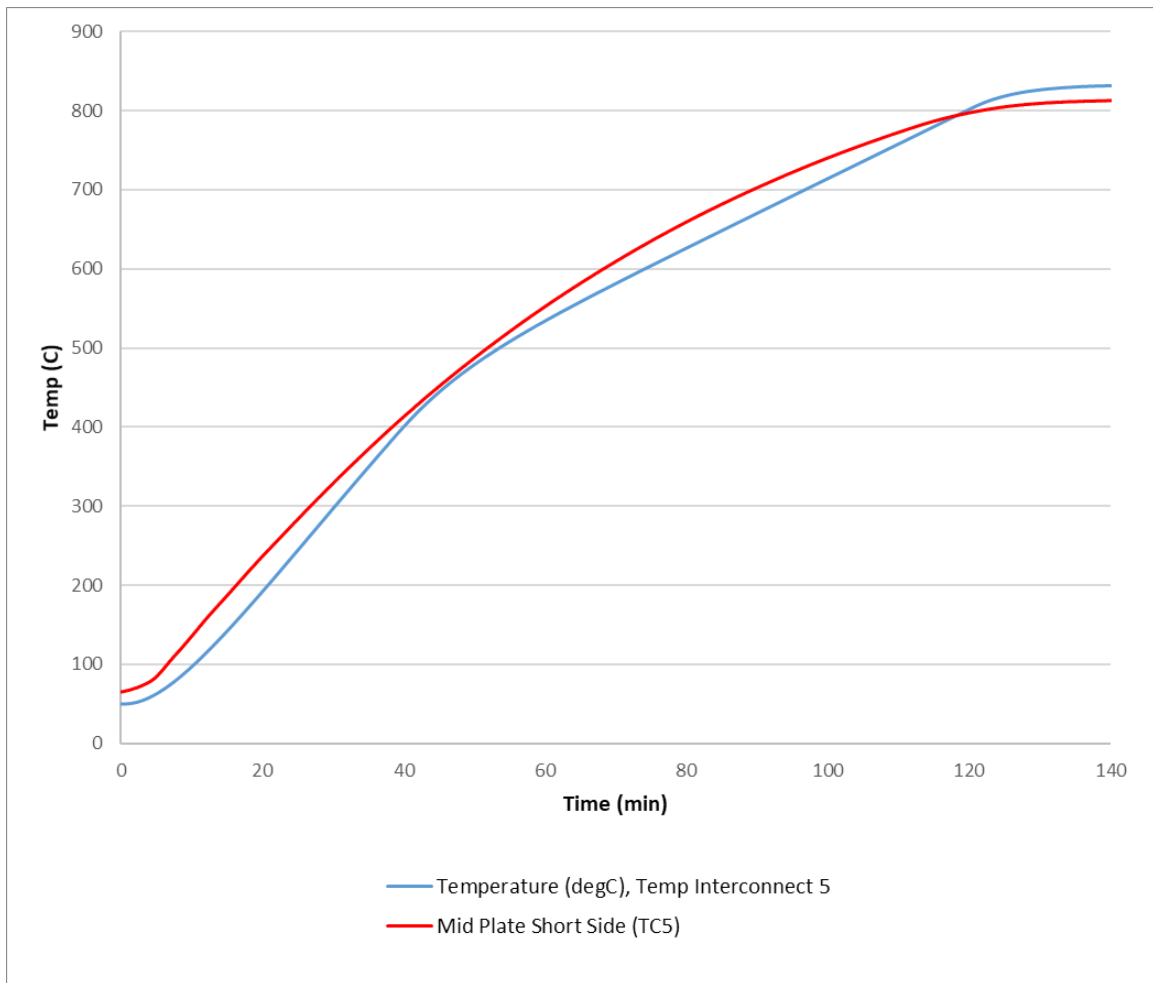


Figure 6-10: COMSOL Transient Model for TC5 (blue) vs. Empirically Recorded Results for TC5 (red)

Figure 6-10 contains both the thermal model (blue) and test recorded data (red). There is a slight offset throughout the transient where the thermal model results are slightly lower than the thermocouple readings. However, the offset is less than 15

degC at any given time and the time constants of the transient matches within a minute.

6.2.2 Transient Results

Figure 6-11 is a plot containing the analytical results of the heater warm-up period compared to the SOXE warm-up heater.

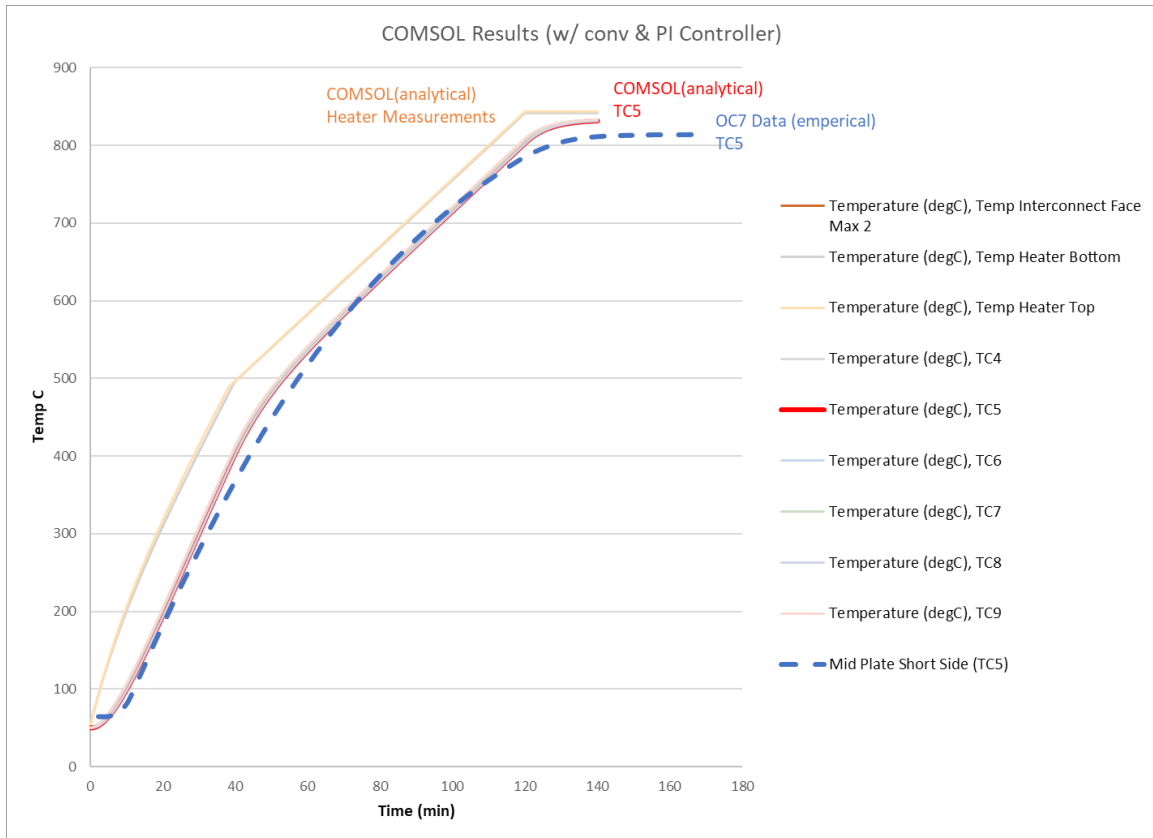


Figure 6-11: Analytical Heater Temperature (Orange) and SOXE Internal Temperature vs. Time

Two main questions can be answered on this plot:

1. How long after the heaters reach steady-state temperature will the SOXE stack reach temperature
2. Is there a time difference between layers within the SOXE stack reaching the target temperature

Regarding the first question, there is a time offset between the heater reaching its target steady-state temperature and the SOXE stack reaching steady-state. The heater reaches steady-state at approximately 120 minutes. About 15 minutes later, at 135 minutes, the SOXE stack approaches an appropriate internal temperature. This

information can be used to reduce the warm-up period by about 45 minutes from the current warm-up period time (180 minutes).

The difference between individual layers thermal warm-up time constants is nominal based on the results in Figure 6-11. The various thermocouple locations are plotted and overlaying each other. The maximum time difference is on the order of minutes between layers, showing that there is relatively consistent thermal transients within SOXE stack.

This model recorded temperatures for all points of interest on each interconnect and cell. However the data available is vast and therefore can be found in the appendix.

Chapter 7

Model Improvement Plan

Due to time constraints of this study, the detailed thermal model has limitations that should be expanded on for further understanding of the system. The modes of the thermal cycle that are not incorporated in the current model are the last three steps, which are called out in Chapter 2:

3. Compressor "ON" Transient Flow
4. Compressor "ON" Steady-State (Electrolysis)

The primary physics that should be added to the model is the thermal impact from the gaseous flow through SOXE (step 3) and the thermal impact from the electrolysis chemical reaction while MOXIE is actively producing oxygen in steady-state (step 4). This interaction is not included in this paper and should be included in the model improvements and validated using the empirical data from the Perseverance mission.

7.1 Next Steps

Compressor "ON" Transient Flow

The model is already set-up with fluid flow internal to SOXE. The flow velocity value shall be added in the inlet tube to the model system. There may be complications with meshing and the current solver selected as the flow is introduced.

With flow introduced, convection shall be added to the modelled physics, referencing Equation 4.6. The input pressure is needed to close the solver loop. It may be acceptable to use the compressor output pressure as the input to the model if no losses are assumed.

The intent of this study is to characterize the thermal impact from the introduction of flow through the SOXE. The initiation of flow through SOXE inherently activates the endothermic reaction via electrolysis. Modelling the flow independently will be able to quantify the thermal impact from just the convection of the flow.

Compressor "ON" Steady-State (Electrolysis)

Adding the endothermic reaction that occurs from electrolysis to the thermal model may be simplified as adding an equation-based heat sink derived from the calculations. This would be applied to the surface areas along the gas flow path within the SOXE stack. This can be done separately or with the gaseous flow as an interaction. A thorough study would provide both the independent endothermic impact and the interaction impact.

Appendix A

Steady-State Results

MEMORANDUM

Author: Justine Schultz

Software: COMSOL Model Thermal_Transient_V16

Date: 7/30/2021

Rev: 8/3/2021

Request

Use COMSOL analytical model to varying Heater SS temperatures for +/-10 degC, +/-5 degC, and baseline heater temperatures. Model run is for steady-state heater state prior to compressor being turned on (no O2 production/airflow). The baseline heater is set to 843.7C and 841.8C for the top heater and bottom heater, respectively.

Assumptions

- Ambient T= 20 degC
- Mars Atmospheric Pressure & gravity
- Steady-State Criteria
- OC6, OC7, OC8 SS data used for baseline run data-matching, ref. Appendix

Methodology

The baseline heater temps, which are defined as

- Top heater = 843.7C
- Bottom heater = 841.8C

Were used as a reference point to match OC data. The results of the baseline study can be found on page 3.

The steady-state parameter sweep was conducted using the following input heater conditions

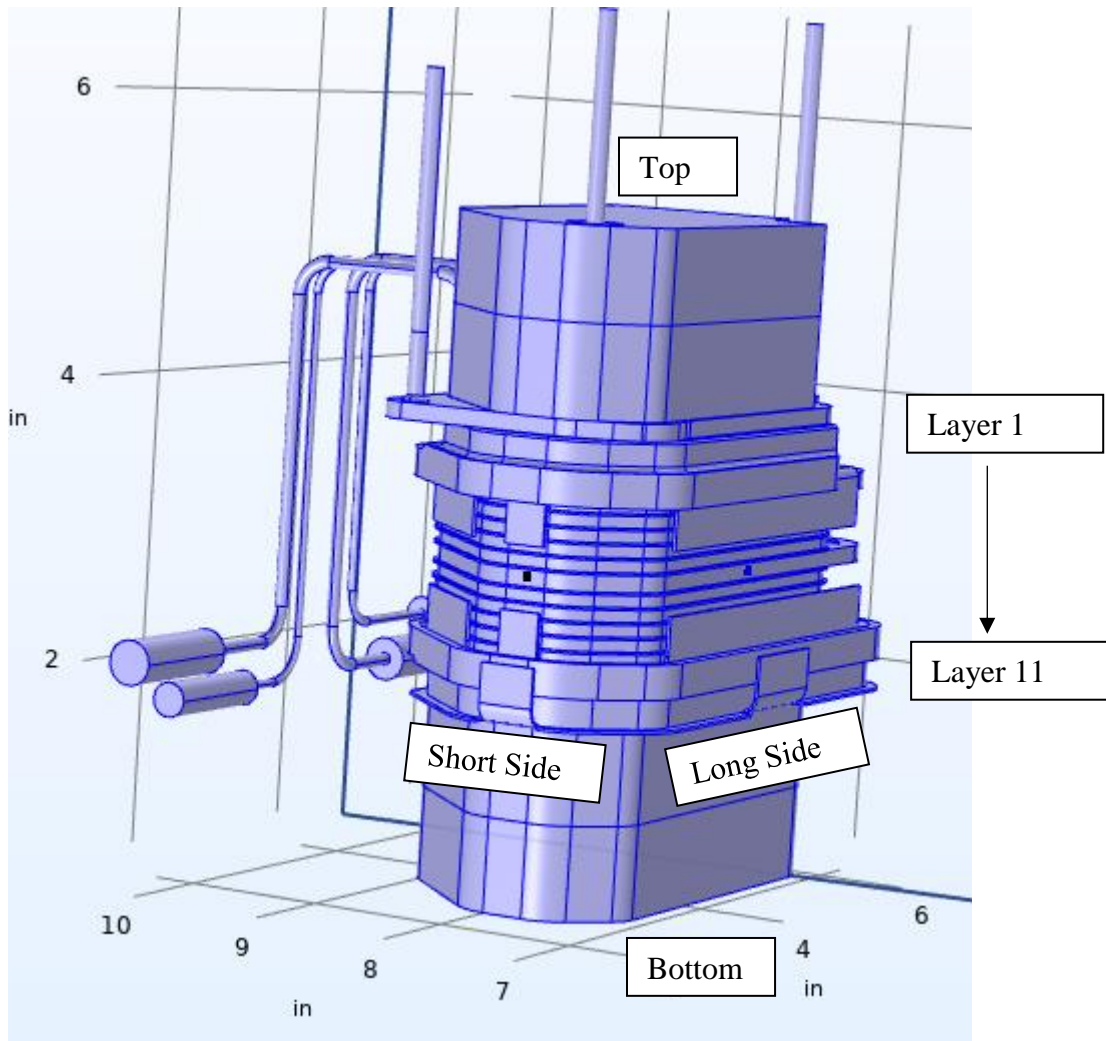
Delta Heater T (deg C)	Bottom Heater (deg C)	Top Heater (deg C)
-10	831.8	833.7
-5	836.8	838.7
0	841.8	843.7
5	846.8	848.7
10	851.8	853.7

Labeling and Notation

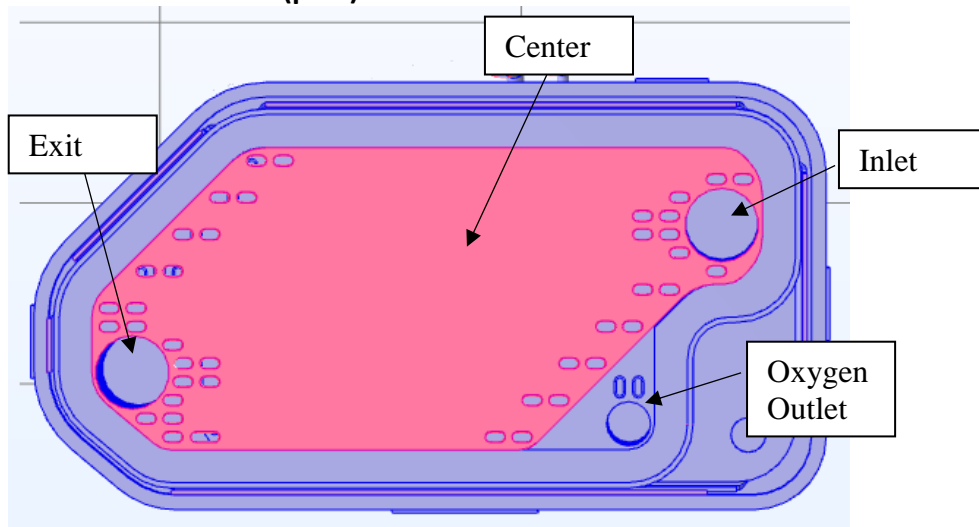
Oxygen Outlet Temps- Average surface temp of circumference and nearby surrounding location

Exit & Inlet Temps- Average edge temp of circumference

Center Temp- Average, Min, or Max surface temp. Note- Min or Max temp could be located in any point on center surface area & may change location for different conditions.

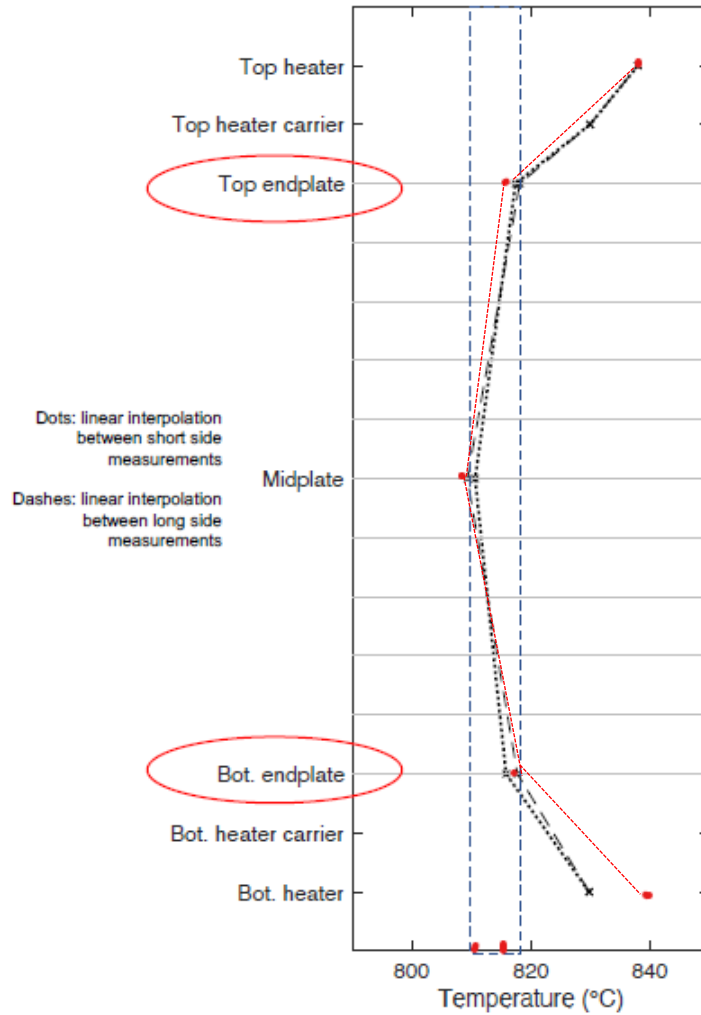


Interconnect Center (pink)



**Thermocouple Comparison, Heater Temp Sweep
Empirical Data: JAS 006 OC 13**

	Top Heater	Top Carrier	Top End Plate (TC4)	Midplate (TC5)	Bottom End plate (TC6)	Bottom Heater
JSA 006 OC 13	843.7	833	816	810	814	838
Delta T=-5C	838.7	828.10	809.66	804.48	811.7	836.8
Delta T=-0C	843.7	833.13	814.71	809.52	816.76	841.8
Delta T=+5C	848.7	838.05	819.59	814.33	821.65	846.8



BASELINE

**Table 2: Model Output Average Volume Temps for Each Layer of SOXE Cell at Base Temp
(Top Heater=843.7C, Bottom Heater =841.8C)**

	Temp Inter-connect 1	Temp Inter-connect 2	Temp Inter-connect 3	Temp Inter-connect 4	Temp Inter-connect 5	Temp Inter-connect 6	Temp Inter-connect 7	Temp Inter-connect 8	Temp Inter-connect 9	Temp Inter-connect 10	Temp Inter-connect 11
Model Temp (Deg C)	815.07	812.62	811.44	810.7	810.3	809.97	810.67	811.43	812.52	814.04	817.1

**Table 3: Detailed Model Output Temps for Each Layer of SOXE Cell at Baseline Heater
(Top Heater=843.7C, Bottom Heater =841.8C), All values in degC**

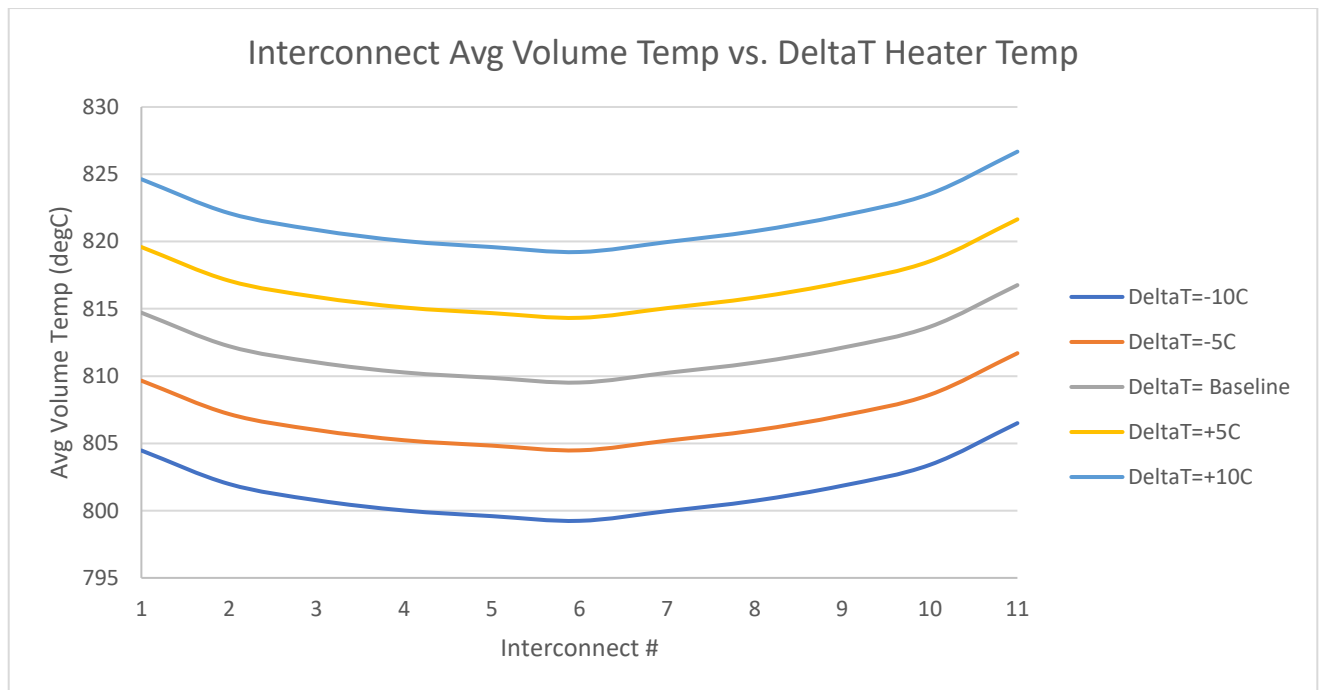
	Temp Interconnect Inlet	Temp Interconnect Exit	Temp Interconnect Oxygen Outlet	Temp Interconnect Center Max	Temp Interconnect Center Min	Temp Interconnect Center Avg
Cell 1	812.48	814.48	811.21	819.35	809.63	816.96
Cell 2	810.92	812.96	810.4	813.06	809.6	814.07
Cell 3	810.1	811.88	809.85	811.72	809.34	812.59
Cell 4	809.56	811.18	809.54	810.92	809.03	811.63
Cell 5	809.28	810.81	809.48	810.5	808.75	811.1
Cell 6	809.29	810.74	810.01	810.42	808.64	810.98
Cell 7	809.8	811.08	810.89	810.85	809.54	811.33
Cell 8	810.58	811.73	812.06	811.61	810.64	812.06
Cell 9	811.63	812.7	813.59	812.74	811.82	813.2
Cell 10	813	814.06	815.92	814.38	813.2	814.82

RESULTS

Below are the average volume temperature values for each layer of SOXE.

Table 4: Average Volume Temp of Each Layer, varied Heater Temp (degC)

Temp Top/ Bottom Heater	Heater Delta T	Interconnect #										
		1	2	3	4	5	6	7	8	9	10	11
833.7/ 831.8	-10	804.47	801.98	800.77	800.01	799.59	799.24	799.96	800.73	801.85	803.4	806.5
838.7/ 836.8	-5	809.66	807.18	805.99	805.23	804.83	804.48	805.2	805.96	807.07	808.61	811.7
843.7/ 841.8	0	815.07	812.62	811.44	810.7	810.3	809.97	810.67	811.43	812.52	814.04	817.1
848.7/ 846.8	5	819.59	817.09	815.88	815.1	814.68	814.33	815.05	815.83	816.96	818.53	821.65
853.7/ 851.8	10	824.63	822.11	820.86	820.04	819.59	819.22	819.96	820.77	821.94	823.54	826.68



Average Volume Temp of Each Layer for Delta Heater Temp

**Table 5: Detailed Model Output Temps for Each Layer of SOXE Cell at -10C Heater Temps
(Top Heater=833.7C, Bottom Heater =831.8C), All values in degC**

	Temp (degC) Interconnect Inlet	Temp (degC) Interconnect Exit	Temp (degC) Interconnect Oxygen Outlet	Temp (degC) Interconnect Center	Temp (degC) Interconnect Center Min	Temp (degC) Interconnect Center Max
Layer 1	801.83	803.88	800.56	806.38	798.99	808.8
Layer 2	800.25	802.33	799.72	802.43	798.93	803.45
Layer 3	799.41	801.23	799.15	801.05	798.65	801.94
Layer 4	798.85	800.5	798.8	800.23	798.31	800.95
Layer 5	798.55	800.1	798.74	799.78	798.02	800.41
Layer 6	798.56	800.03	799.28	799.69	797.9	800.27
Layer 7	799.07	800.37	800.19	800.13	798.82	800.63
Layer 8	799.88	801.03	801.4	800.92	799.94	801.37
Layer 9	800.96	802.02	802.96	802.07	801.15	802.53
Layer 10	802.37	803.41	805.31	803.75	802.56	804.17

**Table 6: Detailed Model Output Temps for Each Layer of SOXE Cell at -5C Heater Temps
(Top Heater=838.7C, Bottom Heater =836.8C), All values in degC**

	Temp (degC) Interconnect Inlet	Temp (degC) Interconnect Exit	Temp (degC) Interconnect Oxygen Outlet	Temp (degC) Interconnect Center	Temp (degC) Interconnect Center Min	Temp (degC) Interconnect Center Max
Layer 1	807.03	809.07	805.77	811.56	804.19	813.98
Layer 2	805.46	807.53	804.94	807.63	804.14	808.64
Layer 3	804.63	806.44	804.38	806.27	803.87	807.14
Layer 4	804.08	805.72	804.05	805.45	803.55	806.17
Layer 5	803.79	805.34	803.99	805.02	803.26	805.64
Layer 6	803.8	805.27	804.53	804.94	803.14	805.51
Layer 7	804.31	805.61	805.42	805.37	804.06	805.87
Layer 8	805.11	806.26	806.62	806.15	805.17	806.6
Layer 9	806.18	807.25	808.16	807.29	806.36	807.76
Layer 10	807.57	808.62	810.51	808.96	807.77	809.39

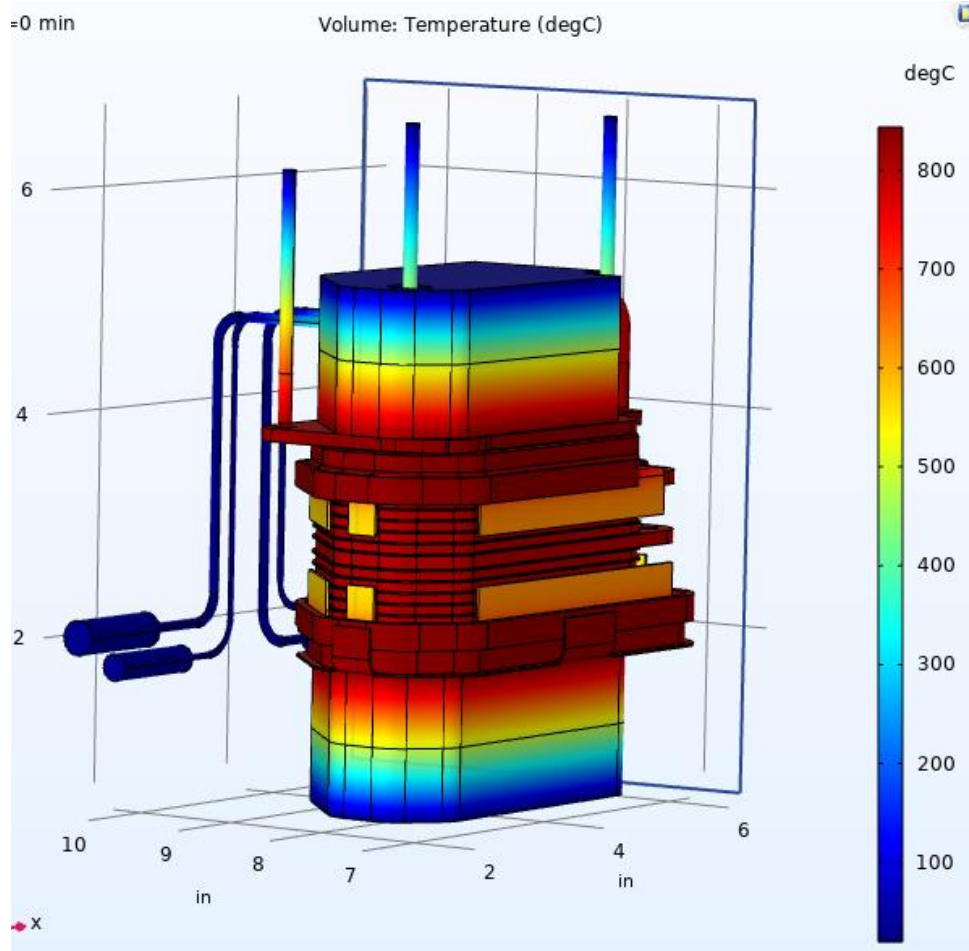
**Table 7: Detailed Model Output Temps for Each Layer of SOXE Cell at +5C Heater Temps
(Top Heater=848.7C, Bottom Heater =846.8C), All values in degC**

	Temp (degC) Interconnect Inlet	Temp (degC) Interconnect Exit	Temp (degC) Interconnect Oxygen Outlet	Temp (degC) Interconnect Center	Temp (degC) Interconnect Center Min	Temp (degC) Interconnect Center Max
Layer 1	816.96	818.99	815.68	821.51	814.1	823.94
Layer 2	815.37	817.44	814.83	817.54	814.04	818.56
Layer 3	814.51	816.33	814.24	816.16	813.76	817.04
Layer 4	813.95	815.59	813.9	815.32	813.41	816.05
Layer 5	813.65	815.19	813.83	814.87	813.11	815.5
Layer 6	813.65	815.12	814.37	814.78	812.99	815.36
Layer 7	814.17	815.46	815.29	815.22	813.91	815.72
Layer 8	814.98	816.13	816.51	816.02	815.04	816.47
Layer 9	816.08	817.13	818.09	817.19	816.26	817.64
Layer 10	817.5	818.53	820.46	818.88	817.69	819.3

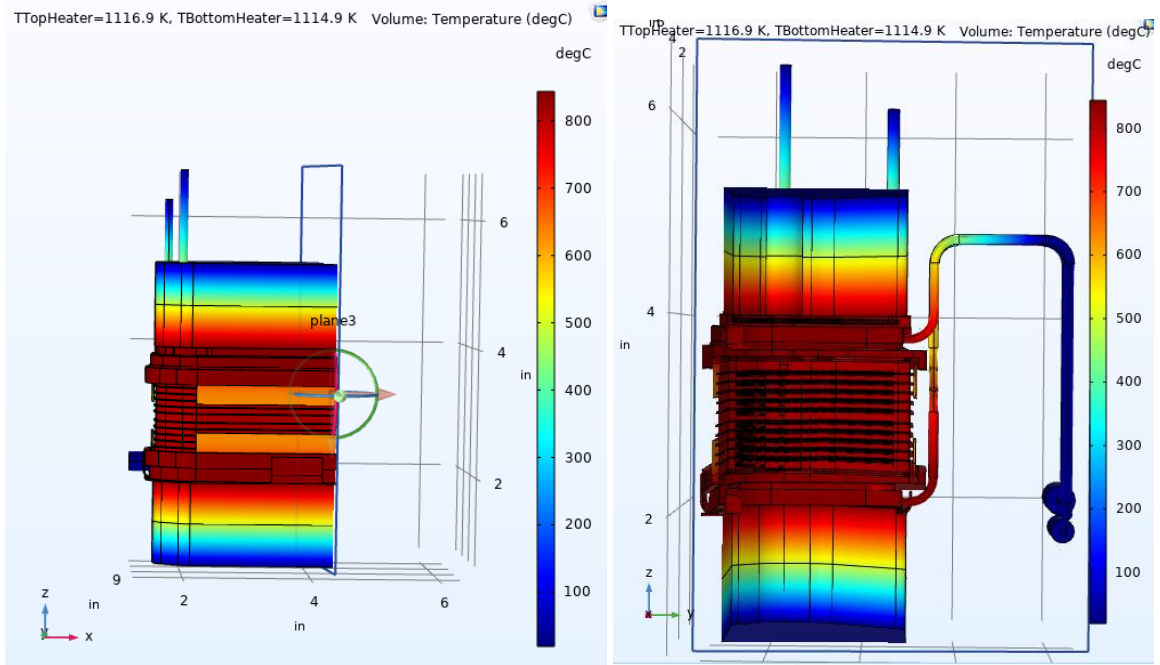
**Table 8: Detailed Model Output Temps for Each Layer of SOXE Cell at +10C Heater Temps
(Top Heater=853.7C, Bottom Heater =851.8C), All values in degC**

	Temp (degC) Interconnect Inlet	Temp (degC) Interconnect Exit	Temp (degC) Interconnect Oxygen Outlet	Temp (degC) Interconnect Center	Temp (degC) Interconnect Center Min	Temp (degC) Interconnect Center Max
Layer 1	822	824.01	820.72	826.55	819.16	828.98
Layer 2	820.4	822.45	819.82	822.56	819.07	823.56
Layer 3	819.5	821.31	819.19	821.14	818.74	822.01
Layer 4	818.9	820.53	818.8	820.26	818.36	820.99
Layer 5	818.57	820.1	818.72	819.77	818.02	820.41
Layer 6	818.55	820.01	819.28	819.67	817.89	820.26
Layer 7	819.09	820.36	820.23	820.12	818.83	820.63
Layer 8	819.93	821.05	821.5	820.95	820	821.41
Layer 9	821.07	822.08	823.12	822.16	821.25	822.61
Layer 10	822.53	823.51	825.51	823.89	822.72	824.3

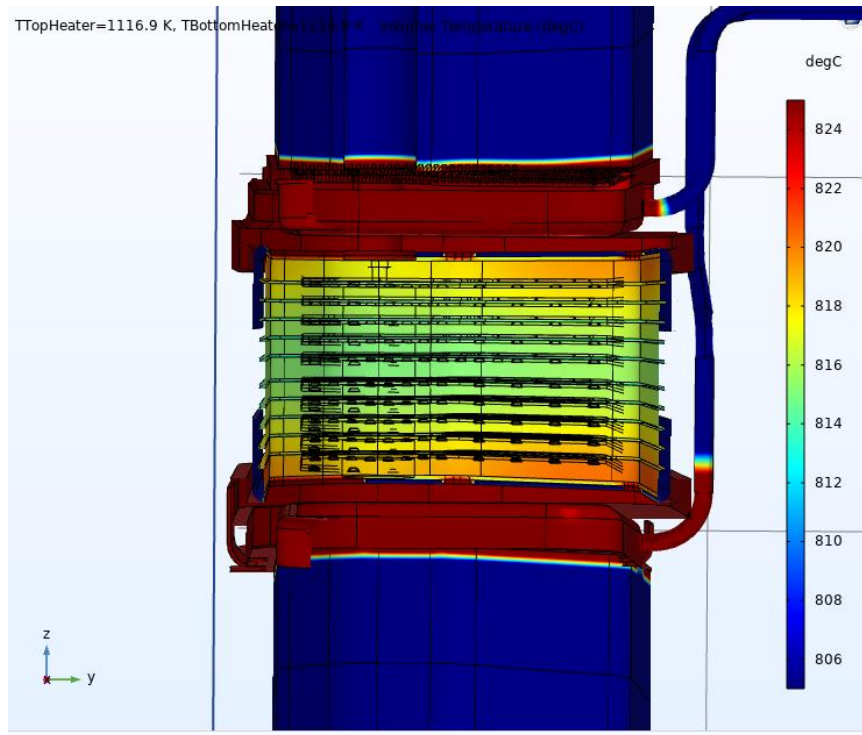
3D Temperatures Plots



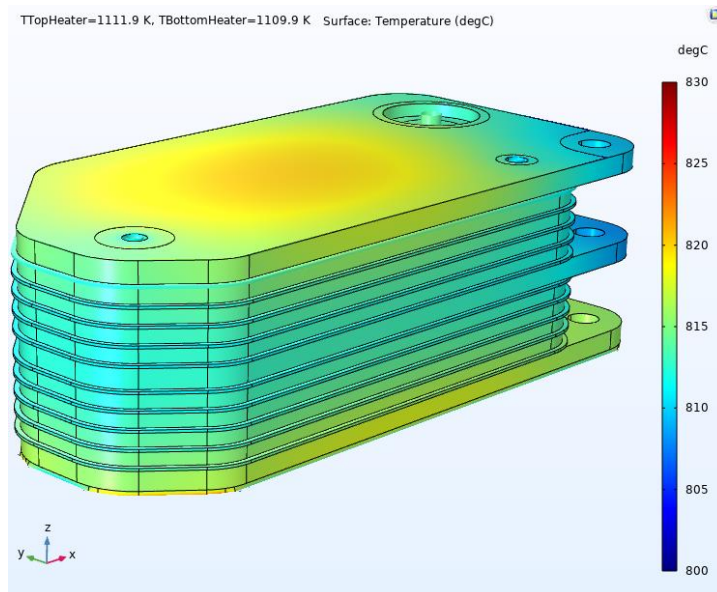
Overall Stack Assembly Temperatures



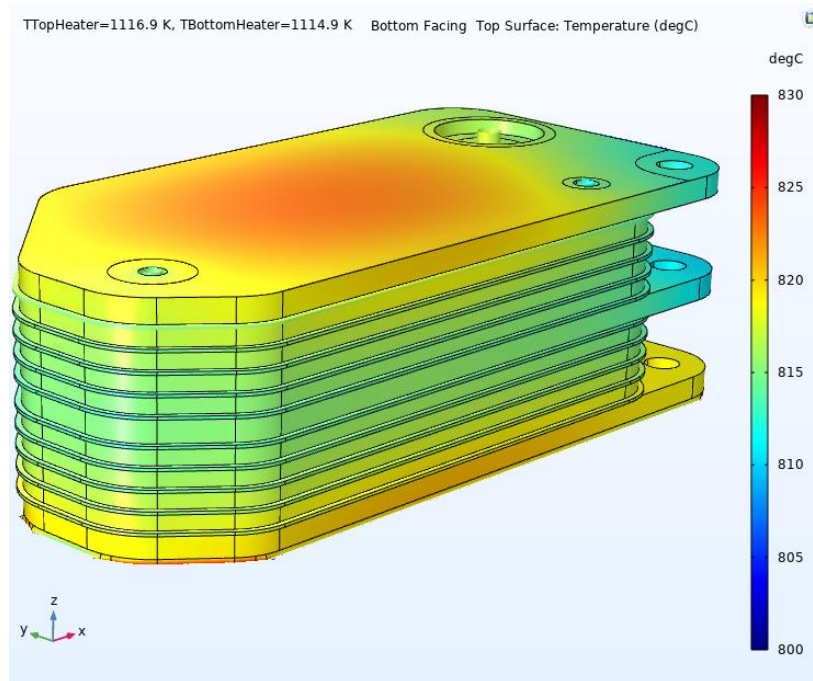
Plane 3, Cross-section for Volume Temp Z-Y



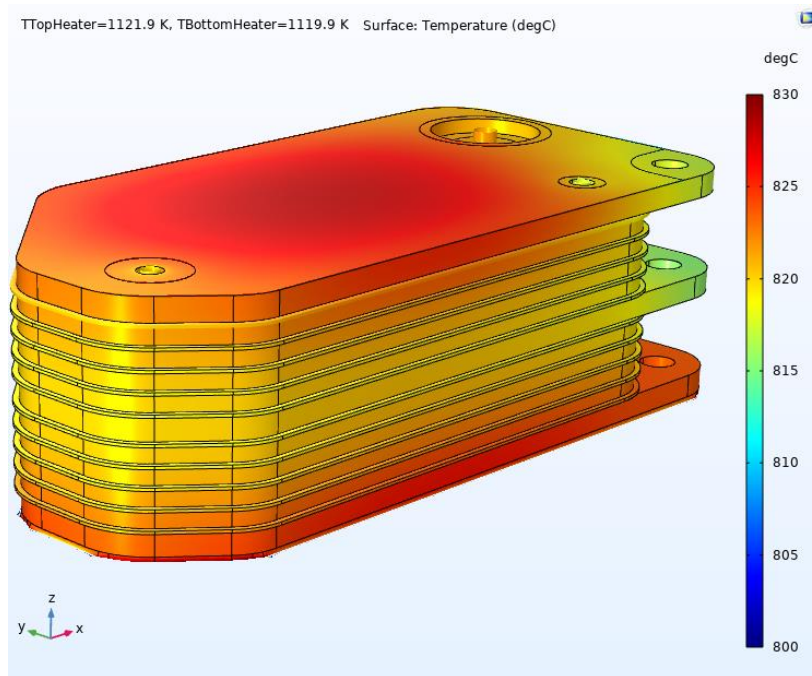
Plane 3 Adjusted Temperature Range to View Temperature profile



Overall Stack Temperature, Heater Delta T = -5C



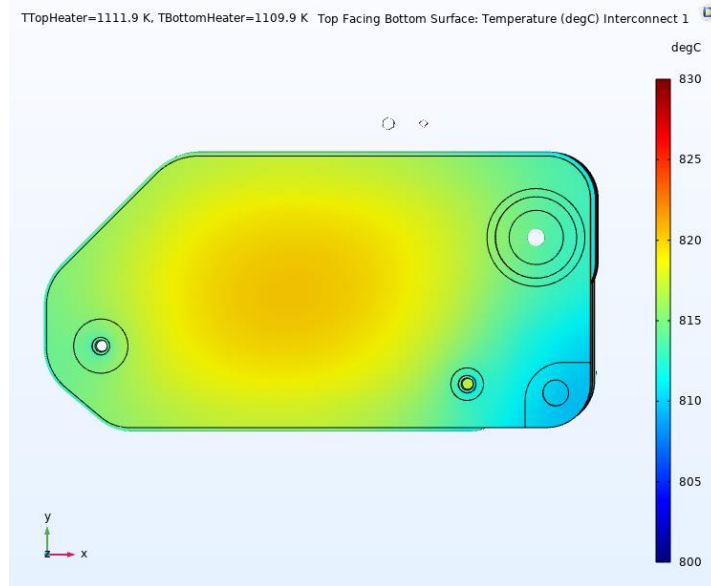
Overall Stack Temperature, Heater Delta T = 0C



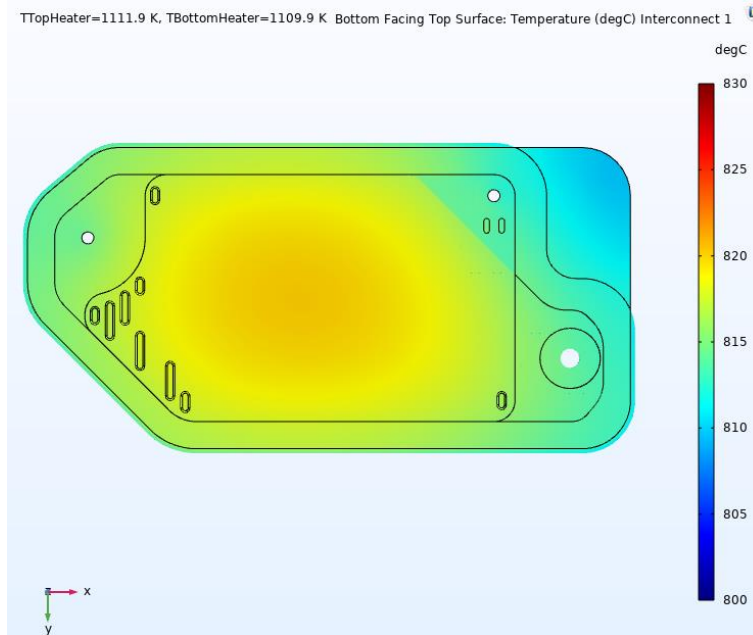
Overall Stack Temperature, Heater Delta T = +5C

INTERCONNECTS

INTERCONNECT 1: Bottom Heater=838.7C, Top Heater= 836.8C

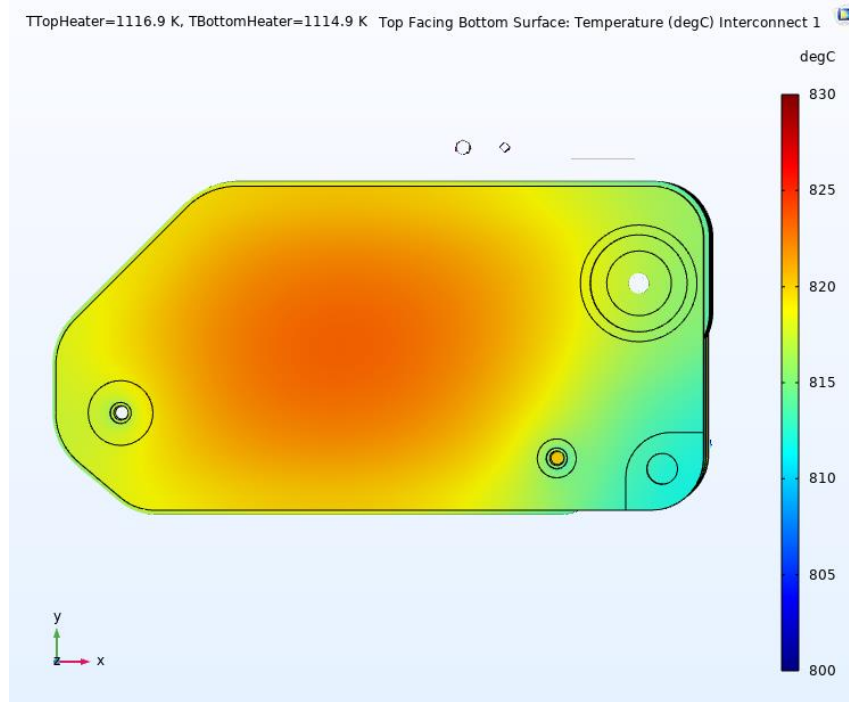


Delta = -5C Top Facing Bottom , Interconnect 1

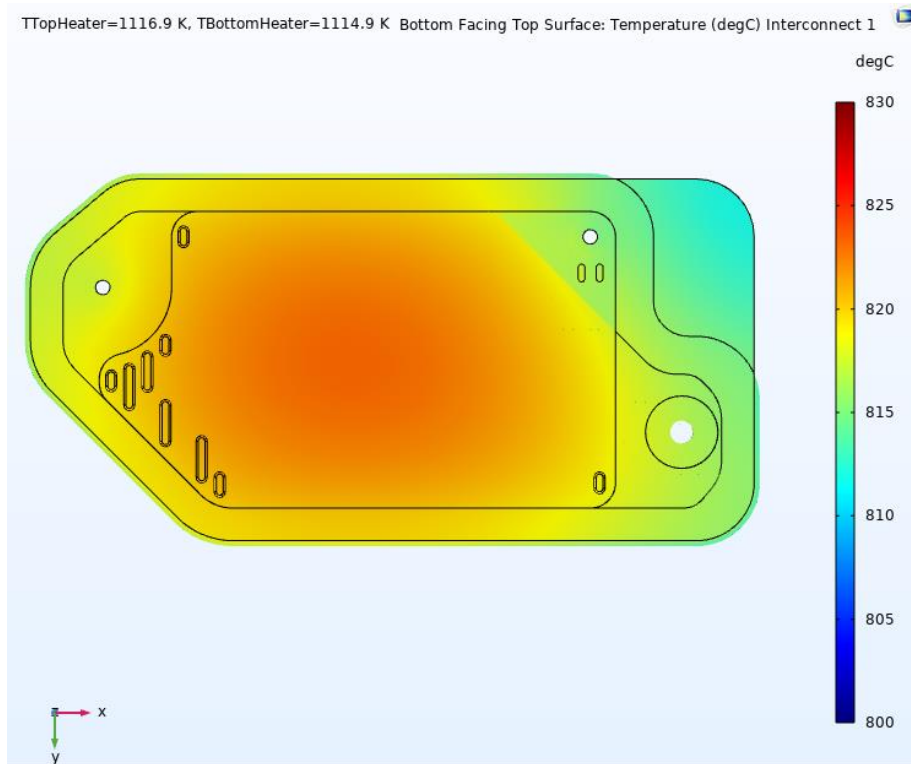


Delta T = -5C Interconnect 1 Bottom Facing Top

INTERCONNECT 1: Bottom Heater=843.7C, Top Heater= 841.8C

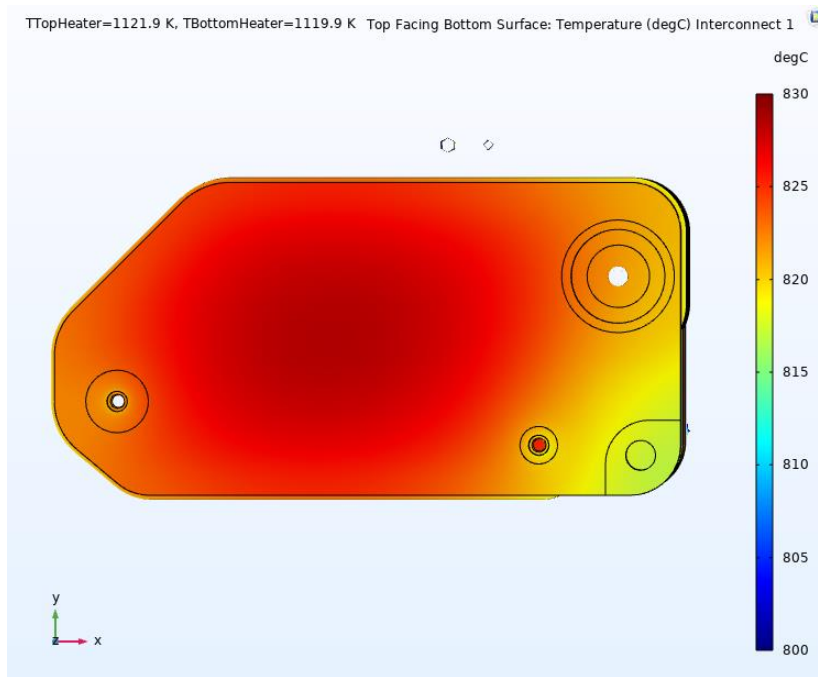


Interconnect 1 Delta =0C Top Facing Bottom

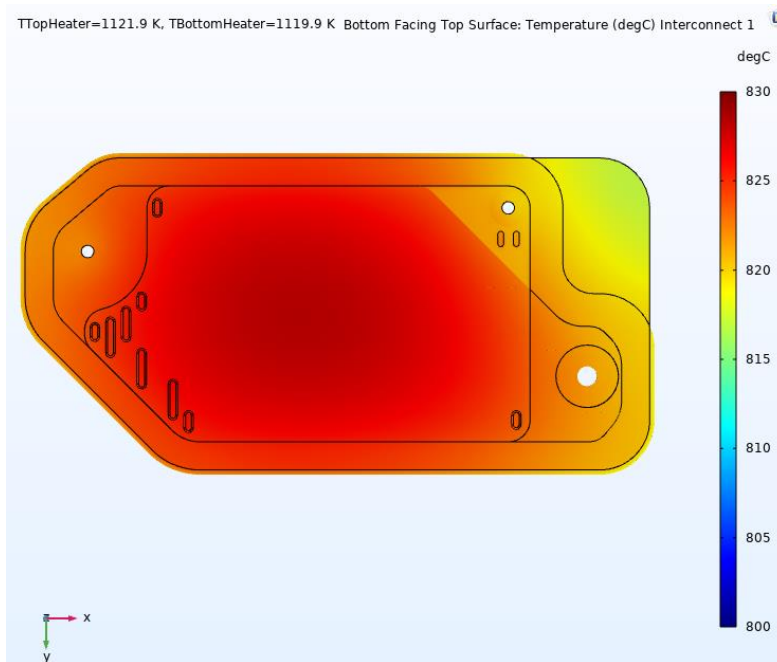


Delta T = 0C Interconnect 1 Bottom Facing Top

INTERCONNECT 1: Bottom Heater=848.7C, Top Heater= 846.8C

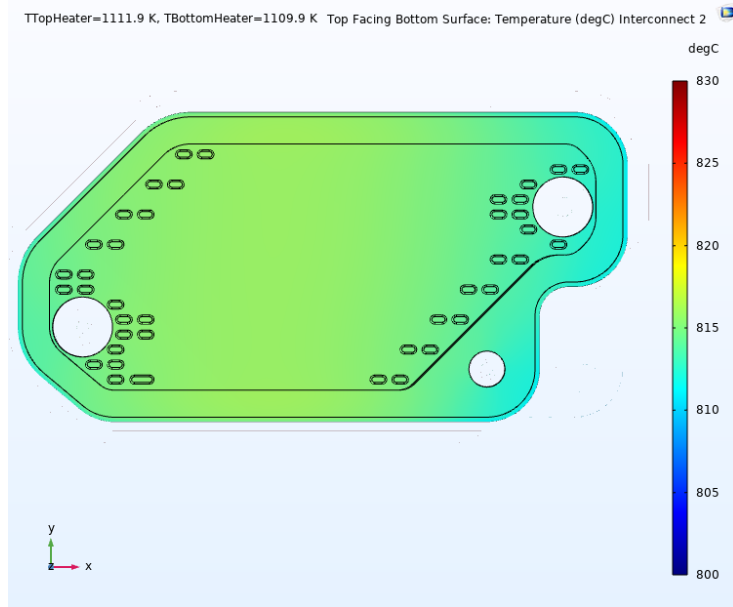


Delta T = +5C Interconnect 1 Top Facing Bottom

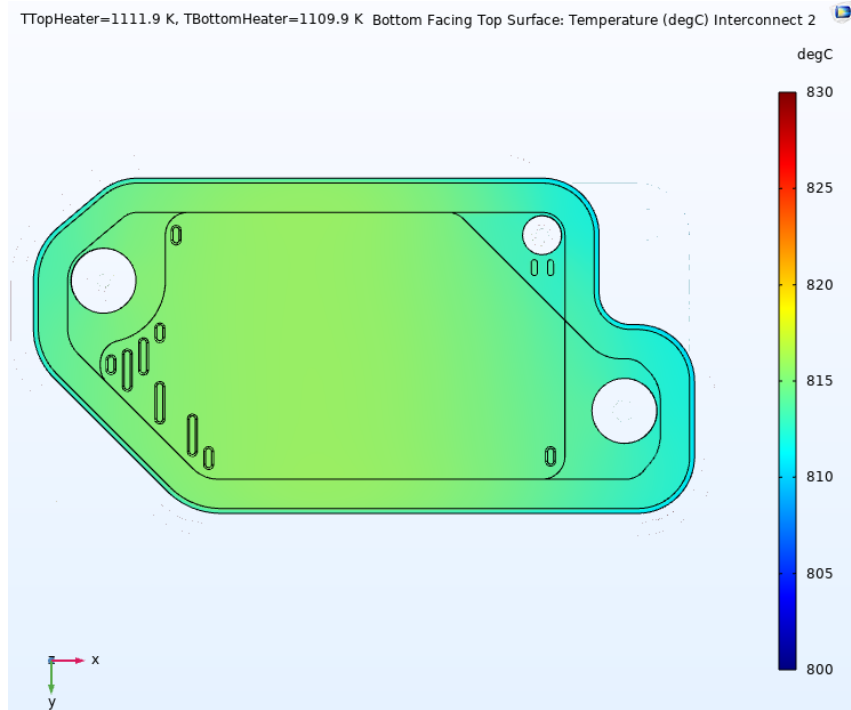


Delta T = +5C Interconnect 1 Bottom Facing Top

INTERCONNECT 2: Bottom Heater=838.7C, Top Heater= 836.8C

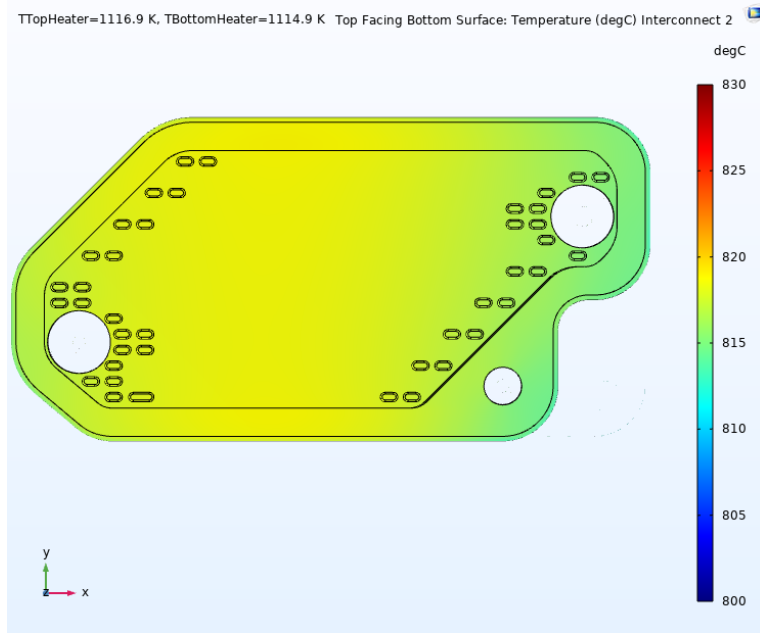


Delta T = -5C Interconnect 2, Top Facing Bottom

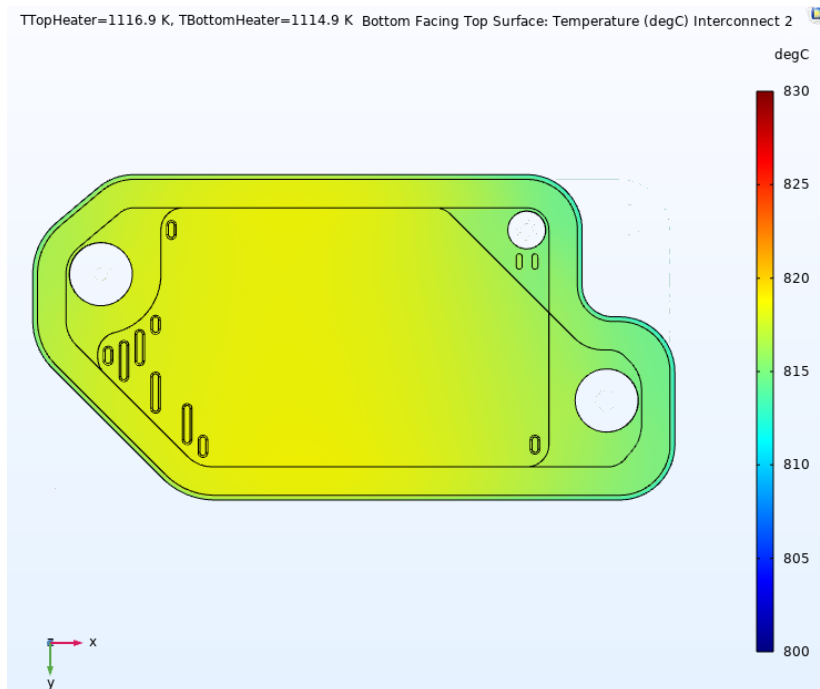


Delta T = -5C Interconnect 2 Bottom Facing Top

INTERCONNECT 2: Bottom Heater=843.7C, Top Heater= 841.8C

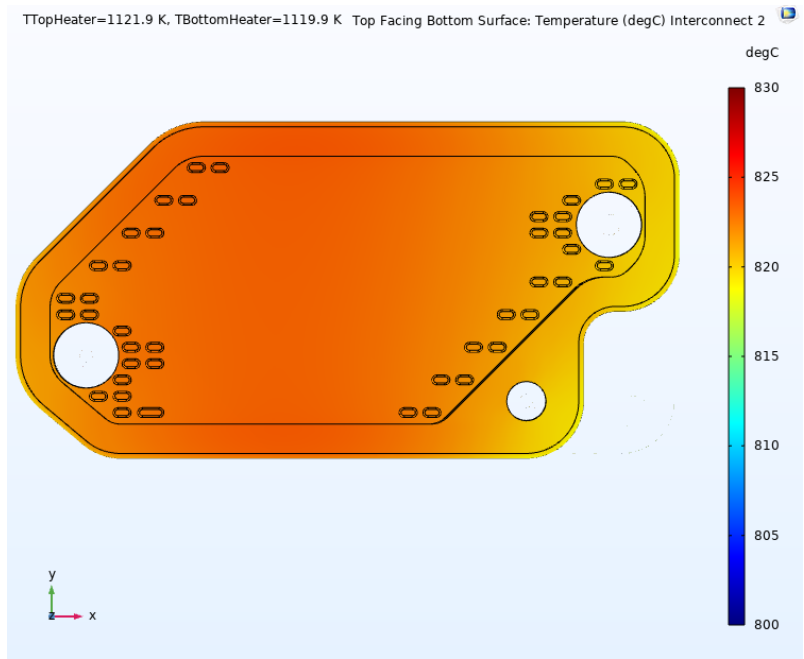


Delta T = 0C Interconnect 2 Top Facing Bottom

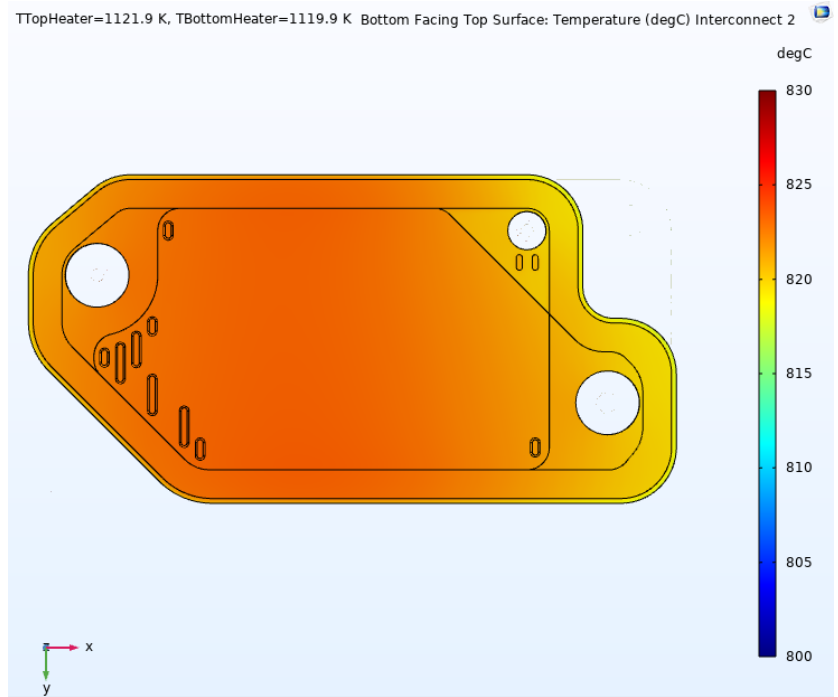


Delta T = 0C Interconnect 2 Bottom Facing Top

INTERCONNECT 2: Bottom Heater=848.7C, Top Heater= 846.8C

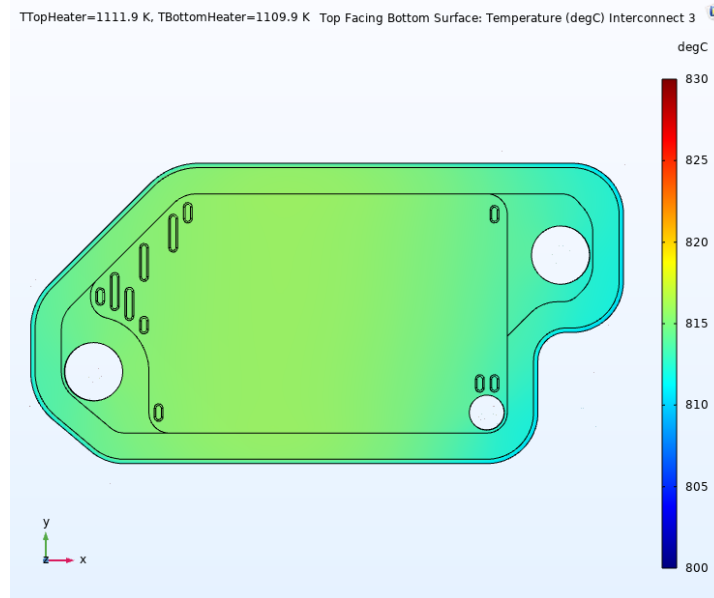


Delta T = +5C Interconnect 2, Top Facing Bottom

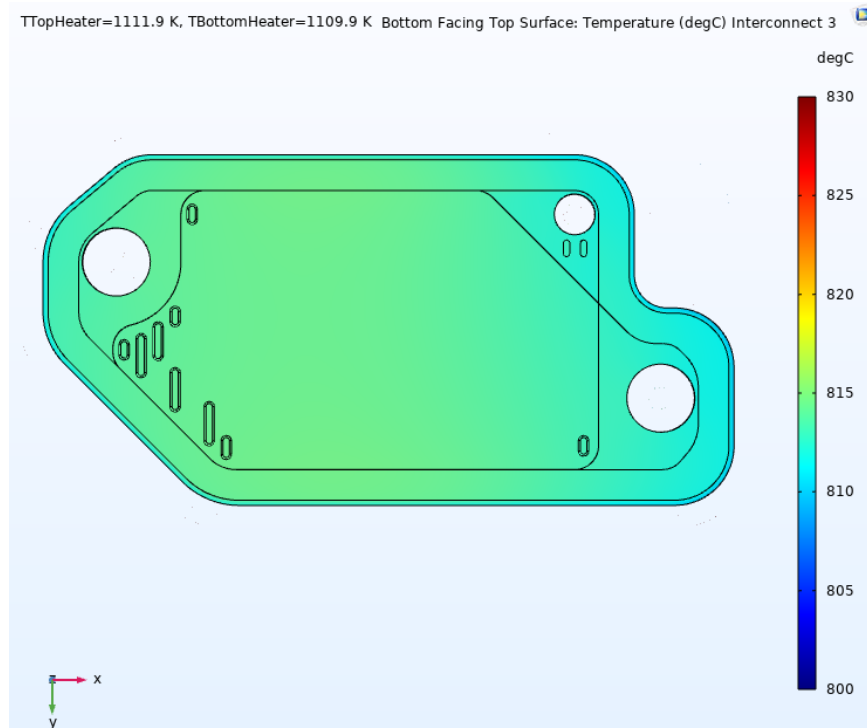


Delta T = +5C Interconnect 2 Bottom Facing Top

Interconnect 3: Bottom Heater=838.7C, Top Heater= 836.8C

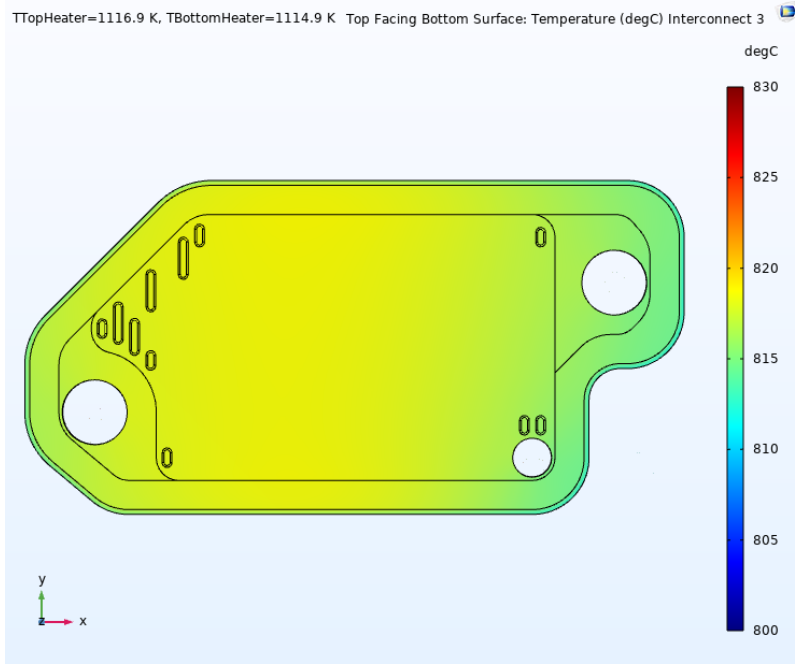


Delta T = -5C Interconnect 3 Top Facing Bottom

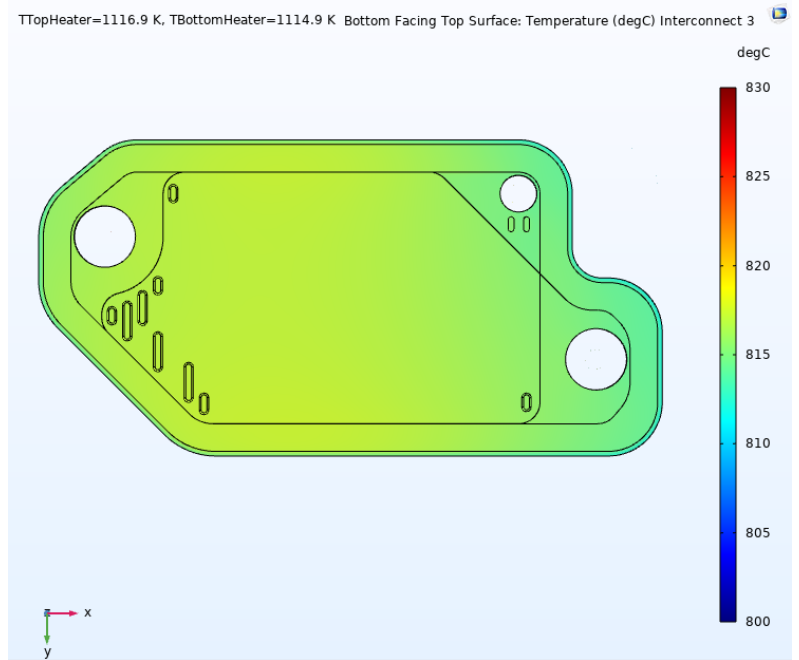


Delta T = -5C Interconnect 3 Bottom Facing Top

INTERCONNECT 3: Bottom Heater=843.7C, Top Heater= 841.8C

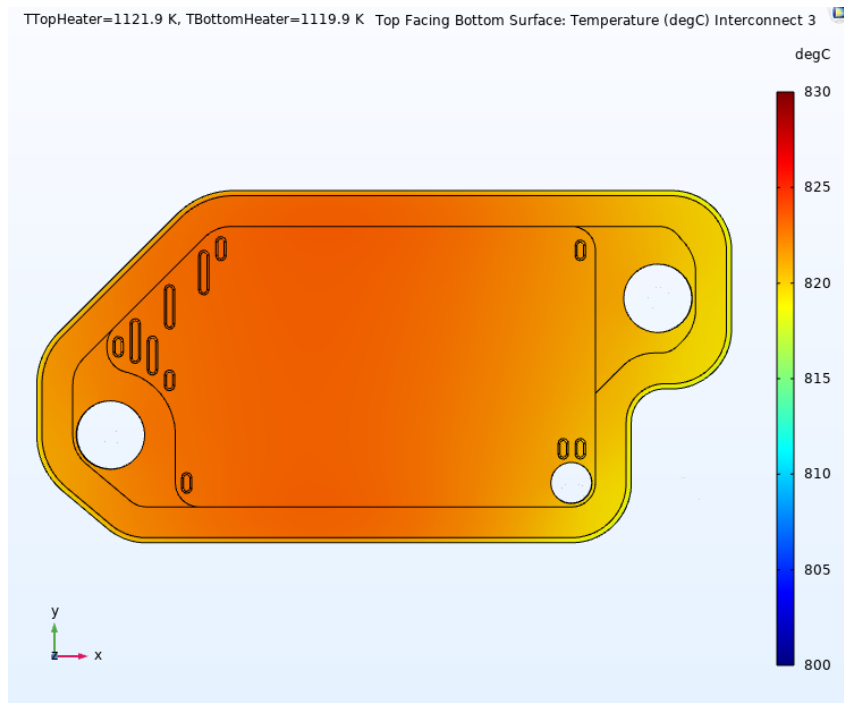


Delta T = 0 Interconnect 3 Top Facing Bottom

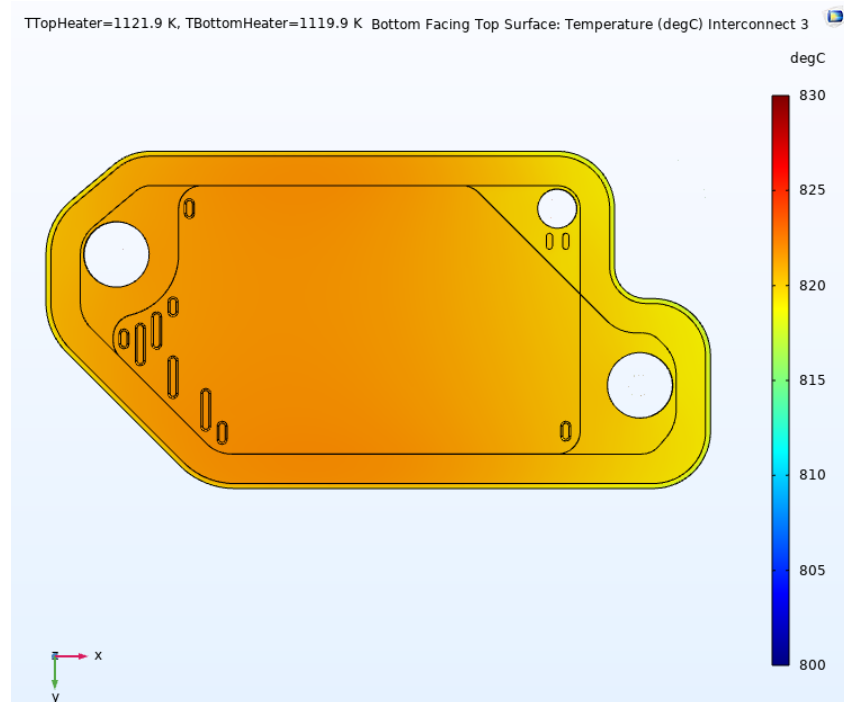


Delta T = 0C Interconnect 3 Bottom Facing Top

INTERCONNECT 3: Bottom Heater=848.7C, Top Heater= 846.8C

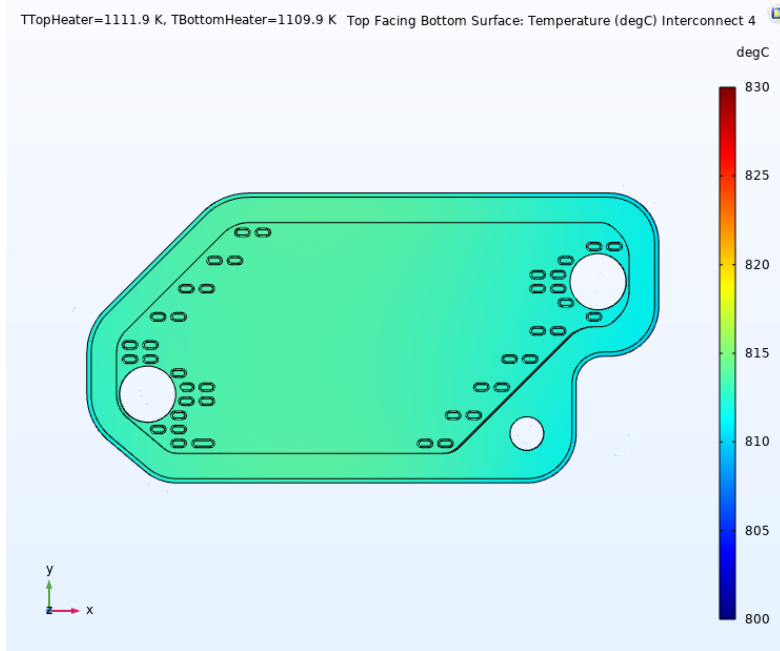


Delta T = +5C Interconnect 3 Top Facing Bottom

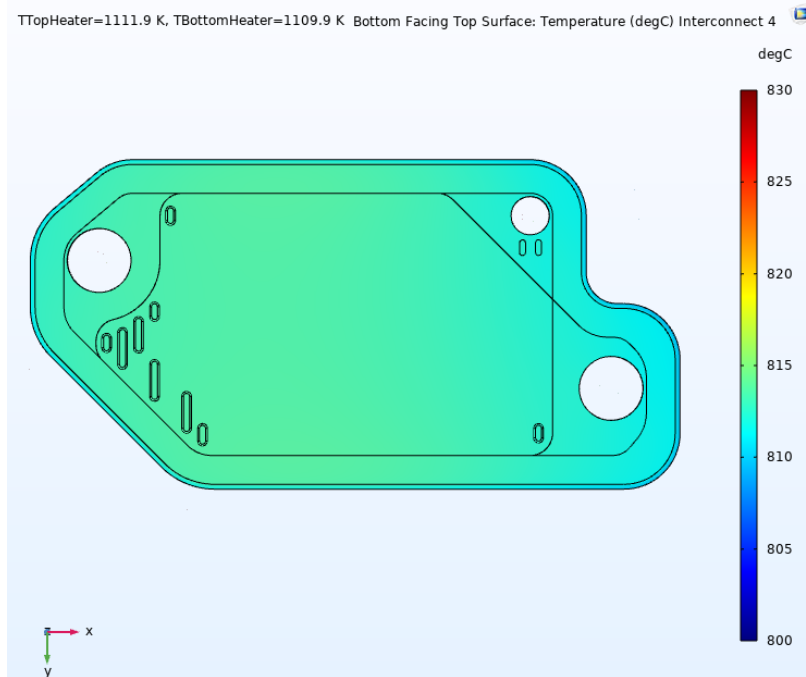


Delta T = +5C Interconnect 3 Bottom Facing Top

Interconnect 4: Bottom Heater=838.7C, Top Heater= 836.8C

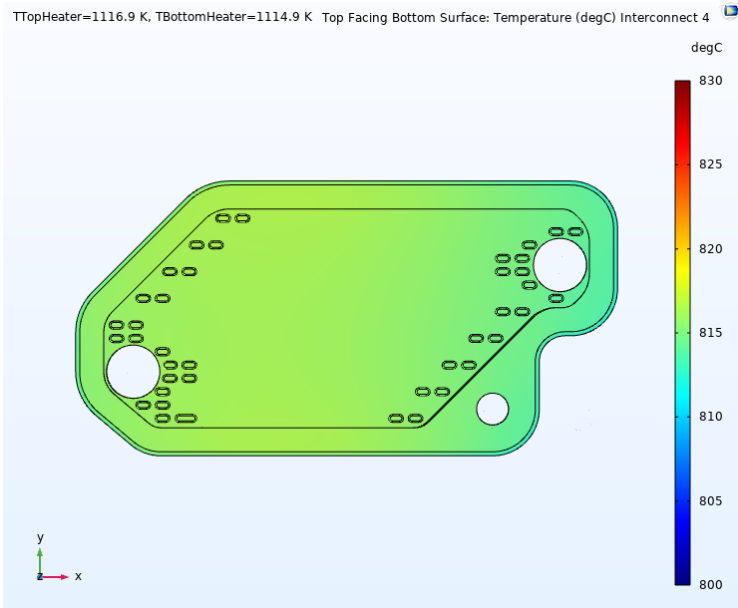


Delta T = -5C Interconnect 4 Top Facing Bottom

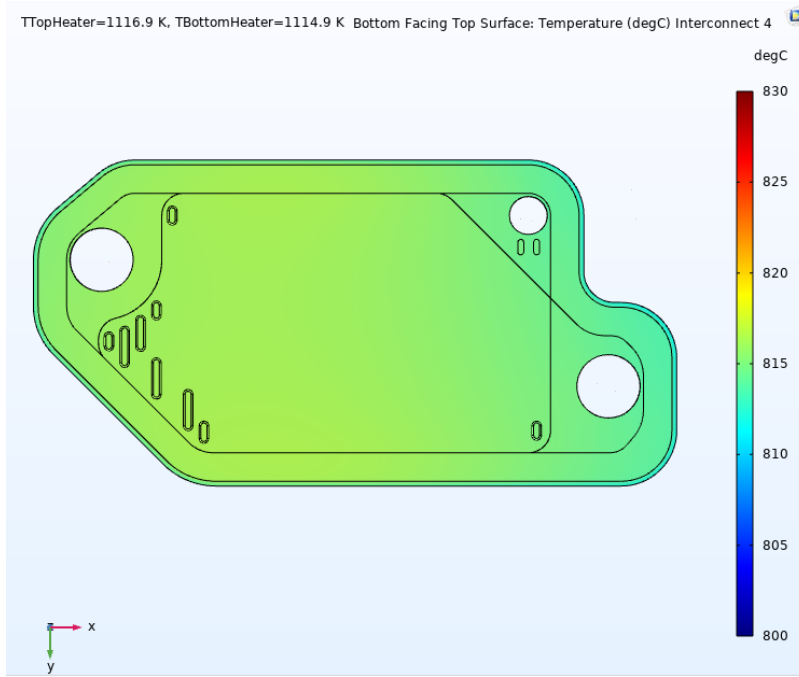


Delta T = -5C Interconnect 4 Bottom Facing Top

INTERCONNECT 4: Bottom Heater=843.7C, Top Heater= 841.8C

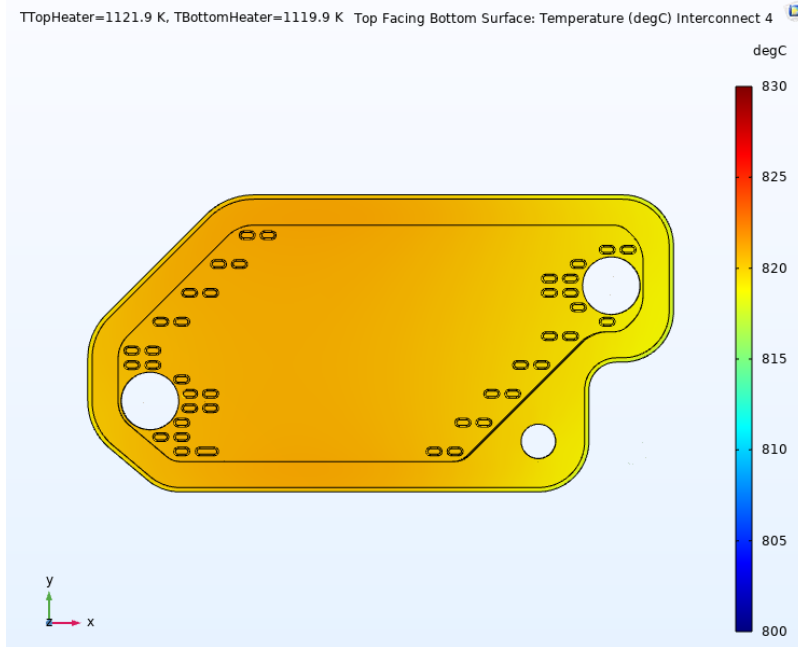


Delta T = 0C Interconnect 4 Top Facing Bottom

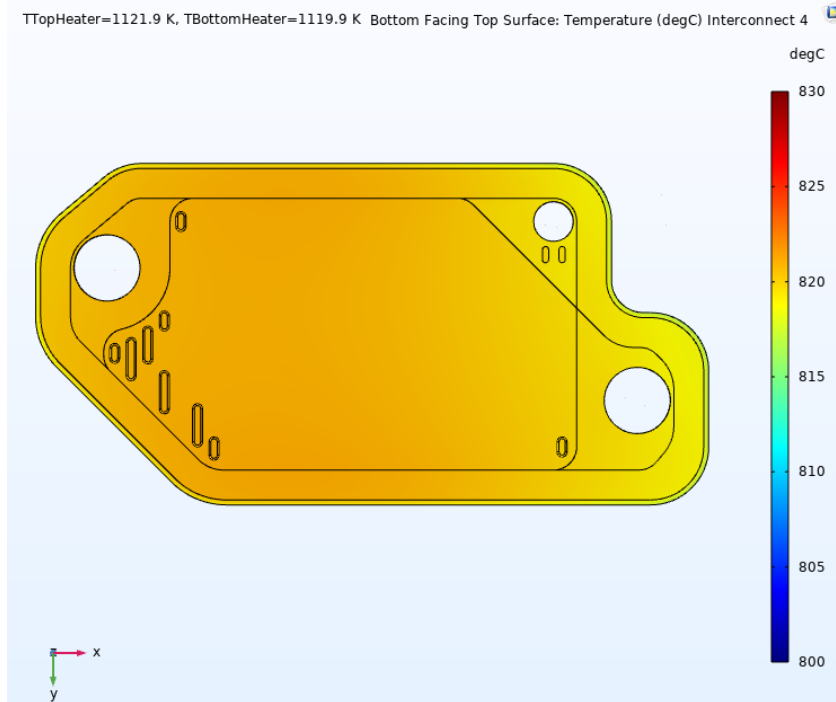


Delta T = 0C Interconnect 4 Bottom Facing Top

INTERCONNECT 4: Bottom Heater=848.7C, Top Heater= 846.8C

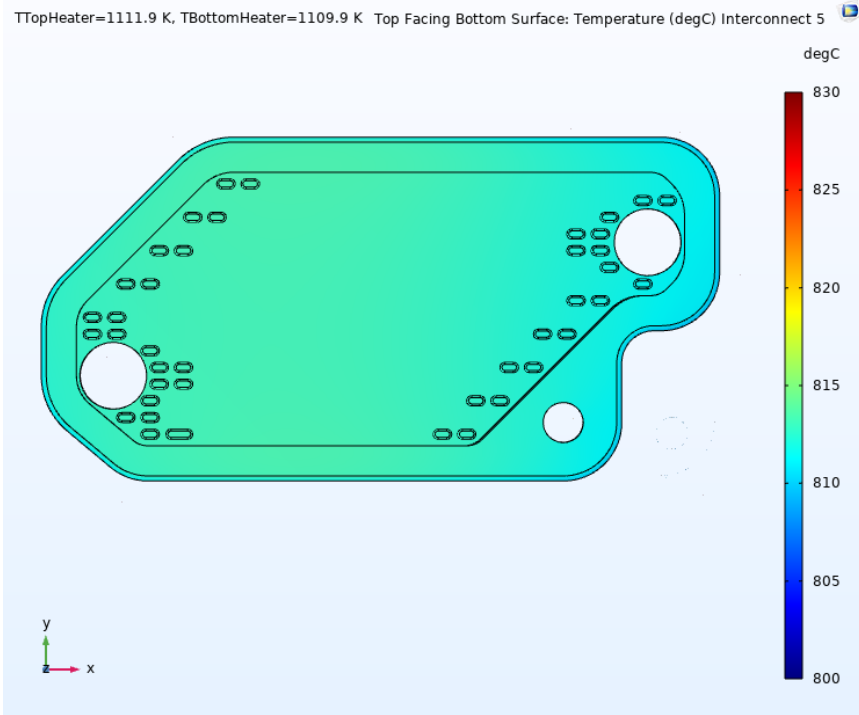


Delta T = +5C Interconnect 4 Top Facing Bottom

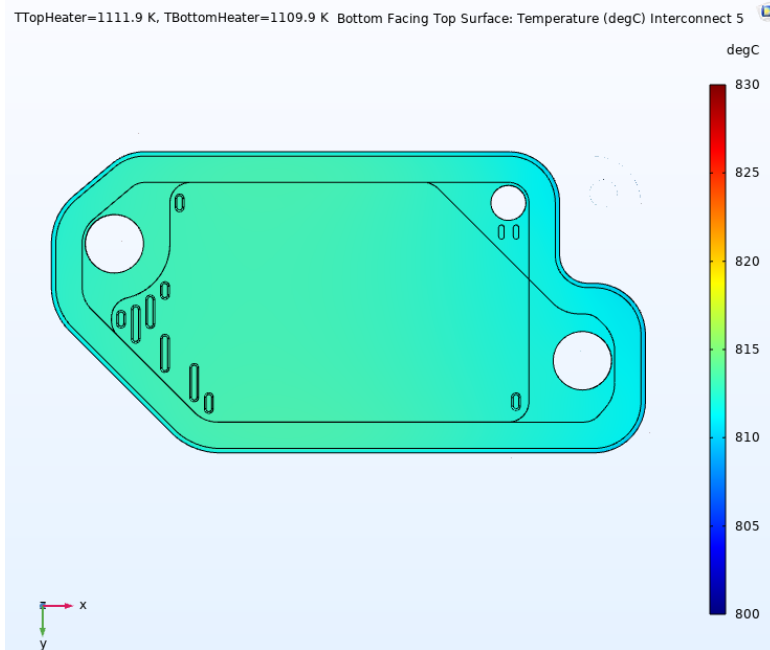


Delta T = +5C Interconnect 4 Bottom Facing Top

Interconnect 5: Bottom Heater=838.7C, Top Heater= 836.8C

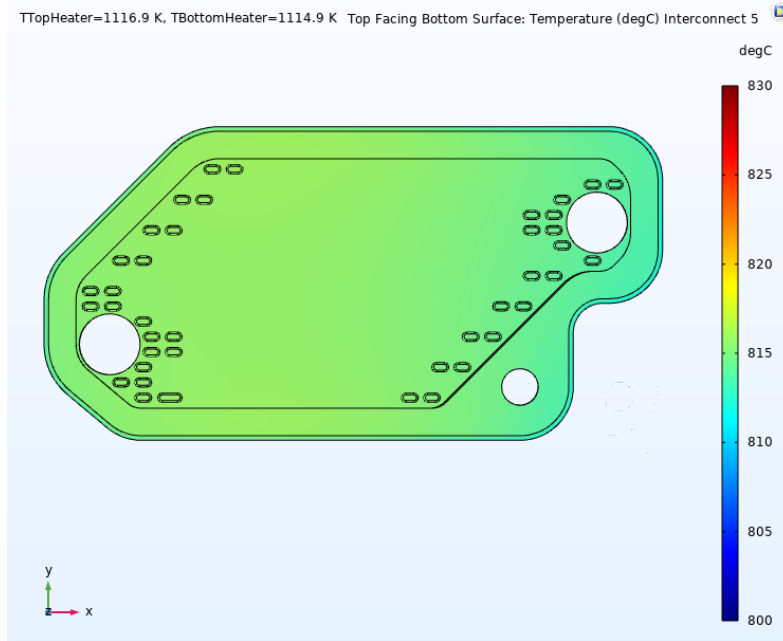


Delta T = -5C Interconnect 5 Top Facing Bottom

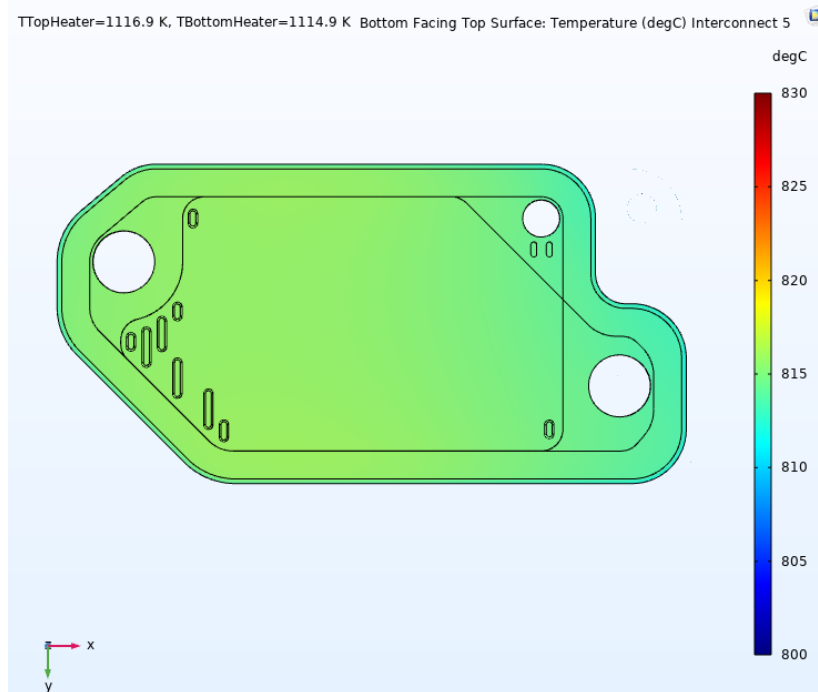


Delta T = -5C Interconnect 5 Bottom Facing Top

INTERCONNECT 5: Bottom Heater=843.7C, Top Heater= 841.8C

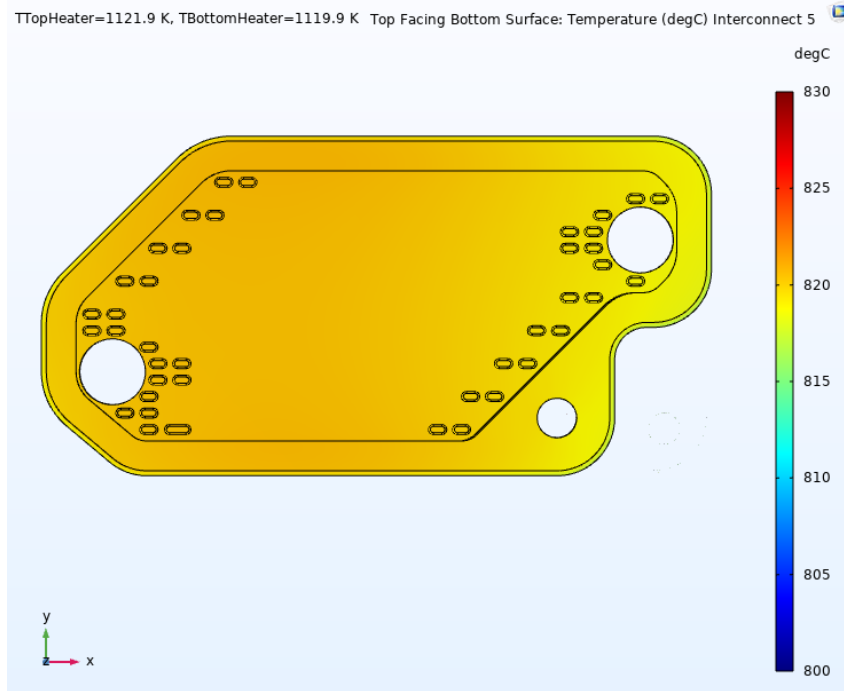


Delta T = 0C Interconnect 5 Top Facing Bottom

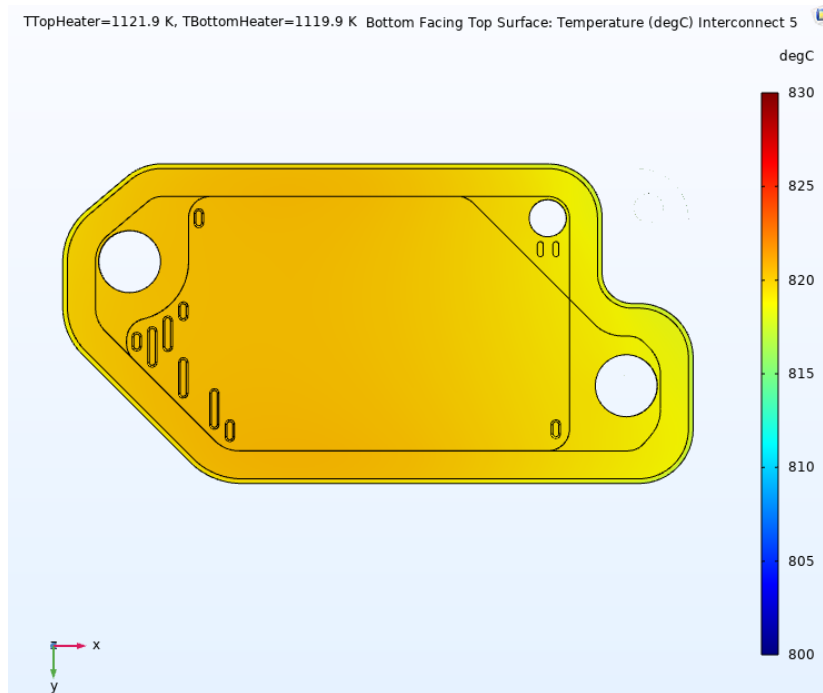


Delta T = 0C Interconnect 5 Bottom Facing Top

INTERCONNECT 5: Bottom Heater=848.7C, Top Heater= 846.8C



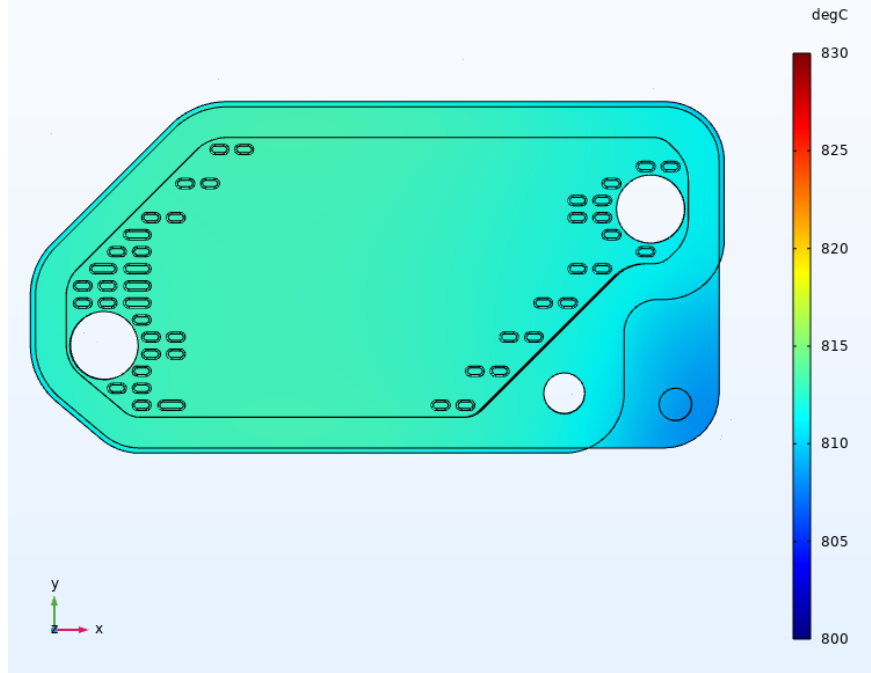
Delta T = +5C Interconnect 5 Top Facing Bottom



Delta T = +5C Interconnect 5 Bottom Facing Top

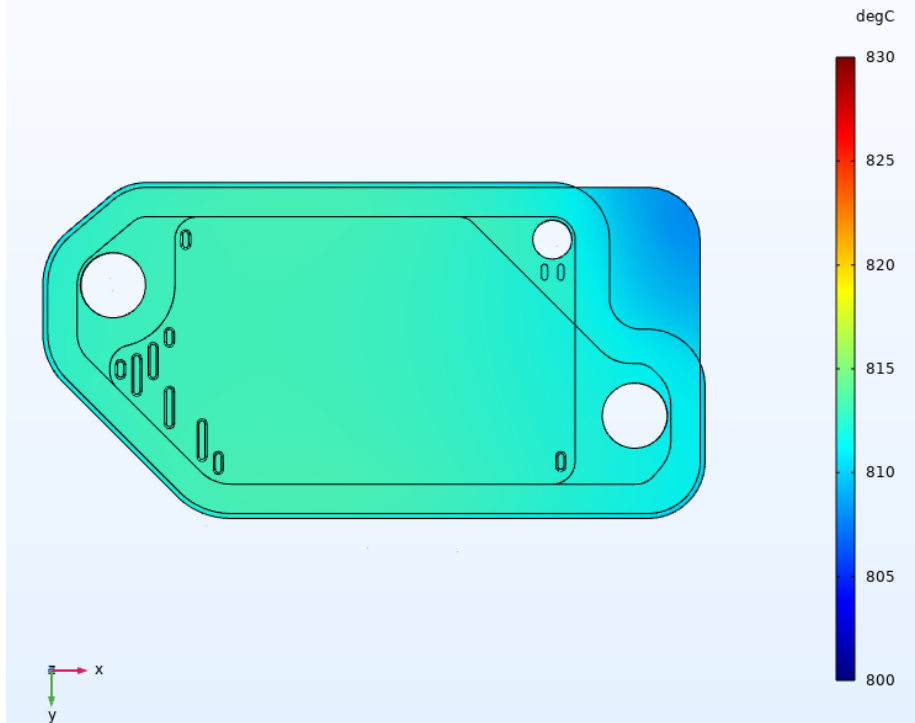
Interconnect 6: Bottom Heater=838.7C, Top Heater= 836.8C

TTopHeater=1111.9 K, TBottomHeater=1109.9 K Top Facing Bottom Surface: Temperature (degC) Interconnect 6



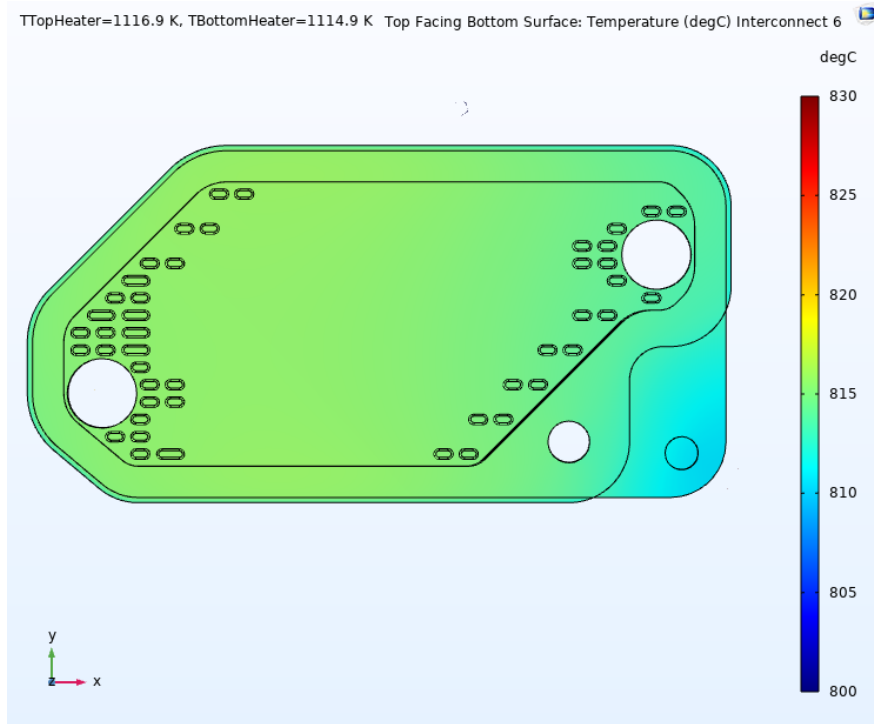
Delta T = -5C Interconnect 6 Top Facing Bottom

TTopHeater=1111.9 K, TBottomHeater=1109.9 K Bottom Facing Top Surface: Temperature (degC) Interconnect 6

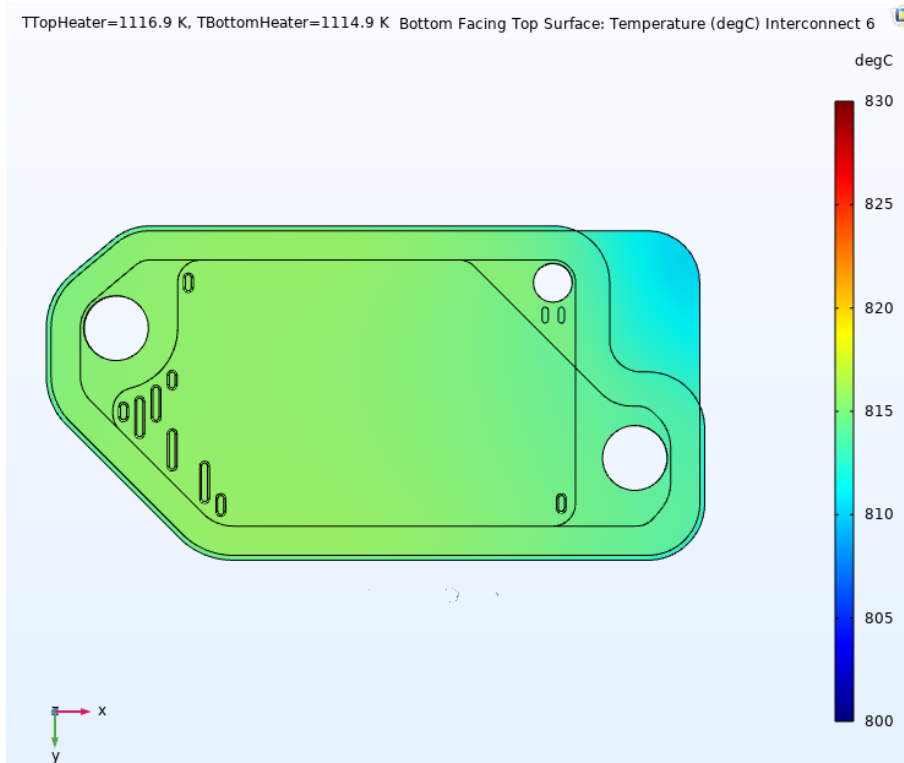


Delta T = -5C Interconnect 6 Bottom Facing Top

INTERCONNECT 6: Bottom Heater=843.7C, Top Heater= 841.8C

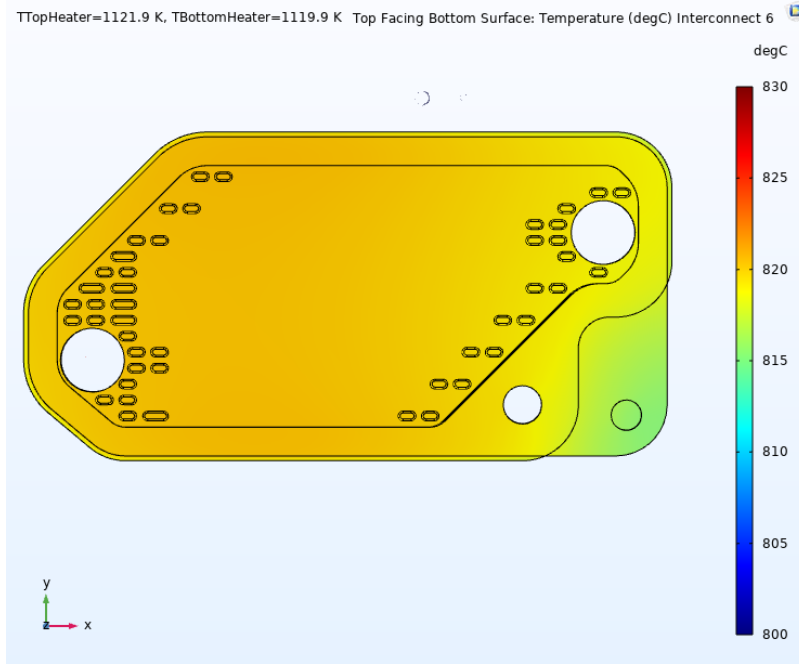


Delta T = 0C Interconnect 6 Top Facing Bottom

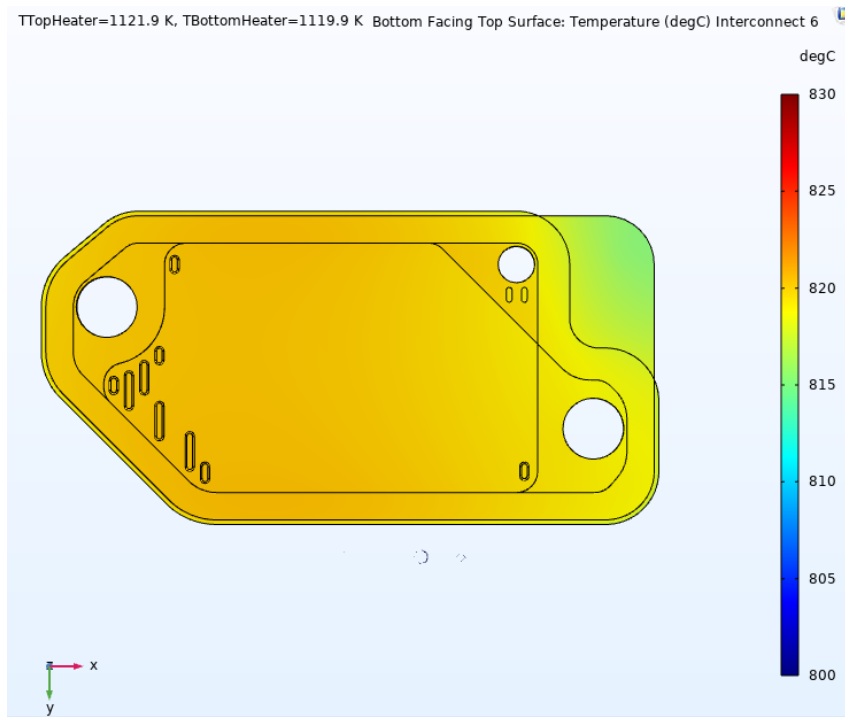


Delta T = 0C Interconnect 6 Bottom Facing Top

INTERCONNECT 6: Bottom Heater=848.7C, Top Heater= 846.8C

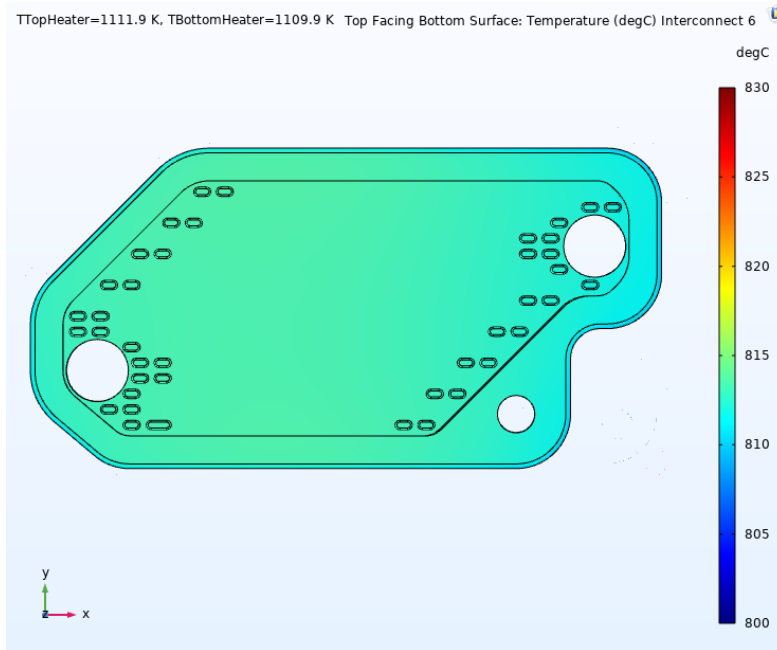


Delta T = +5C Interconnect 6 Top Facing Bottom



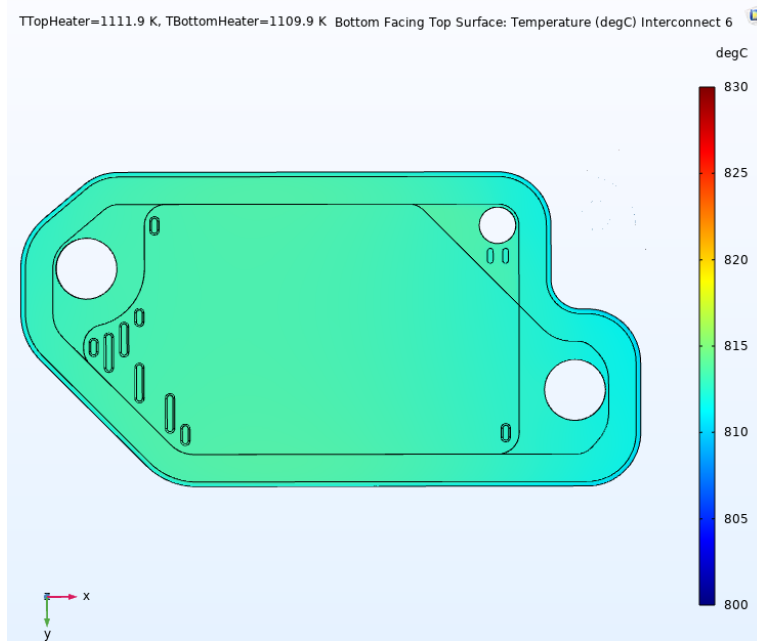
Delta T = +5C Interconnect 6 Bottom Facing Top

Interconnect 7: Bottom Heater=838.7C, Top Heater= 836.8C



Interconnect 7

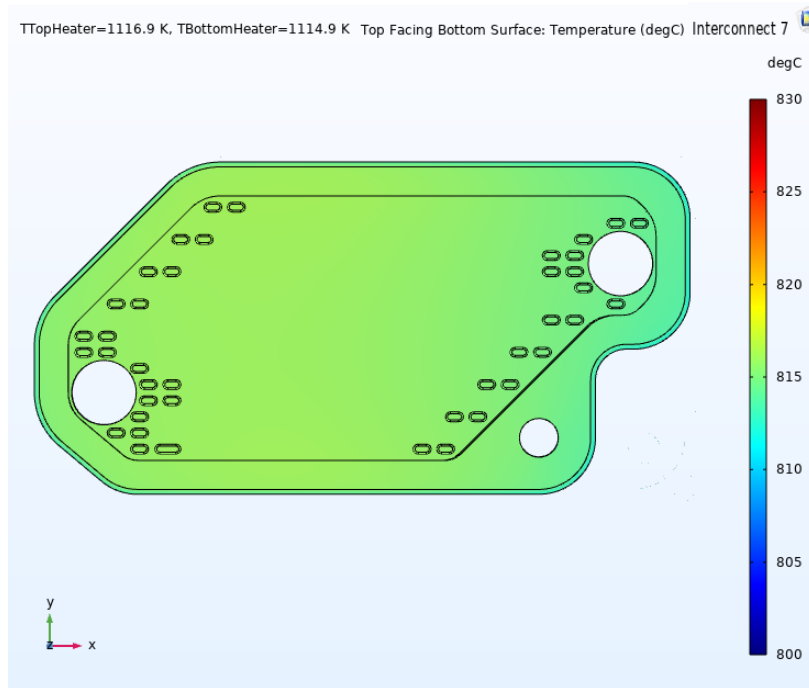
Delta T = -5C Interconnect 7 Top Facing Bottom



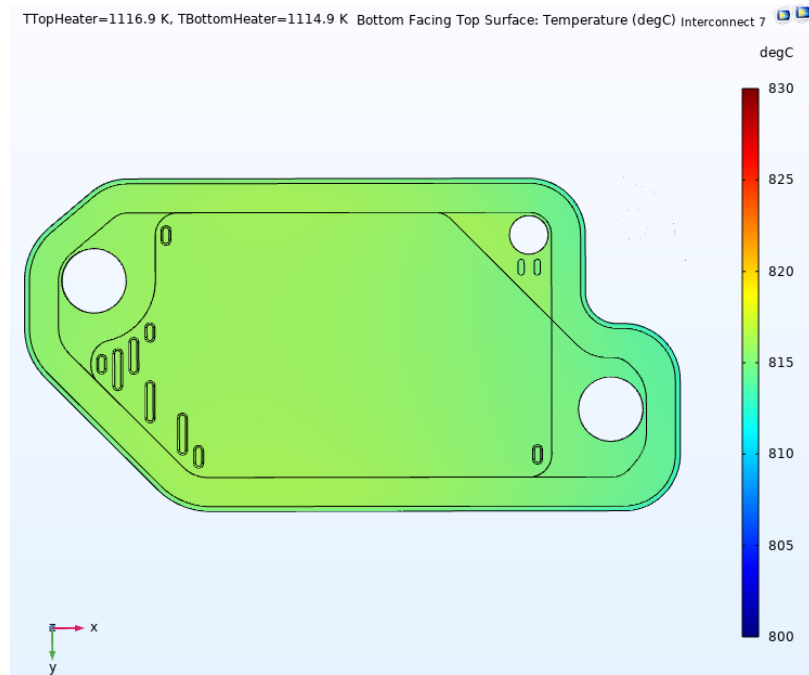
Interconnect 7

Delta T = -5C Interconnect 7 Bottom Facing Top

INTERCONNECT 7: Bottom Heater=843.7C, Top Heater= 841.8C

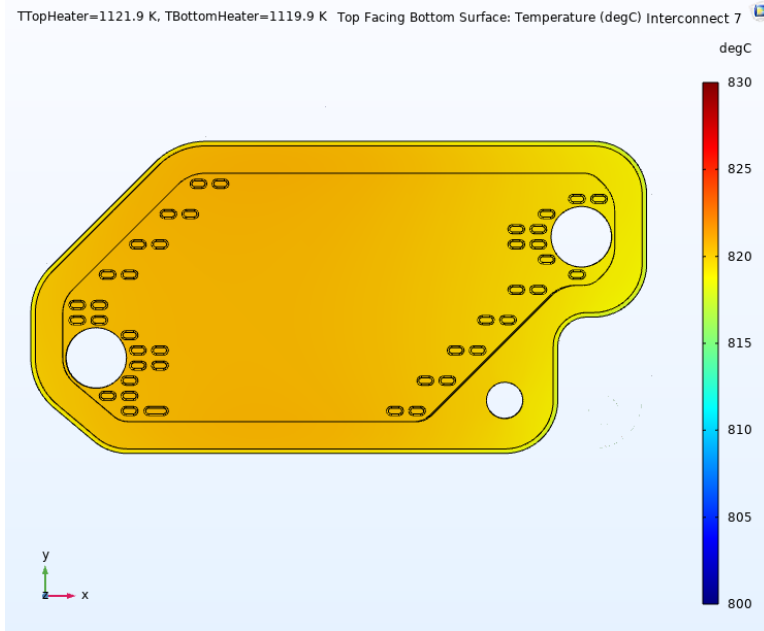


Delta T = 0C Interconnect 7 Top Facing Bottom

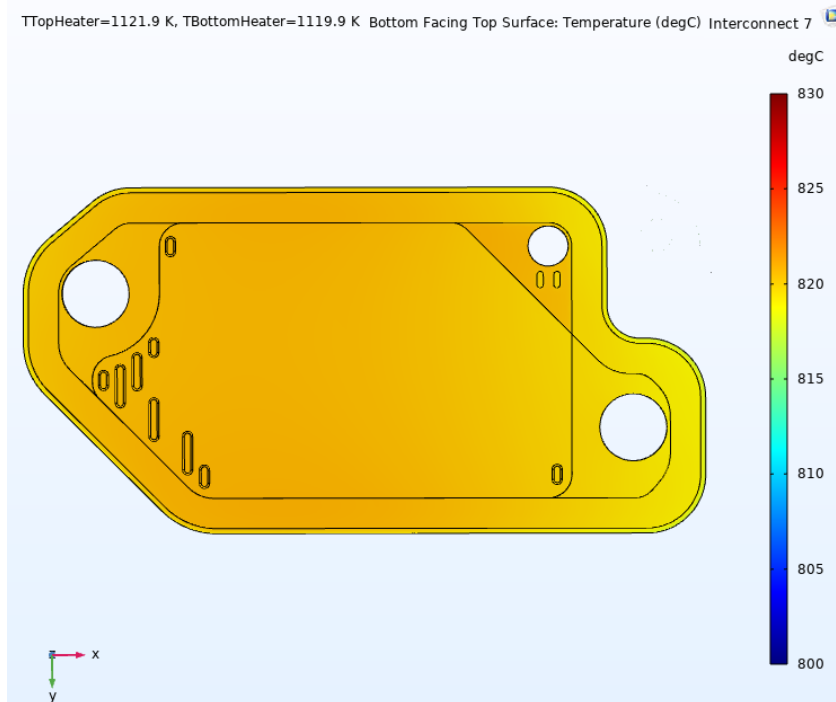


Delta T = 0C Interconnect 7 Bottom Facing Top

INTERCONNECT 7: Bottom Heater=848.7C, Top Heater= 846.8C

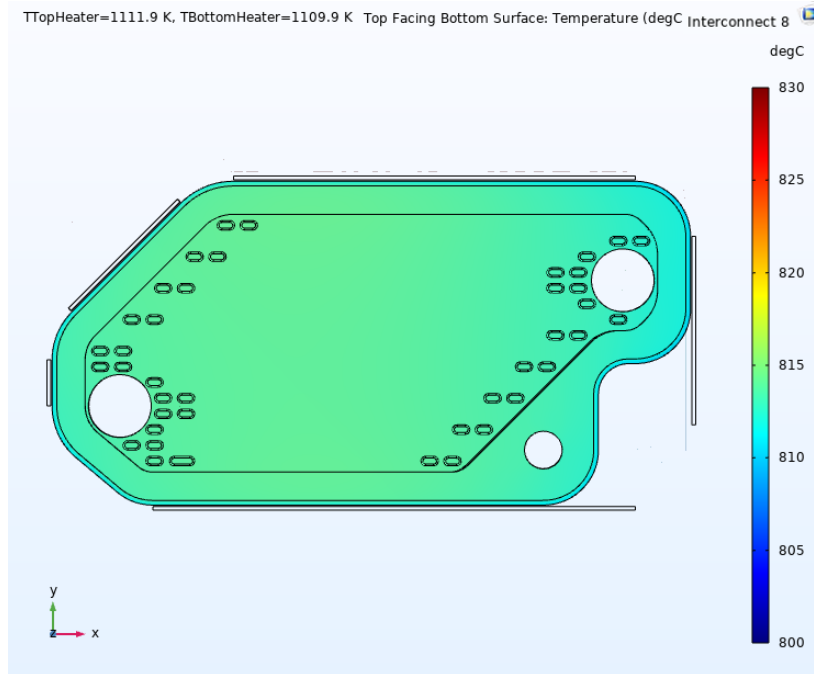


Delta T = +5C Interconnect 7 Top Facing Bottom

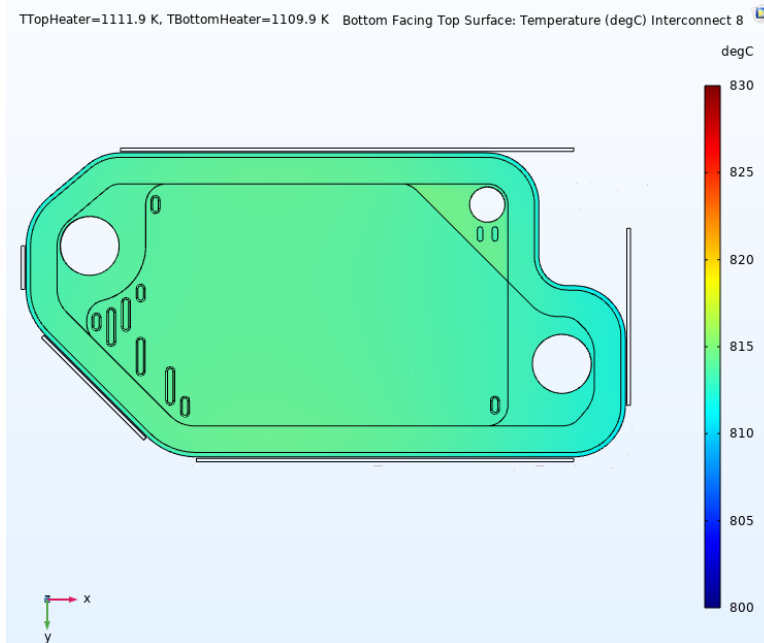


Delta T = +5C Interconnect 7 Bottom Facing Top

Interconnect 8: Bottom Heater=838.7C, Top Heater= 836.8C

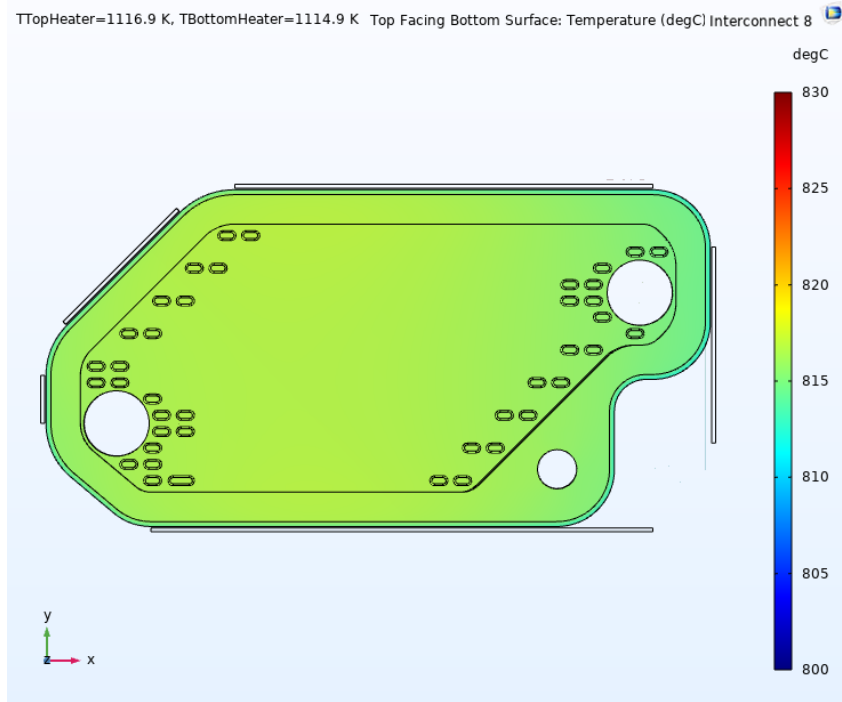


Delta T = -5C Interconnect 8 Top Facing Bottom

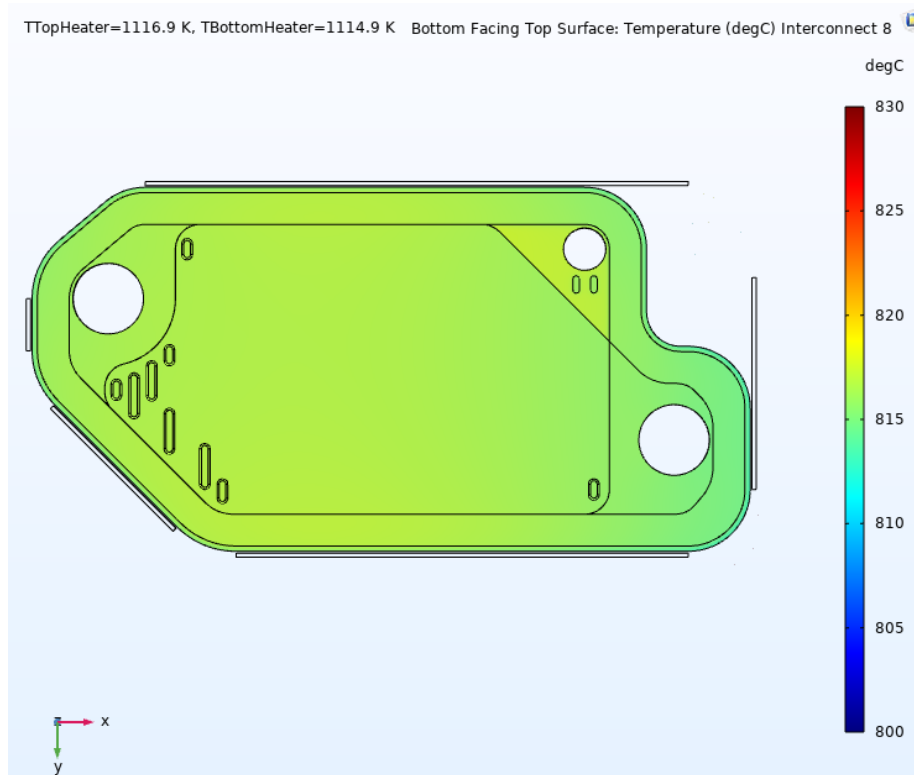


Delta T = -5C Interconnect 8 Bottom Facing Top

INTERCONNECT 8: Bottom Heater=843.7C, Top Heater= 841.8C

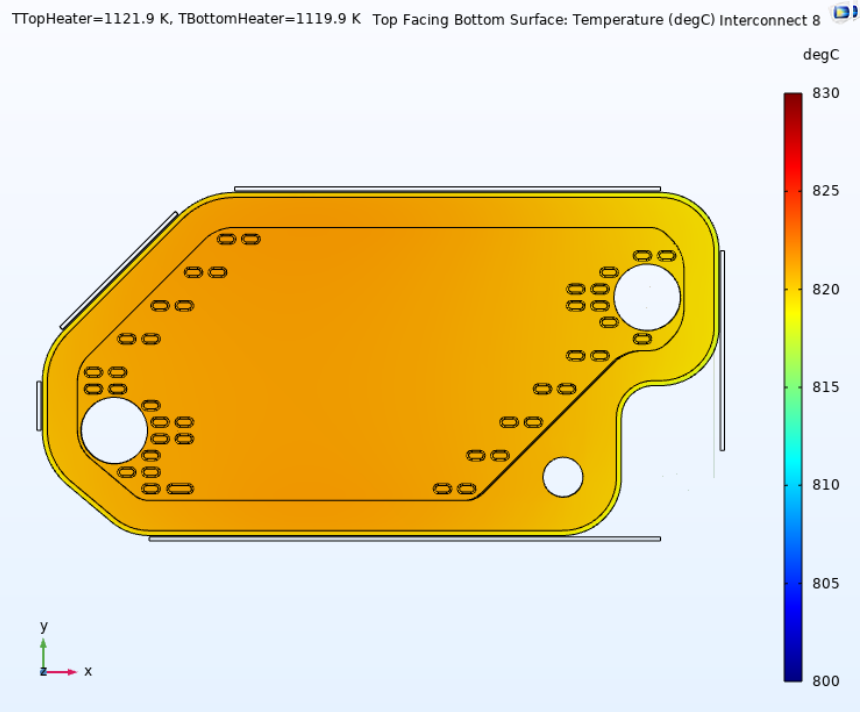


Delta T = 0C Interconnect 8 Top Facing Bottom

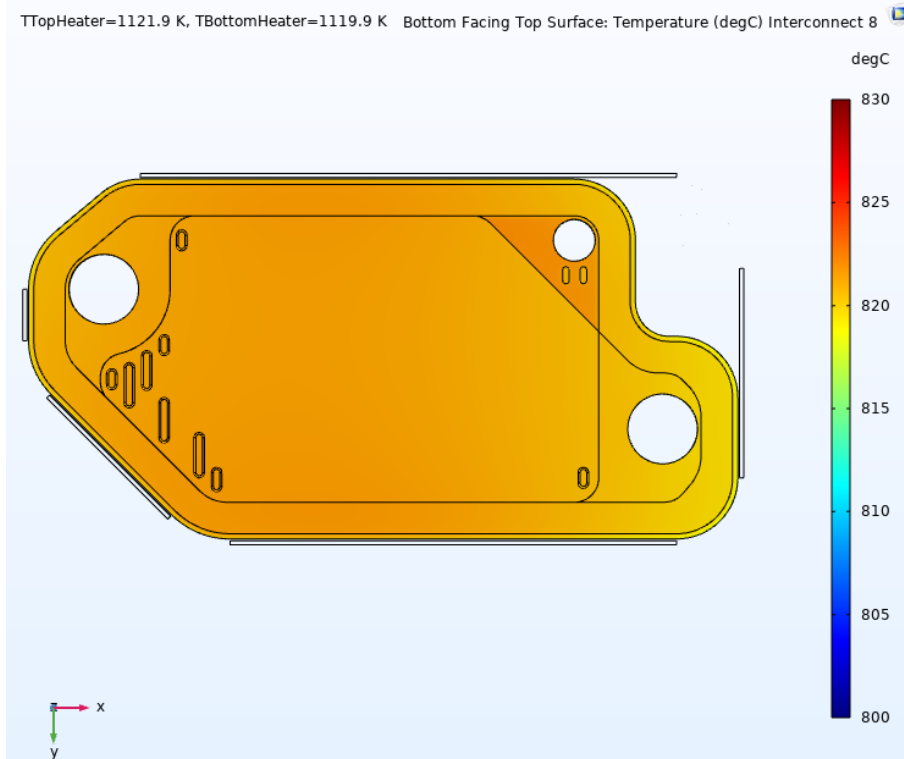


Delta T = 0C Interconnect 8 Bottom Facing Top

INTERCONNECT 8: Bottom Heater=848.7C, Top Heater= 846.8C

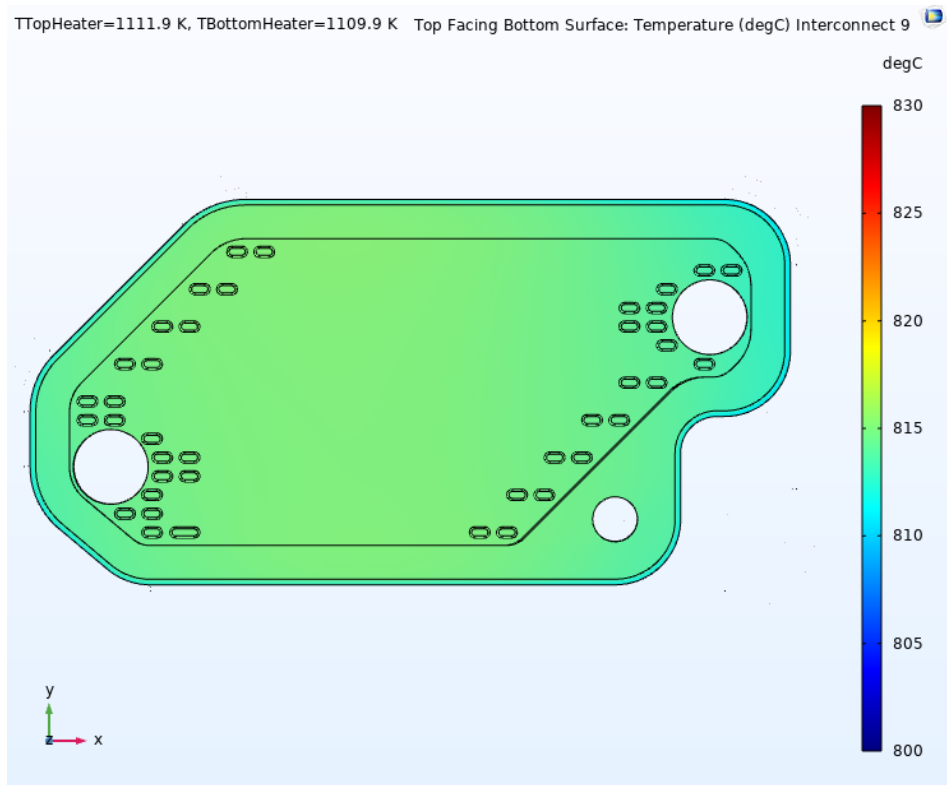


Delta T = +5C Interconnect 8 Top Facing Bottom

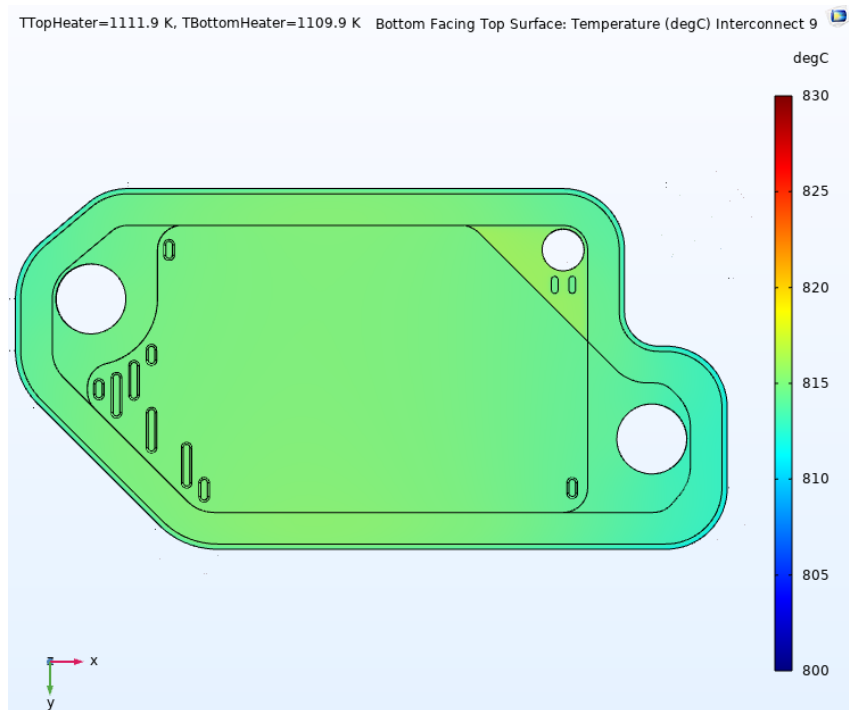


Delta T = +5C Interconnect 8 Bottom Facing Top

Interconnect 9: Bottom Heater=838.7C, Top Heater= 836.8C

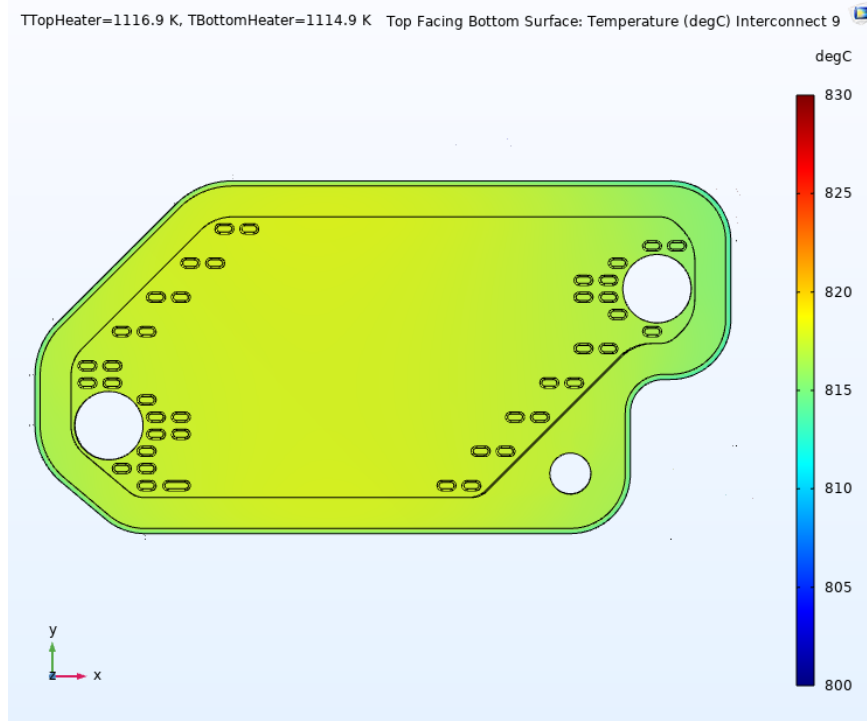


Delta T = -5C Interconnect 9 Top Facing Bottom

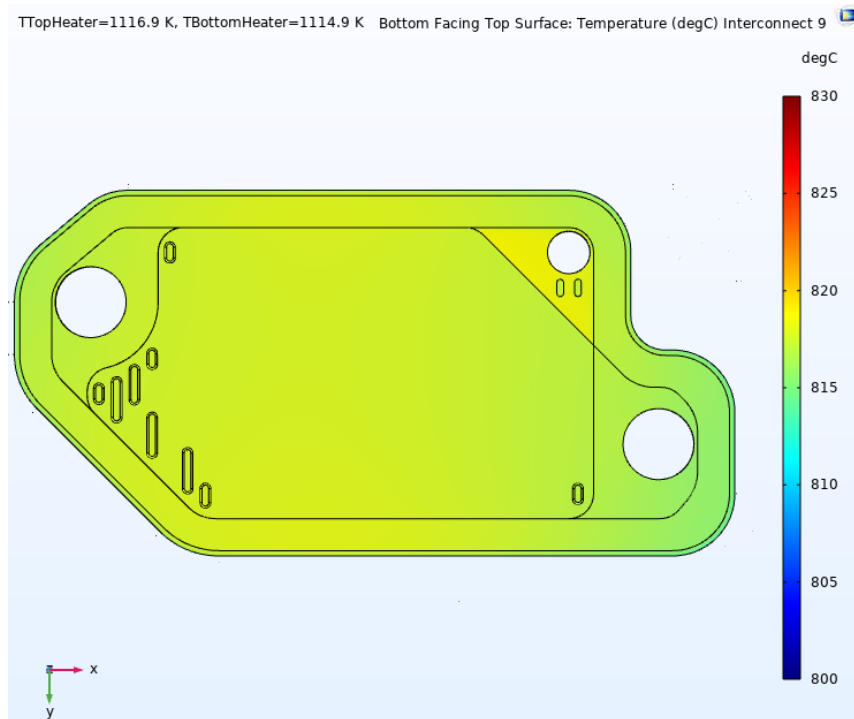


Delta T = -5C Interconnect 9 Bottom Facing Top

INTERCONNECT 9: Bottom Heater=843.7C, Top Heater= 841.8C

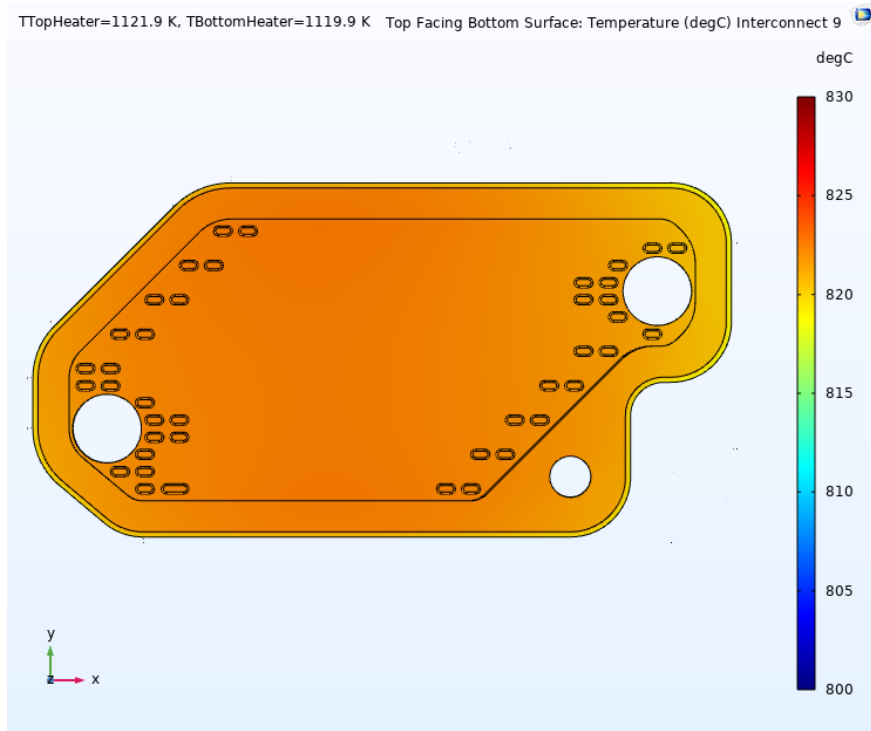


Delta T = 0C Interconnect 9 Top Facing Bottom

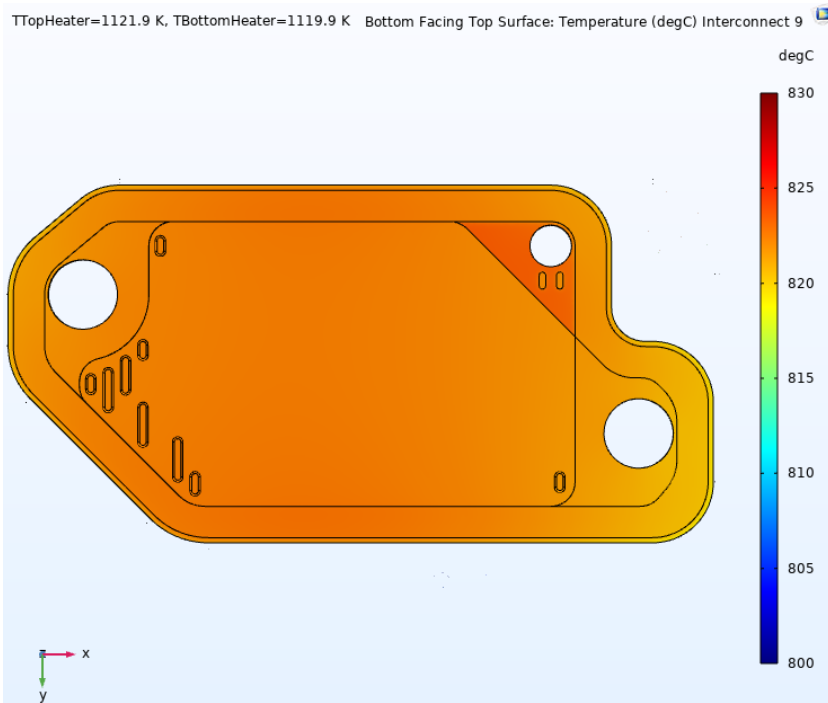


Delta T = 0C Interconnect 9 Bottom Facing Top

INTERCONNECT 9: Bottom Heater=848.7C, Top Heater= 846.8C

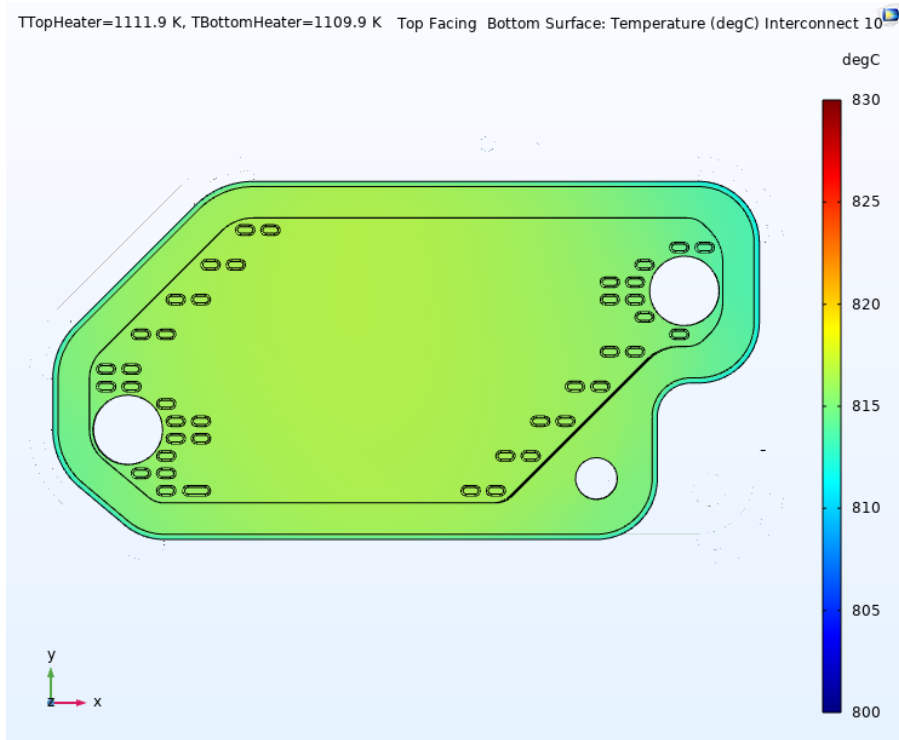


Delta T = +5C Interconnect 9 Top Facing Bottom

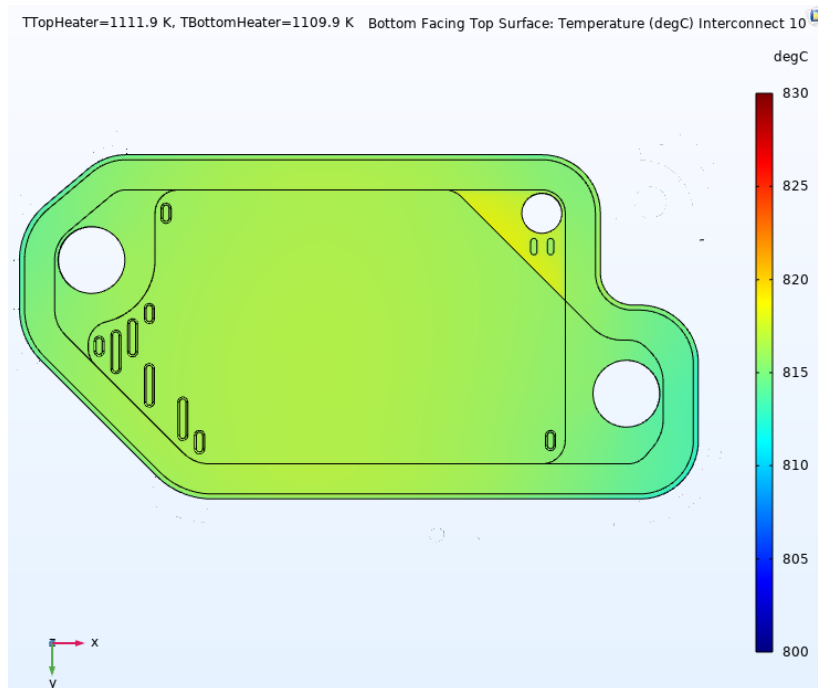


Delta T = +5C Interconnect 9 Bottom Facing Top

Interconnect 10: Bottom Heater=838.7C, Top Heater= 836.8C

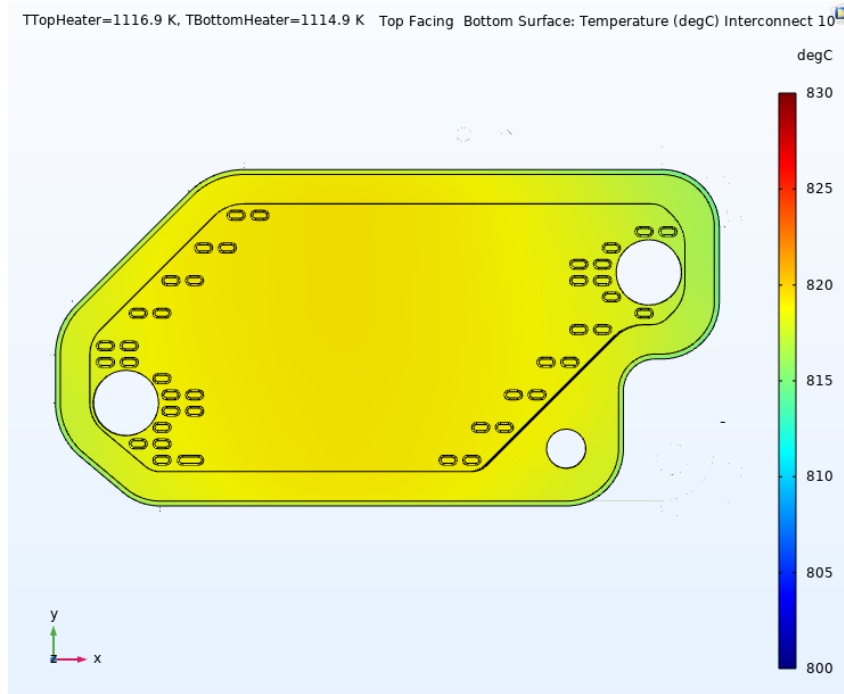


Delta T = -5C Interconnect 10 Top Facing Bottom

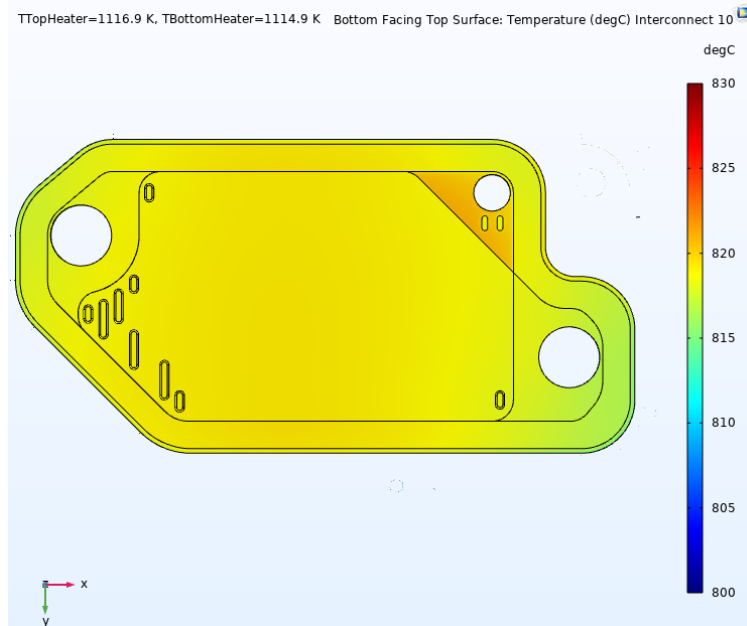


Delta T = -5C Interconnect 10 Bottom Facing Top

INTERCONNECT 10: Bottom Heater=843.7C, Top Heater= 841.8C

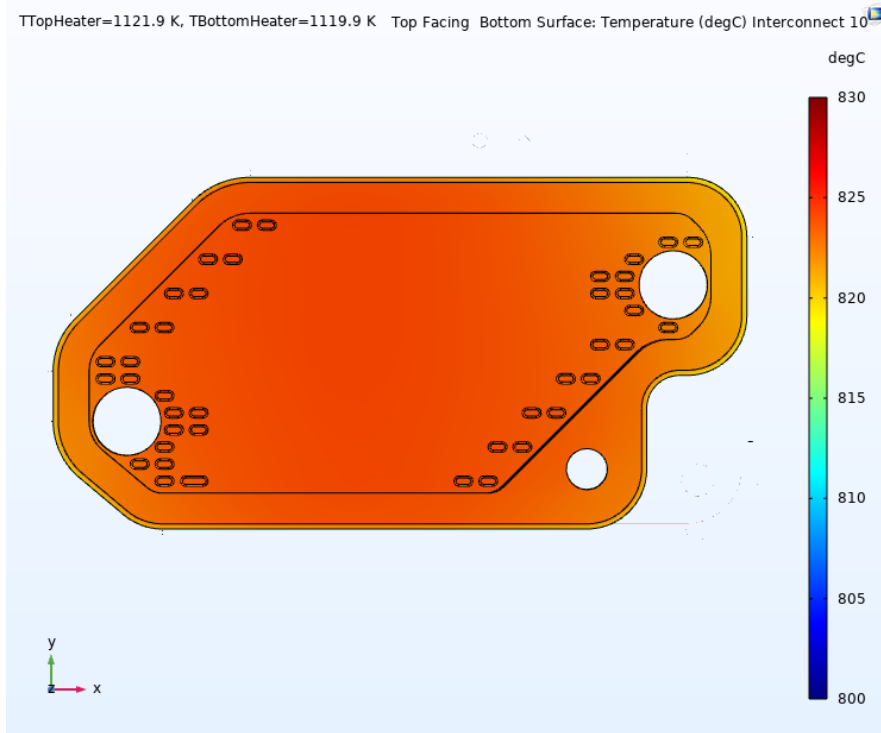


Delta T = 0C Interconnect 10 Top Facing Bottom

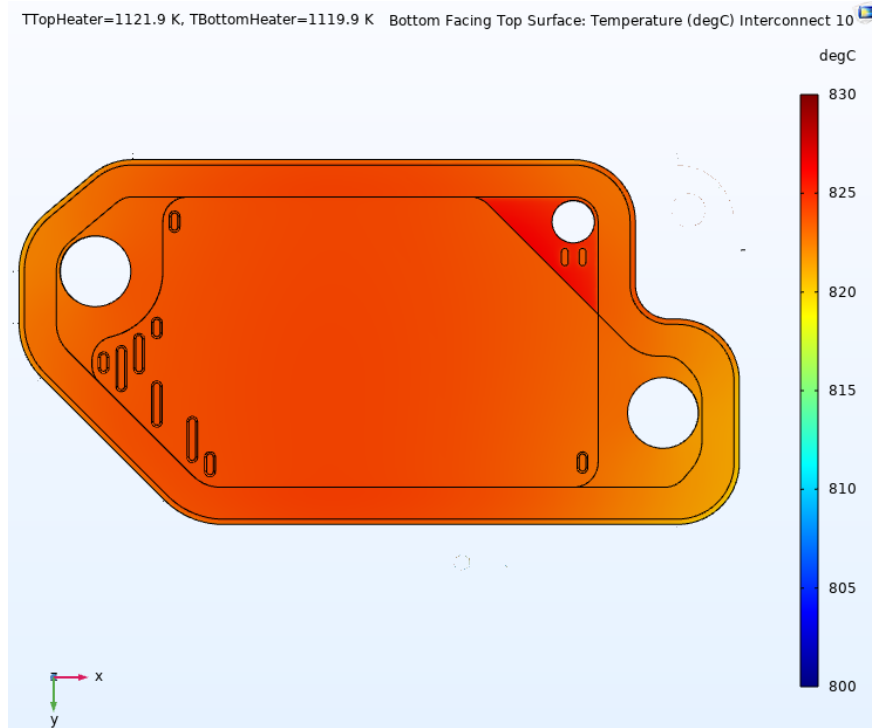


Delta T = 0C Interconnect 10 Bottom Facing Top

INTERCONNECT 10: Bottom Heater=848.7C, Top Heater= 846.8C

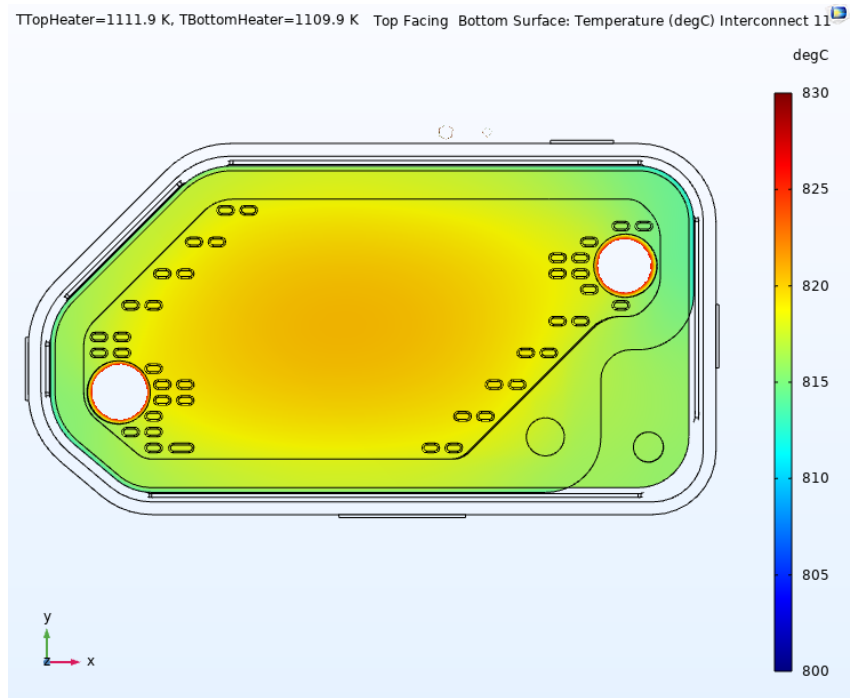


Delta T = +5C Interconnect 10 Top Facing Bottom

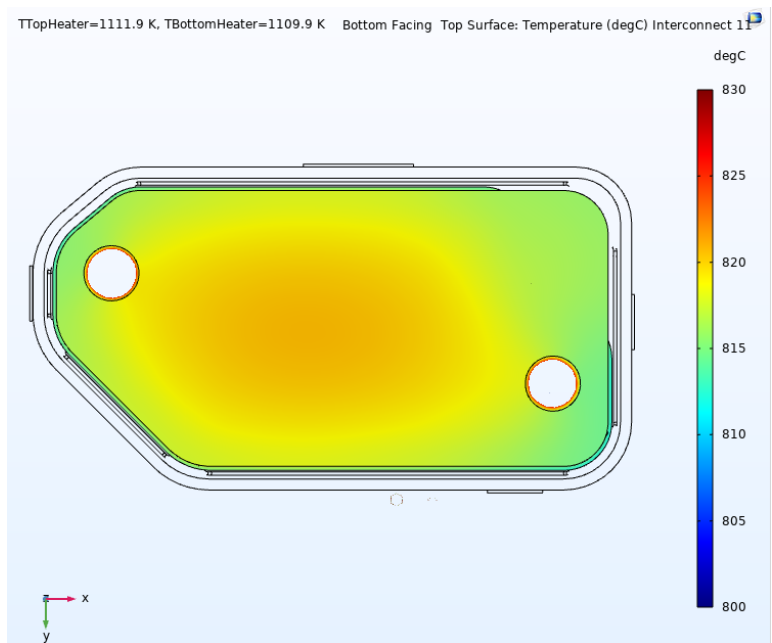


Delta T = +5C Interconnect 10 Bottom Facing Top

Interconnect 11: Bottom Heater=838.7C, Top Heater= 836.8C

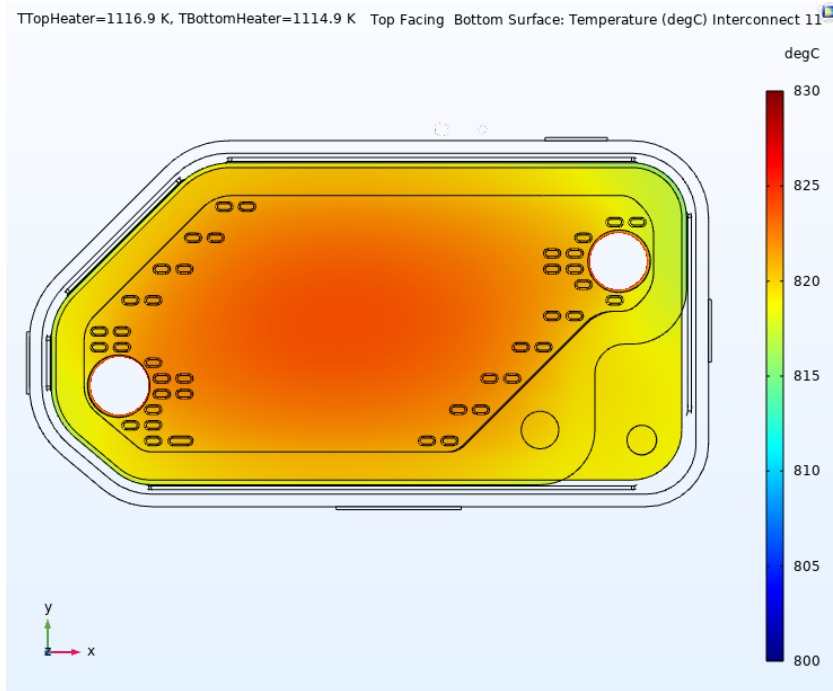


Delta T = -5C Interconnect 11 Top Facing Bottom

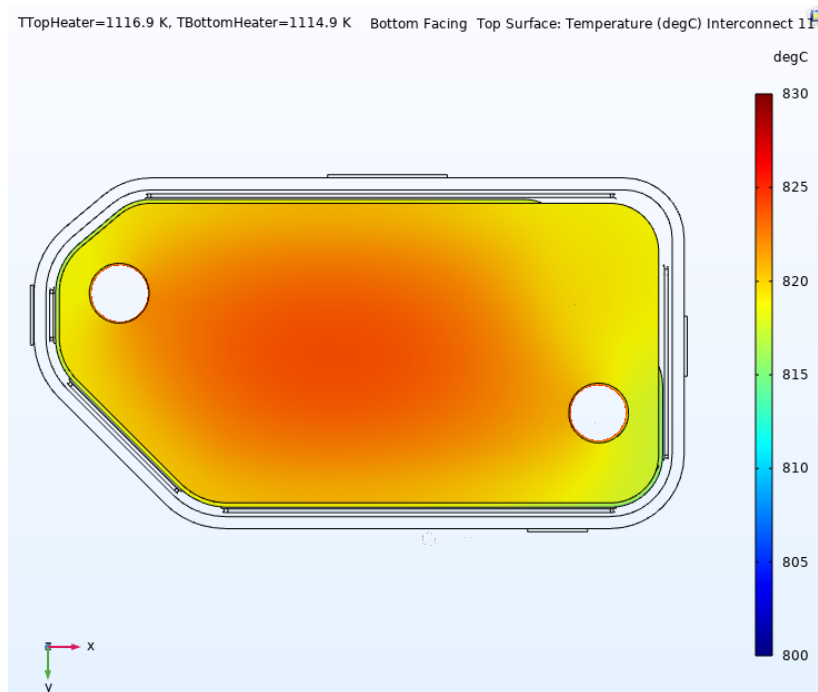


Delta T = -5C Interconnect 11 Bottom Facing Top

INTERCONNECT 11: Bottom Heater=843.7C, Top Heater= 841.8C

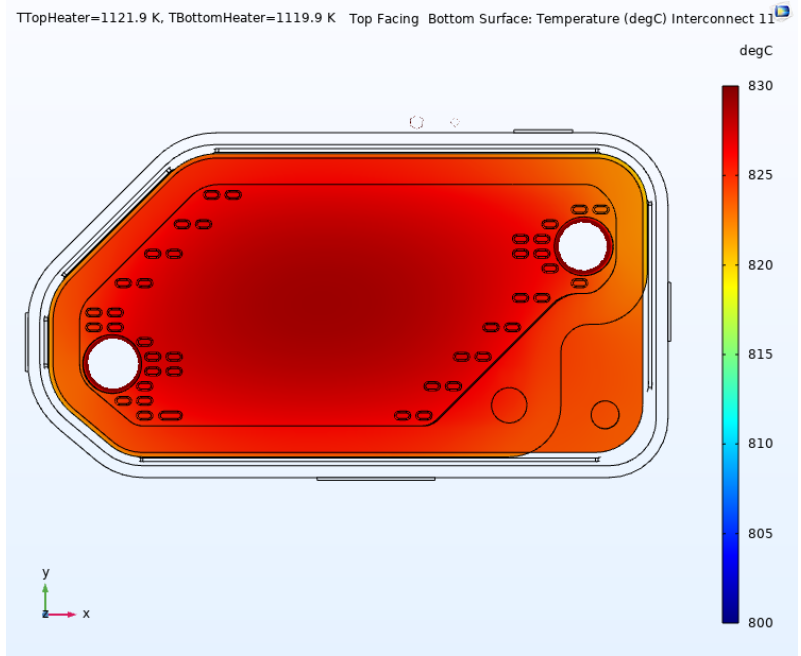


Delta T = 0C Interconnect 11 Top Facing Bottom

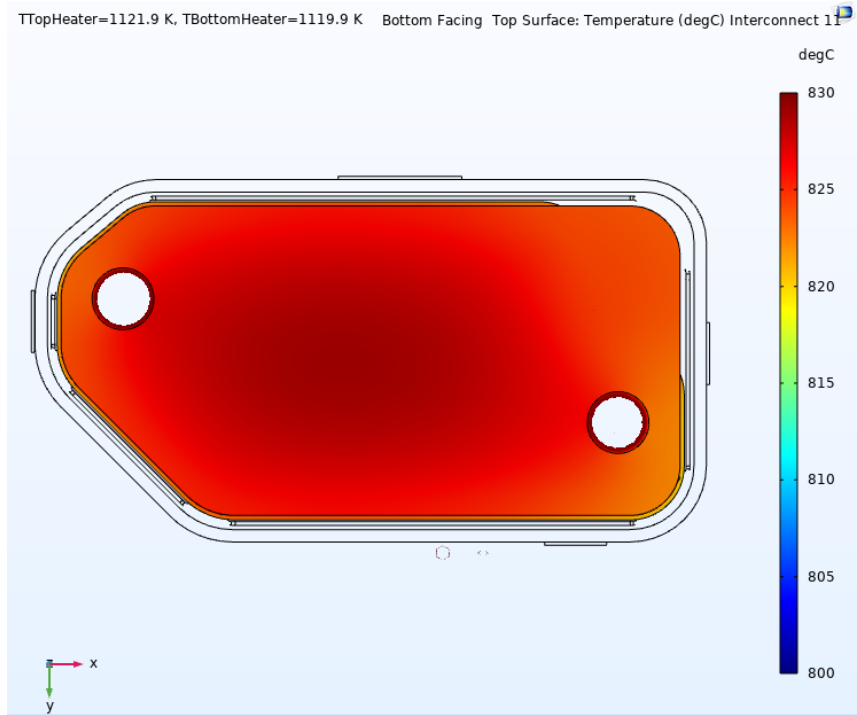


Delta T = 0C Interconnect 11 Bottom Facing Top

INTERCONNECT 11: Bottom Heater=848.7C, Top Heater= 846.8C



Delta T = +5C Interconnect 11 Top Facing Bottom



Delta T = +5C Interconnect 11 Bottom Facing Top

APPENDIX

**Delta Error Used for Data Matching Baseline Heater Temp (T_emperical-Tmodel)
Emperical Data JAS 006, OC07, OC8
(Baseline Heater Temp Bottom Heater=841.8C, Top Heater= 843.7C)**

*All temps in degC	O2 End Plate Short Side (TC4)	Mid Plate Short Side (TC5)	CO2 End Plate Short Side (TC6)	O2 End Plate Long Side (TC7)	Mid Plate Long Side (TC8)	CO2 End Plate Long Side (TC9)
Baseline Model Temp	817.65	815.15	818.78	820.06	815.58	820.08
OC07 Temps	820.49	813.89	818.78	821.39	812.28	820.1
Model Error Delta	-2.84	1.26	0	-1.33	3.3	-0.02
OC08 Temp	817.19	809.79	815.18	818.28	809	817.19
Model Error Delta	0.46	5.36	3.6	1.78	6.58	2.89

Bibliography

- [1] Aboobaker, A. SOXE Cell Temperature Testing, NASA Jet Propulsion Laboratory. 2017.
- [2] Aboobaker, A. SOXE Thermal Testing, NASA Jet Propulsion Laboratory. 2016.
- [3] Jenny Hua and A.Aboobaker. Material Property Tables. JPL: Internal Communications.
- [4] AZO Materials. Copper Alloy (UNS C15715) Material Data Sheet. Retrieved from: <https://www.azom.com/article.aspx?ArticleID=8814>: :text=UNS%20C15715%20is%20an%20aluminium,good%20elevated%2Dtemperature%20mechanical%20properties. 2013.
- [5] COMSOL. "Automatic (Newton) and Automatic Highly Nonlinear (Newton). Retrieved from "https://doc.comsol.com/5.5/doc/com.comsol.help.comsol/comsol_ref_solver.27.149.html". Accessed : 01.09.2016.
- [6] COMSOL. The Heat Transfer Module User Guide. Retrieved from <https://doc.comsol.com/5.4/doc/com.comsol.help.heat/HeatTransferModuleUsersGuide.pdf>.
- [7] B. Drake. Mars Design Reference Architecture 5.0. NASA/SP-2009-566-ADD, 2008.
- [8] A. Greenbaum. Iterative Methods for Linear Systems. Frontiers in Applied Mathematics. Vol. 17. SIAM., 1997.
- [9] Joseph Hartvigsen. Oxygen Production from Mars Atmosphere Carbon Dioxide Using Solid Oxide Electrolysis. *GCS Transactions*, 129(0094-5765):82-87, 2016.
- [10] M.H. Hecht. The Mars Oxygen ISRU Experiment (MOXIE) on the Mars 2020 Rover. 3rd International Workshop on Instrumentation for Planetary Mission. Vol 1980, 2016.
- [11] Eric Hinterman. System Modeling, Graphical User Interface Development, and Sensors Testing for the Mars Oxygen In-Situ Resource Utilization Experiment (MOXIE). Massachusetts Institute of Technology , June 2018.
- [12] M.H. Hecht and J.Hoffman. Mars Oxygen ISRU Experiment (MOXIE). *Space Science Review*. Vol. 217: 9, 2021.

- [13] Jon Ebert. Simulating Feedback Control of Thermal Systems. Video Webinar. Retrieved from: <https://www.comsol.com/video/simulating-feedback-control-thermal-systems>, 2022.
- [14] Ivar Kjelberg. Minimum Element Quality Statistic Documentation. COMSOL Solver Forum (2015). Retrieved from: <https://www.comsol.com/forum/thread/96191/Minimum-element-quality-statistic-documentation>. Accessed: 07.25.2021, 2015.
- [15] Jet Propulsion Laboratory. "SOXE Thermal Design and Analysis". Mars 2020 Project. California Institute of Technology. Internal Thermal Review, Internal Communication, 2020.
- [16] Forrest E. Meyen. Thermodynamic model of Mars Oxygen ISRU Experiment (MOXIE). *Acta Astronautica*. Vol 78: 2953, 2017.
- [17] NASA Jet Propulsion Laboratory, California Institute of Technology. . Mars 2020 Project 08 Thermal Review. Internal Technical Review: Internal Communication.
- [18] Donald Rapp. The Mars Oxygen ISRU Experiment (MOXIE) on the Mars 2020 Rover. AIAA SPACE Forum. "AIAA SPACE 2015 Conference and Exposition", 2015.
- [19] R. Zubrin. "The Case for Mars". New York City, NY: Simon Schuster. pg: "16,157,165", 1996.